UNIVERSITÀ DEGLI STUDI DI BOLOGNA

FACOLTÀ DI INGEGNERIA

Dottorato di Ricerca in Automatica e Ricerca Operativa

XV Ciclo

ADVANCED ROBOTIC HANDS: DESIGN AND CONTROL ASPECTS

Ph.D. Thesis

Luigi Biagiotti

Coordinatore
Prof. Alberto Tonielli

Tutore
Prof. Claudio Melchiorri

Anni Accademici 2000–2002

To Francesca and Calimero

Acknowledgements

The author thanks the Department of Electronics, Computer Science and Systems (DEIS) of the Faculty of Engineer of the University of Bologna for the received support and the staff of the Laboratory of Automation and Robotics (LAR) for the help in the experimental part of the thesis.

A special thank to professor Claudio Melchiorri, the author is grateful to him for the patience and the encouragement shown during these years.

Contents

List of Figures

List of Tables

Chapter 1

Introduction

1.1 Presentation of the work

In last decades, there has been a growing interest towards the development of advanced robotic hands, that is robotic end-effectors able to reproduce the functional capabilities (and in some cases the structure) of the human hand. The applications of such devices can be various: when the goal is to perform, by means of a robotic system, activities which foresee physical interactions (e.g. grasping and manipulation of some objects) with an unstructured environment, the use of an advanced end-effector is necessary. A typical application field is those of space activities, where robotic systems aim to replace human beings in the accomplishment of tasks, which are too dangerous, time consuming or simply annoying.
However, despite the wide potential applications of these devices, no real examples can be found and their use remains limited to research laboratories. As a matter of fact the high-level capabilities of dexterous hands to perform manipulation tasks imply, as a side-effect, high complexity of their mechanical structure, their sensory equipment and the control strategies. This is mainly due to technological limits: the human hand is the ideal target of each researcher in the field of dexterous manipulation but the tools (actuators, sensors...) currently available are still far from their biological models (muscles, receptors...).
The structural complexity of dexterous robotic hands leads to high costs and very poor reliability of the developed prototypes. Therefore an important requirement to encourage the diffusion of such devices will be their general simplification. This need is well summarized by the title of a paper of Bicchi [1]:

"Hands for dexterous manipulation and robust grasping: a difficult road toward simplicity"

Several are the ways to achieve this simplification. Obviously, technological improvements (concerning actuators, materials, sensors...) can allow an improvement of the overall system. The implementation of suitable control strategies can help to manage the complexity of such devices. The adoption of new design criteria (which are currently tied to the traditional robotics) can lead to simplified mechanical structures.
But, in general, the problem of complexity has been not faced by the designers of dexterous

robotic hands, whose target is to prove the effectiveness of a particular structure, rather than to make an “usable” device. Moreover, often the attention is mainly devoted to the physical design and development of the robotic hands, rather than to control problems tied to these devices. It is widespread the (wrong) idea that the control must be added (and hence designed) in a second phase. Therefore, some impressive examples of dexterous robotic hands are indeed able to perform only simple manipulation tasks, since the control is not adequate. Conversely, there are some devices which are purposely designed to validate control algorithms for dexterous manipulation, but usually they have simple structures and they can not be defined hands.

1.2 Contents of the thesis

Aim of this thesis, is to show how a simplification of advanced robotic hands can be achieved without prejudicing their functional capabilities. Different aspects are considered (control issues, technological improvements, new design criteria) and the results are shown by means of devices and prototypes carried out at LAR (Automation and Robotics Laboratory).

The thesis have been structured in the following way:

- In **Chapter 2**, starting from a review of some noticeable robotic hands developed over the last three decades, the state of art in robotic manipulation is analyzed with the purpose of emphasizing trends and open problems that currently characterize this research field.
- In **Chapter 3**, a robotic gripper purposely designed for space applications is presented. Despite a trends towards anthropomorphic hands has been recognized, the design of this device aims to demonstrate the effectiveness of a not-anthropomorphic structure to perform complex operations.
- The research activity, reported in **Chapter 4**, aims to validate the use of a new sensing element for mechanical “strain” in the robotic field. In particular, this new transducer (directly built on a deformable substrate) could replace traditional strain-gauge technology in force/torque sensors manufacturing, encouraging a deeper integration between mechanical and electronic part. The final result will be a general simplification and a considerable reduction of the dimensions of force sensors, which could be easily integrated in those structures where the available room is very narrow, such as the fingers of a robotic hand.
- **Chapter 5** presents the development of a controller able to drive a complex robotic system, such as a multifingered robotic hand, during the interaction with the environment in order to perform grasp and manipulation tasks. In particular a suitable strategy has been recognized in the impedance controller approach, which has been adapted to solve specific problems of dexterous robotic end-effectors. The achieved control algorithm has been implemented and experimentally validated on the DLR Hand II.
- **Chapter 6** describes the development, from the early idea to a working prototype, of a new kind of articulated robotic fingers, that is the basic element which will form a new hand for dexterous manipulation. This research summarizes in real terms the idea

developed over this thesis and in this sense it is the right conclusion of the overall work; in particular it shows how, by means of a proper integration between the design of the physical structure (mechanical frame as well as sensory equipment) and the choice of the control strategies, it is possible to achieve a general simplification of robotic devices for dexterous manipulation.

Chapter 2

An overview on advanced robotic hands

In this Chapter, starting from a review of some noticeable robotic hands developed over the last three decades, the state of art in robotic manipulation is analyzed with the purpose of emphasizing trends and open problems that currently characterize this research field. In particular, this study takes into account the different aspects, that contributes to the overall dexterity of a robot end-effector, such as kinematics configuration, sensory equipment and control strategies.

2.1 What is an advanced robotic hand?

In the last decades, a number of robotic end-effectors has been developed in the laboratories of universities and institutions (e.g. [2, 3, 4, 5, 6, 7]). Main aim of these robotic devices is to reproduce the functional capabilities (and often the structure) of the human hand, and hence are usually named "hands".

In particular, it can be easily recognized that the two main skills of a human hand are:

- *prehension*, i.e. the hand's ability to grasp and hold objects of different size and shape;
- *apprehension*, or the hand's ability to understand through active touch.

In this sense, the human hand is both an *output* and *input* device (see [8]). As output device, it can apply forces in order to obtain stable grasps or perform some procedures of manipulation while, as input device, besides providing information about the state of the interaction with the object during the task, it is capable to explore an unknown environment.
Both the characteristics are desirable in a robotic hand, which must operate in unknown environments and execute complex operations. As a matter of fact manipulation and exploration

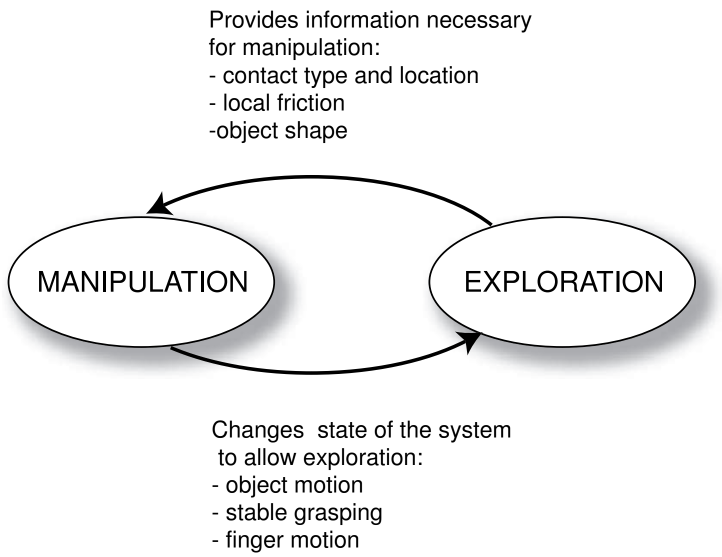

Figure 2.1: Reciprocal dependence between manipulation and haptic exploration.

capabilities are closely connected (as shown by Klatzky and Lederman, [9]). If we consider that a pure manipulation occurs when the object is perfectly known and conversely a pure exploration when the object is unknown but fixtured, it is clear as most part of dexterous manipulation tasks comes from their combination (in literature it is possible to find many examples of simultaneous manipulation and exploration [10], [11]): in general, we use manipulation for exploration and *vice versa*, Fig. 2.1.

2.1.1 The meaning of dexterity

A rigorous definition, widely accepted in the robotic manipulation letterature, states that:

dexterity (for a robotic end-effector) is "the capability of changing the position and orientation of the manipulated object from a given reference configuration, to a different one, arbitrarily chosen within the hand workspace" [1].

Despite of its precision, the previous statement does not give a complete idea of what dexterity is, and basically this definition appears tied to the kinematic structure of a robotic end-effector. On the contrary, (as shown in Fig. 2.1) dexterous manipulation is the result of several components including not only mechanics features, but also sensing capabilities, control strategies ...

In a broader sense, "dexterity" means the capability of an end-effector, operated by a suitable robotic system, to *autonomously* perform tasks with a certain *level of complexity.* In this sense the terms dexterous and *advanced* are used as synonym, even if the former refers to the functional capabilities of robot hands, the latter to the features which allow such capabilities. In general growing levels of dexterity are obviously associated with an increase of complexity.

The dexterity domain for robotic hands can be roughly divided in two main areas, that are *grasping* and *internal manipulation*.
Grasping is intended as constraining objects inside the end-effector with a constraint configuration that is substantially invariant with time (the object is fixed with respect to the hand workspace), while internal manipulation means controlled motion of the grasped object inside the hand workspace, with constraint configuration changing with time. Further subdivisions of these two domains have been widely discussed in the literature (different grasp topologies on one side [12], different internal manipulation modes based on internal mobility and/or contact sliding or rolling on the other side [1]).

2.1.2 The role of anthropomorphism

As above mentioned, the designers of robotic hands try often to reproduce not only the functional capabilities of the human hand but also its structure. That seems natural if we look at the level of dexterity of our hand, but it is worth to notice that "anthropomorphism" and "dexterity" are quite different concepts. As a matter of fact, the term "anthropomorphism" points at the capability of a robotic end-effector to mimic the human hand, partly or totally, as far as shape, size, consistency, and general aspect (including color, temperature, and so on) are considered. As the word itself suggests, anthropomorphism is related to external perceivable properties, and is not, itself, a measure of what the hand can do. On the contrary, "dexterity" is related to actual functionality and not to shape or aesthetic factors.
It is possible to find in the literature anthropomorphic end-effectors with very poor dexterity level, even if they are called hands, as the tasks they perform are limited to very rough grasping procedures [13]. Similarly, we can find smart end-effectors, capable of sophisticated manipulation procedures, without any level of anthropomorphism, e.g the DxGrip-II [14]. Anthropomorphism itself is neither necessary nor sufficient to achieve dexterity, even if it is quite evident that the human hand achieves a very high level of dexterity and can be considered a valid model for dexterous robotic hands.
Moreover, anthropomorphism may be a desirable goal in the design of robotic end-effectors for the following reasons:

- the end-effector can operate on a man-oriented environment, where tasks may be executed by the robot or by man as well, acting on items, objects or tools that have been sized and shaped according to human manipulation requirements;
- the end-effector can be tele-operated by man, with the aid of special-purpose interface devices (e.g. a data-glove), directly reproducing the operator's hand behavior;
- it may be specifically required that the robot has a human-like aspect and behavior, e.g. humanoid robots for purposes of entertainment, assistance, and so on.

2.1.3 A key-word in robotic hands design: the integration

Besides the dexterity or the anthropomorphism, a desirable feature (often underestimated) in the design of a robotic end-effector is the *integration*. This term has several meanings, but all

of them are fundamental in robot hands design.
As a matter of fact, a right integration between mechanical parts, sensors and electronics systems and control algorithms is one of the most stressed concepts in the design of robotic devices and automatic systems in order to achieve structural simplification, increase of reliability, and drop of costs. In particular this is true for a dexterous robot hands, which usually are extremely complex devices with quite small dimensions. Moreover, as will be shown in following sections, the dexterity and the functional capabilities of robot hands are the result of several contributions, which must balanced as much as possible. Therefore it is very important to properly match mechanical structure and sensory apparatus and also a medium-complexity hand can be dexterous and effective if an adequate mix has been done.
But, considering a robotic end-effector, *integration* concerns also the relation between the hand to be designed and the rest of the robotic system, considering both the physical parts of the system (*structural integration*) and the way they interact or cooperate in order to accomplish manipulation tasks (*functional integration*). Structural integration has great influence on overall hands design (and in particular the mechanical one), while functional integration is mainly a conditioning goal as far as control strategies and task planning procedures are concerned.
Two different concepts about the structural integration of robotic hands are described in the literature, which can be summarized with the following formula:

- Modular Hands (MH), Fig. 2.2.a;
- Integrated design Hands (IH), Fig. 2.2.b.

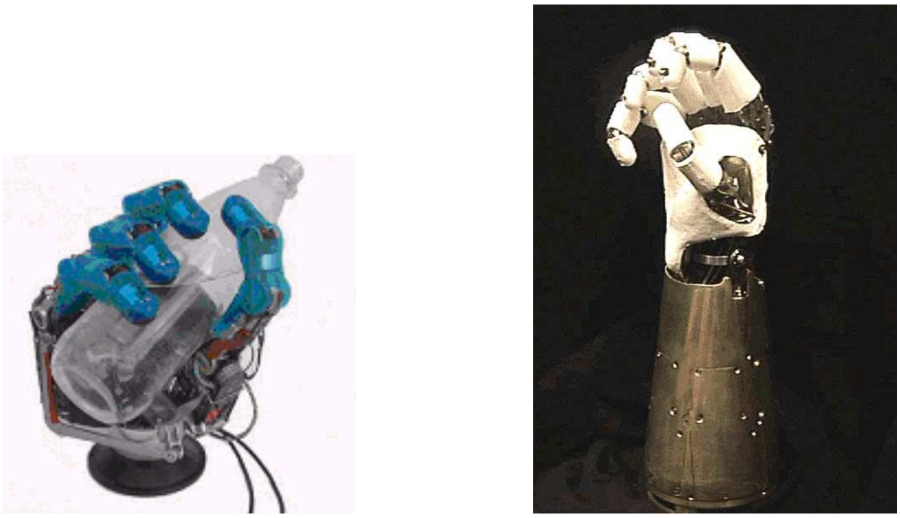

(a) (b)

Figure 2.2: Example of modular hand (DLR Hand II) (a) and of hand-arm structural integration (Robonaut Hand) (b).

In the former case, the hand is considered like an independent device to be applied at the end of an arm: the same hand can be applied to any kind of arm because it has been designed

independently of it (examples of this approach are the DLR Hands [3, 4], the Barret Hand [15], the Salisbury's hand [16],...).
In the latter case, reproducing the biological model, the hand is considered a non-separable part of the arm, deeply integrated with it: the hand and the arm are jointly designed and cannot be conceived as separate subsystems (as examples of this approach we can remember the Robonaut hand [17, 5], the UB Hand [18, 19]).
The main difference between these two approaches is that a modular hand must contain all its functional components (actuators, sensors, electronics, etc:), while an integrated system (hand + arm) can distribute these components in the whole structure, placing them where room is available.

2.2 Some comparative indices

In order to make a clear and objective comparison of different robotic hands presented in the literature some indices have been defined. These indices refer to the different aspects which characterize a robotic end-effector (as reported in Sec. 2.1), such as the degree of anthropomorphism and the level of dexterity resultant from both the kinematic configuration and the sensory apparatus.

2.2.1 An anthropomorphism index

From the observation of the many robotic end-effectors inspired by the human hand, it is clear that the level of achieved resemblance with a human hand is greatly variable from case to case, although all of them are defined as anthropomorphic hands.
Therefore an interesting problem arises: *what are the components of anthropomorphism and how the achieved level of anthropomorphism can be quantified?*
With the main aim of trying a comparison between different designs an anthropomorphism index (in the following denoted as α_x) has been constructed. That has been determined considering the following aspects:

- *Kinematics*. This aspect considers the presence of the main morphological elements (principal upper fingers, secondary upper fingers, opposable thumb, palm). Each of them, whose value ranges between 0 and 1 (according to the number of articulations inside each finger, in comparison with the human case), gives a different contribution to the kinematic evaluation score, weighted by the factor w_{1i};
- *Contact surfaces*: extension and smoothness of the contact surfaces, that means the capability to locate contacts with objects all over the surface of the available links, and availability of external compliant pads;
- *Size*. This contribution takes into account the actual size of the robotic hand compared with the medium size of a human hand and the "correct" size ratio between all the links.

The index α_x is calculated as the weighted sum of these three aspects, as shown in Fig. 2.3. If we consider the structure of the human hand the final value for α_x will be obviously equal to

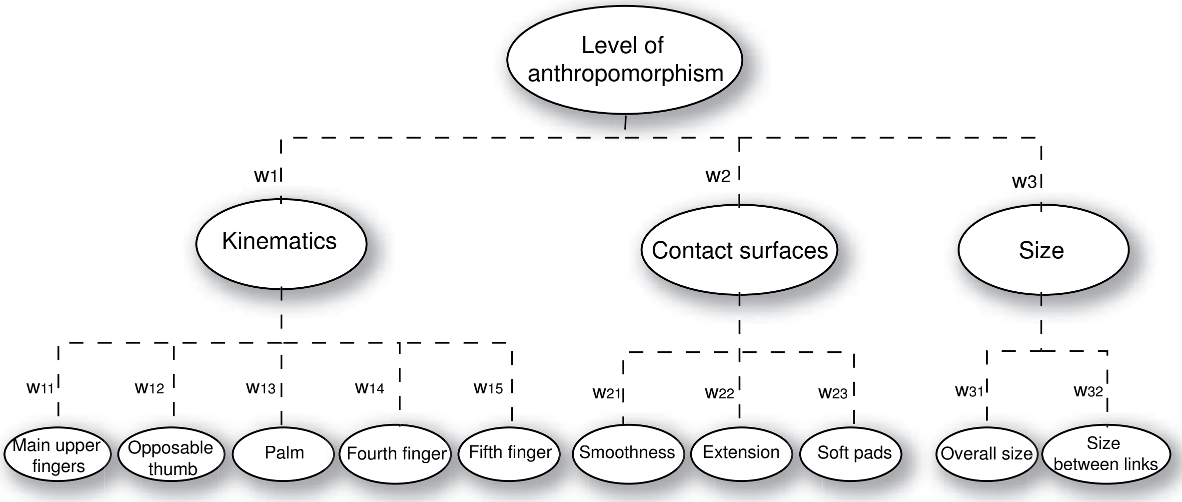

Figure 2.3: Evaluation graph of the anthropomorphism level of a robotic hand.

1, therefore the index associated to a given design (e.g. $\alpha_x = 0.75$) provides an immediate idea of how far from the human shape and aesthetics it places. For example, in Tab. 2.1 the index α_x relative to the UB-Hand, shown in figure Fig. 2.4, is presented [18, 19].

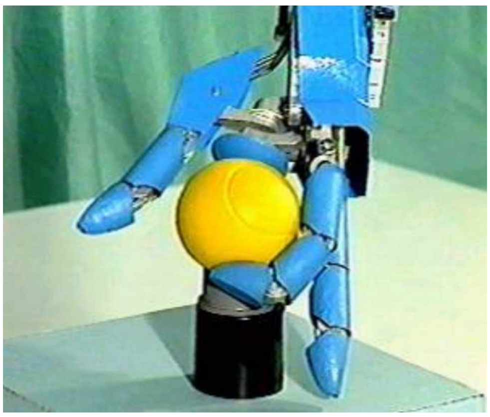

Figure 2.4: The University of Bologna Hand II.

2.2.2 A measure of dexterity

If the notion of dexterity is well settled, the way to achieve it remains debated. The factors affecting the actual capabilities of a robotic end-effector are so many, that often the analysis and above all the synthesis of dexterous hands do not take in the right consideration some of these elements, namely:

- morphological features;

Evaluated Elements and Related Weights		Value	Result
Kinematics ($w_1 = 0.6$)	Main Upper Fingers ($w_{11} = 0.3$)	1	0.18
	Opposable Thumb ($w_{12} = 0.3$)	0.8	0.144
	Palm ($w_{13} = 0.2$)	0.8	0.096
	Fourth Finger ($w_{14} = 0.1$)	0	0
	Fifth Finger ($w_{15} = 0.1$)	0	0
Contact Surfaces ($w_2 = 0.2$)	Smoothness ($w_{21} = 0.33$)	0.9	0.0594
	Extension ($w_{22} = 0.33$)	0.9	0.0594
	Soft Pads ($w_{23} = 0.33$)	0.3	0.0198
Size ($w_3 = 0.2$)	Overall Size ($w_{31} = 0.5$)	1	0.1
	Size Between Links ($w_{32} = 0.5$)	0.9	0.09
Total			0.745

Table 2.1: Evaluation of the anthropomorphism level (index α_x) of the UB Hand II.

- sensory equipment;
- control algorithms;
- task planning strategies;
- ...

As a matter of fact, a very simple end-effector like a rigid stick can be used for very sophisticated object-pushing tasks if used by a robot with visual and force feedback, while a complex articulated hand without adequate control can limit its dexterity to trivial self-adapting encompassing grasps. Evaluating the design of a robotic hand, for example examining its kinematical configuration or its sensory equipment, we can define a *potential dexterity* intrinsically related to its structure.

Potential Dexterity of a given mechanical structure

It is quite evident that the potential dexterity of an articulated five-finger hand is better than that of a rigid stick, but it is obvious at the same time that much of the potential dexterity of such a complex structure can be wasted if proper actuation or sensory system are not adopted and suitable control procedures are not implemented. The evaluation of potential dexterity of an articulated hand depending on its kinematical configurations (e.g. evaluation of manipulation ellipsoid) has been widely discussed in the literature, as reported in [1].
This kind of analysis requires the knowledge of some mechanical details and parameters, which are often unavailable. An alternative (but certainly more rough) way to quantify the potential dexterity of a robotic hand is considering its functional capabilities (allowed by the features of its mechanical structure, such as number of degrees of freedom, smoothness of the contact surfaces,...). In particular two main areas can be recognized:

- hands with capability limited to grasping (simplified kinematical configuration or complex kinematical configuration but reduced number of controlled degrees of freedom)

- hands that are capable of some kind of internal manipulation.

Each of these two areas can be further subdivided in two parts, distinguishing if the capability is limited to fingertip operation or is extended to the other active elements of the hand (whole hand grasp and manipulation). It is a rough subdivision, but can help to distinguish between projects that may look aesthetically similar but in practice achieve quite different levels of operating capabilities. In order to make this comparison easier, an index of the kinematic dexterity can be constructed, by tacking into account the contribution of the different abilities (as shown in figure 2.5).

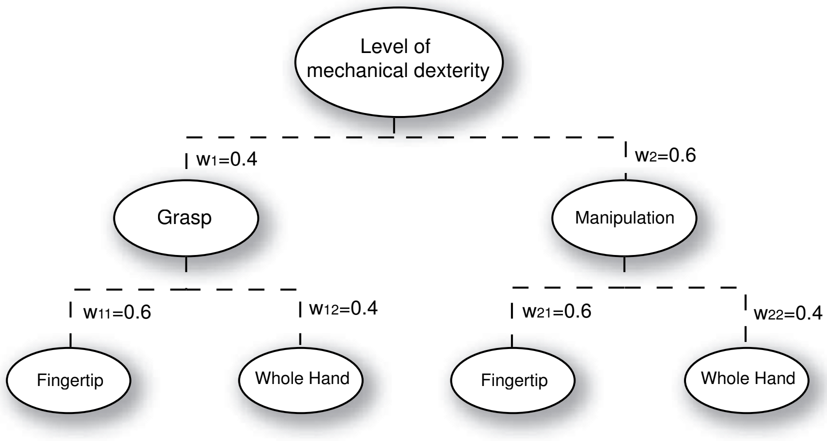

Figure 2.5: Evaluation graph of the kinematic dexterity level of a robotic hand.

2.3 Potential dexterity related to the sensory apparatus

Besides suitable mechanical configurations, dexterous manipulation requires an adequate sensory system. The manipulation of an object needs precise information about the configuration of the hand and the state of the interaction with the environment (typically the grasped object), and often the success (or simply the completion time) of the task depends on the level of this information. Since the human hand can be considered as the best known example of dexterous end-effector, not only its structure but also its sensory system has become a paradigm for the researchers. As a matter of fact, many of them tend to adopt similar sensory configurations even in devices quite simple from the mechanical point of view and not anthropomorphic at all. This is the case of the ROTEX Gripper (see Fig. 2.6) [20], whose equipment includes position, force and tactile sensors.

The internal state of the human hand (position, velocity and force) is known by means of receptors collocated in muscles, tendons, and joint capsules (for a complete overview see [21, 22]). But the key point of human dexterity is the richness of cutaneous information (high-frequencies vibrations, small scale shape or pressure distribution, accelerations and dynamic forces, thermal properties). As a matter of fact, it has been shown that the lack of touch sensation, due for

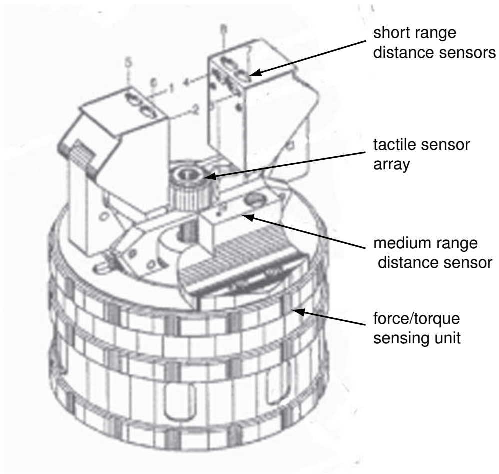

Figure 2.6: Sensory equipment of ROTEX gripper.

example to thick gloves (e.g. in space) degrades the human ability and prolongs the task completion time up to 80%, [23].

If the sensing system of the human hand is the desired target, unfortunately current technologies are still far from their biological models, in particular considering transducers of touch sensations. As a matter of fact, tactile sensors are object of great research efforts and the sensors currently available still present some important problems and functional limitations: basically they can detect the contact point and the magnitude of applied forces (while acceleration or vibration sensors are current under development [24] but not yet available for their integration in advanced robot hands) but they are generally characterized by low reliability, non-linear (hysteresis) phenomena and a large number of electrical connections.

2.3.1 A synthesis of sensing technologies for manipulation

The standard equipment of an advanced robotic end-effector includes, besides sensors directly collocated in the actuators (e.g. encoders), a number of additional sensing elements; in particular three main classes can be identified.

Joint position sensors

Although position sensors on motor shaft are a solution simple, reliable and with a relatively high resolution (considering that the rotor motion is 'reduced' several times by the mechanical transmission), back-lashes and deformations of the motions transmissions can render the measure quite rough. Besides, the use of non-rigidly coupled joints or under-actuated systems makes the *minimal* solution of motor encoders not applicable, since a well-defined relation between the rotor positions and the joint configuration does not exist: in general it depends also on external conditions (e.g. contact with the grasped object). In any case, when a single motor is used to drive more than one joint, and, in general, in order to improve the position measurements, additional position sensors must be added directly (or as close as possible) to the joints in the kinematic chain. Position sensors are based on different physical principles and methods: Hall effect sensors (e.g. the position sensors on the gripper designed by the University of Bologna, [25]), potentiometer, optical sensors (e.g. in the DLR hand I,[26]), and so on.

Interaction sensors

If the sense of touch (and in general force information) is the main reason of human hand dexterity, a robot hand, which will physically interact with the environment, can not leave aside force sensing. The measure of the interaction can be done in different way, but schematically it is possible to find three alternative methods (complete overview are available in [27, 28, 29]); on one hand the force exchanged with the external environment can be known by means of force/torque sensors collocated within the kinematic chain of the end-effector, on the other hand tactile sensors, directly placed on external surface, can provide information on the contact area and force magnitude when the interaction occurs. In the middle, Intrinsic Tactile (IT) can be considered.
Force/torque sensors measure the efforts exerted by fingers, at different levels and in different way: it is possible to detect the torques on finger joints, or consider the tension of tendons (which often are used to transmit the motion in robot hands), or if the mechanical chain is back-drivable measure the force/toruqe provided by the actuators. Other kind of force/torque sensors are able to detect all the components of the applied wrench; basically, the major part of these devices are transducers which measure forces/torques by means of the induced mechanical strains on flexible parts of their mechanical structure. The mechanical strains are in turns measured by elastomers (strain gauges), properly glued on the structure, that change their resistance according to local deformations. Based on a force/torque sensor with known external shape and connected to a link of a manipulator (see Fig. 2.7), the *IT sensor* has the possibility to determine, when a contact is established between the link and an object, both the applied wrench and the position of the contact centroid on the surface of the link. For this reason, the IT sensor can be considered an

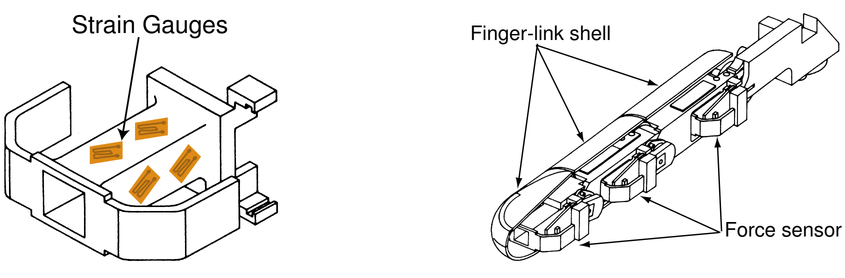

(a) (b)

Figure 2.7: An IT sensor (a) within a finger of the UBHand II (b).

intermediate solution between force sensors and tactile ones, even if one of the main drawbacks of this technology is the fact that they can not detect the difference between one contact and multiple contacts in the same structure (producing in the second case wrong estimations) and measure the shape/extent of the contact area. For this purposes, that is to determine the exact shape and position of contact (possibly not-punctual) area, *tactile sensors* are used. Usually, they consist in a matrix (array) of sensing elements. Each sensing element is referred to as a *taxel* (from "tactile element"), and the whole set of information is called a *tactile image*. Main goal of this class of sensors is to measure the map of pressures over the sensing area, allowing to get geometrical information (position and shape of contacts), as well as knowledge about mechanical properties (e.g. friction coefficient), and to detect when a slip condition occurs. In order to realize this kind of transducers several technologies have been developed, ranging from piezoresistive to magnetic, to optical effects [27, 28].

Additional sensors

Additional sensors can be added for particular applications or to obtain specific capabilities; for example end-effectors for space activities are often equipped with proximity sensors and/or cameras directly installed within the hand [26]. Other classes of sensors, which can increase the dexterity of a robot hand, include accelerations or vibrations sensors [24], but their development is still in progress.

2.3.2 A comparative index

In order to give an immediate idea of the complexity of the adopted solutions in some noticeable examples of robot hands, we have defined an index σ_x which takes into account the sensory equipment. In Table 2.2 the sensory apparatus of the UB Hand II has been considered: the index is the result of evaluation of the three classes defined in the previous section, considered with different weights according to the level of dexterity they can, in authors' opinion, allow.
Sensors that detect the status of the interaction (force/torque and tactile sensors) are considered as preeminent to achieve dexterity. Moreover, it is worth to notice that tactile "array" sensors and intrinsic tactile sensors are treated as alternative: the information they provide are quite different and normally used for different aims (planning the former, control the latter). Tactile capabilities are further specialized considering their peculiar features:

- distribution on the robotic devices (fingertips/phalanges/palm) and number of detectable force/torque components for IT sensors;

- distribution, covering (partial/total of the finger link surfaces), and spatial resolution for tactile array sensors.

The index σ_x can be very useful to compare different designs and to have an immediate idea of how different researchers have faced the problem of dexterity.
Moreover, it provides a measure of the gap with the human hand, whose index is not far from one (not exactly one, because of the lack of some sensors, such as proximity sensors)

Evaluated Elements and Related Weights				Value	Result
Position ($w_1 = 0.2$)	Joint Position Sensors ($w_{11} = 1$)			1	0.2
Interaction ($w_2 = 0.6$)	Force/Torque Sensors ($w_{21} = 0.3$)			0.4	0.072
	Tactile Sensors ($w_{22} = 0.7$)	Intrinsic ($w_{221} = 0.6$)	# Axis ($w_{2211} = 0.5$)	1	0.126
			Placement ($w_{2212} = 0.5$)	1	0.126
		Array ($w_{222} = 0.4$)	Spatial Resolution ($w_{2221} = 0.3$)	0	0
			Covering ($w_{2222} = 0.2$)	0	0
			Placement ($w_{2223} = 0.5$)	0	0
Additional ($w_3 = 0.2$)	Proximity,Vision, Dynamic Force Sensors ($w_{31} = 1$)			0	0
Total					0.524

Table 2.2: Evaluation of the sensory equipment of the UB Hand II.

2.4 A survey on advanced robotic hands

Several robotic hands, more or less dexterous/anthropomorphic, have been developed over the past two decades. The goals of each project were most times rather different, and the results are not easily comparable to the purpose of declaring one project better than another. Anyway, in order to point out the effectiveness of each contribution and to trace the historical evolution of this sector of robotics, a classification of the potential dexterity and level of achieved anthropomorphism of each design can help to outline results, tendencies, open problems and goals for future evolution of research.
In Tab. 2.3-2.10 a survey of some noticeable examples of robotic hands is reported, considering the the main features of the mechanical design, as well as of the adopted sensory system. The review is limited to those projects that clearly addressed the achievement, at a significant level, of both dexterity and anthropomorphism.

From the data collected in the tables, the indices mentioned in Sec. 2.2.1, 2.2.2 have been computed for each hand and graphically displayed in order to give a synthetic idea of the main characteristics of each project and to compare the different designs. In order to give an historical perspective of the considered aspects (anthropomorphism, dexterity,...), the robot hands are presented according to a chronological order.
Firstly, in Fig. 2.8 the anthropomorphism level has been considered: it is clear that in last years (in particular in the last 5-6 years) the interest towards fully anthropomorphic devices has been growing. As a matter of fact the kinematic structure of robotic hands becomes more and more close to the human model and the dissimilarity with our hand mainly concern the size and the "skin". If the former difference is above all due to technological problems (in particular, to the lack of miniaturized actuators), the latter strongly depends on a traditional way of designing robotic devices. Despite it has been recognized that suitable contact surfaces (in particular soft pads) can greatly enhance (besides their appearances) the dexterity of robot hands [45], only in the last years this issue has been explicitly faced and the first endoskeletal structures, apt to be integrated with soft layers, have been presented [46, 47].

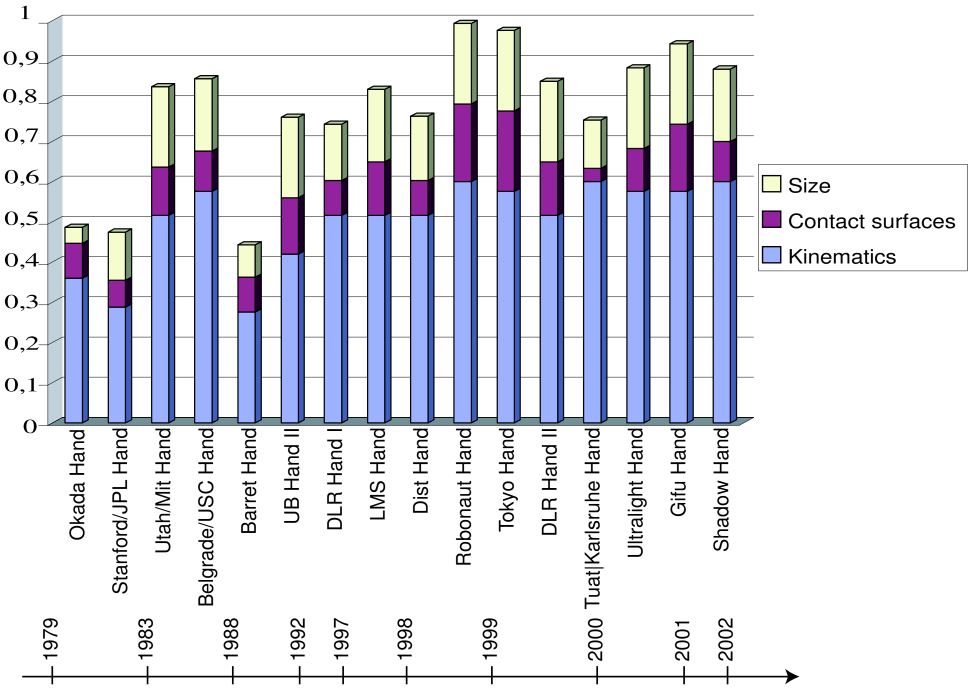

Figure 2.8: Anthropomorphic level of the reviewed robotic hands.

As mentioned in Sec.2.2.1 anthropomorphism and dexterity are orthogonal concepts; this is evident if we consider the other two defined index, that is the degree of dexterity related to the mechanical structure and to the sensory equipment, respectively reported in Fig. 2.9 and 2.10. Tacking into account the mechanical structure, it can not be observed the trend, which characterizes the anthropomorphism level, towards an increase of dexterity. There are examples in the scale of evolution, from very anthropomorphic but low dexterity designs (it is the case of hands simply oriented to adaptable grasp applications, e.g. the Tuat/Karlsruhe Hand [13] and the Laval Hand [48]) to fairly dexterous but less anthropomorphic ones. In Fig. 2.11 possible relations between anthropomorphism and dexterity are displayed, considering some notable examples of robotic hands. These designs are usually associated to very restricted and limiting specifications and precise purposes:

- Salisbury, designing the Stanford/JPL hand, explicitly focus the problem of dexterity, but no considerations about resemblance with the human hand have been done;

- the target of the Tuat/Karlsruhe hand is to exploit the structure of the human hand in order to achieve good grasp capabilities with a very low complexity (only one actuator has been used);

- Robonaut hand aims to substitute the human hand concerning both functional capabilities and shape/structure;

- Barret hand is, according to the definition of its designer, a grasper and therefore neither

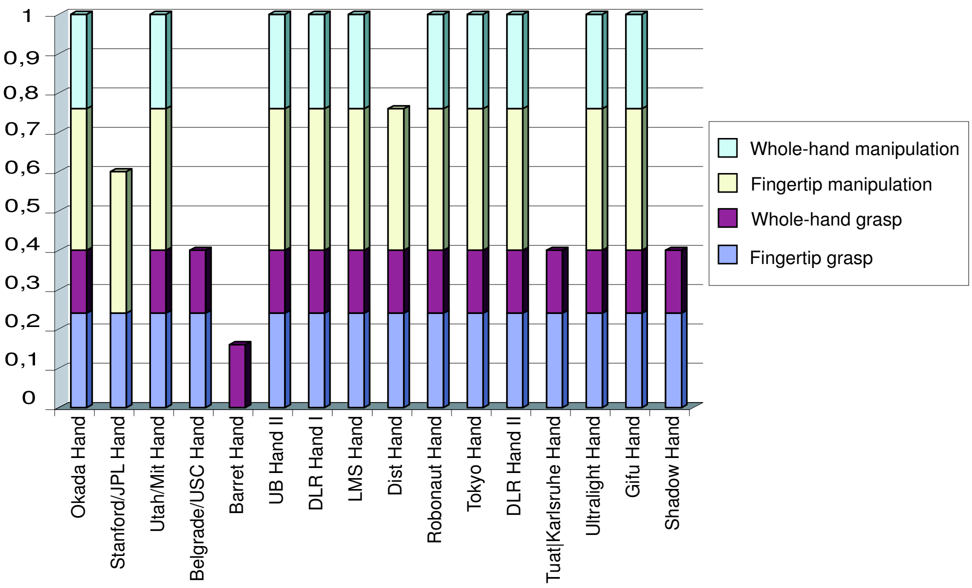

Figure 2.9: Potential dexterity related to the mechanical structure of the reviewed robotic hands.

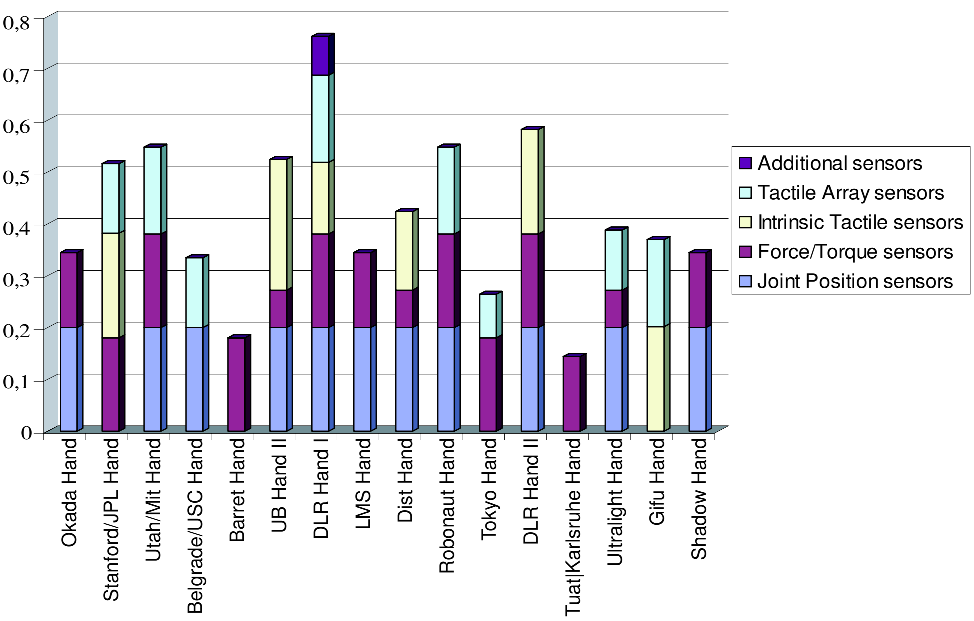

Figure 2.10: Potential dexterity related to the sensory system of the reviewed robotic hands.

anthropomorphism nor high-level of dexterity has been specifically addressed.

High dexterity is usually synonym of complexity. In this sense the designs of the reported robotic hands appear very coherent, according to the criterion of integration between mechanical and electronic parts mentioned in Sec. 2.1.3. As a matter of fact hands showing the highest degrees

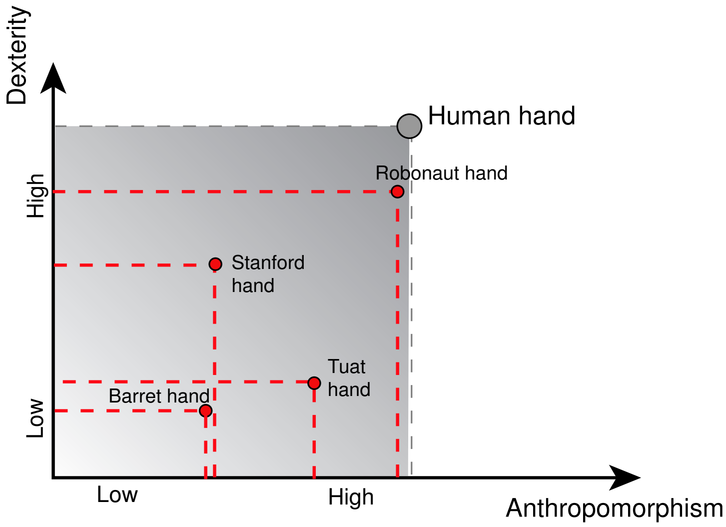

Figure 2.11: Relation between anthropomorphism and dexterity.

of structural dexterity, and therefore the largest number of controlled degrees of freedom and actuators, are characterized by an extremely complex sensing apparatus. Conversely commercial hands (like Barret hand or Shadow hand), that must be particularly reliable and consequently not too complex have only a basic set of sensors.
In any case, if we observe the potential dexterity related to the sensory system, all the projects show high-level equipments (compared with traditional robot manipulators), including positions and force/torque sensors. Moreover the design of such an equipment is somehow incremental, and often additional sensors are employed afterwards. In particular, this is true for tactile sensing: despite the contribution of tactile sensors to the dexterity of robotic hands is widely recognized, their use is not settled yet. From the Fig. 2.10 it is clear that a "final decision" between intrinsic tactile sensors, tactile array sensors, or both has not been definitely made and it is currently an important research topic in the field of robot manipulation.

2.5 Potential or real dexterity? The role of control

As stated by Bicchi [1], citing the Greek philosopher Aristoteles, one of the (old) theories regarding the relationship between human hands and mind claims that "because of his intelligence he (man) has hands". Despite, researches of paleoanthropologists have shown that the converse opinion, which considers the development of the brain of human beings as a result of the structural dexterity of their hands, is preferable, the former theory gives an insight into the importance of the "intelligence"(in a broad sense) in order too obtain the dexterity of an (artificial) hand.
As shown in previous sections, the dexterity of a robot hand is the result of its mechanical structure as well as of its sensory equipment. Adding up the contributions sketched in Fig. 2.9 and Fig. 2.10 it is possible to quantify the overall degree of dexterity of the reviewed hands. At this point, a first consideration is that some of the devices taken into account are not distant

(considering their structure and their features) from the human hand but the tasks they can autonomously perform are still simple and quite far from the human capabilities. Therefore, in order to estimate the real dexterity of a robot hand, the "intelligence", that is control algorithms and task planning strategies, can not be neglected. Indeed, the control is a key element, which puts potential dexterity into real one and is the main reason of the success of the human hand. Because of its "control system", the human hand can fully exploit its complex structure. The same does not happen for robot hands: as qualitatively shown in Fig. 2.12.a their actual dexterity is considerably lower than the dexterity given by their structure and paradoxically some simple devices with suitable control strategies may be more dexterous than a complex robot hand (see Fig.2.12.b). A tangible example of such a smart device is given by Dx-Grip II, a 2-jaw gripper developed by Bicchi et al. [49], able to arbitrarily change the position/orientation of quite general objects, by means of rolling.

A number of theoretical works show that *rolling* and *sliding* can greatly enhance the robot

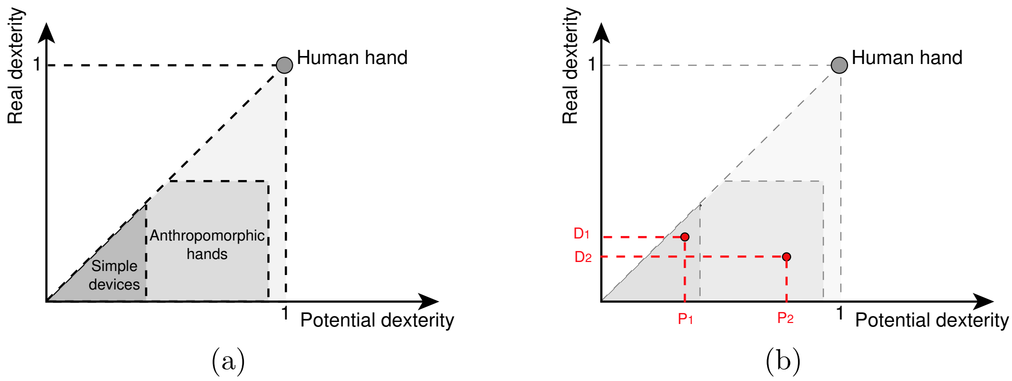

Figure 2.12: Potential versus real dexterity: general case (a) and an example (b).

dexterity [50, 51, 52, 53] but, despite the effectiveness of manipulation by rolling or sliding can be observed also in human beings, these results are not applied to complex robot hands. In the same way, the use of tactile sensors for direct servoing have been the subject of several recent works [11, 54], but practical demonstrations of the achieved results has been done only by means of robotic devices purposely designed.

Table 2.3: Main features of Okada and Stanford/JPL Hands.

	Project denomination	**Okada Hand**	**Stanford/JPL Hand**
Project identification	Reference author(s)	T. Okada	Salisbury
	Research institute	Electrotechnical laboratory, Japan	Stanford University
	Year of presentation	1979	1983
	Reference	[30]	[16, 31, 32]
Picture		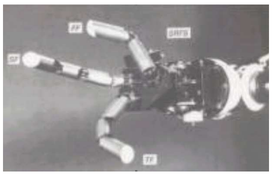	
Mechanical structure:	Arm/hand Integration	MH	IH
Kinematical scheme:	Main upper fingers	✓	✓
	Opposable thumb	✓	✓
	Fourth finger	-	-
	Fifth finger	-	-
	Palm	-	-
	Number of links	12	10
	Number of joints	11	9
	Number of controlled degrees of freedom	11	9
Morphological features:	Size w. r. to a human hand	>	=
	Surfaces apt to contact with objects	Fingertips/Phalanges	Fingertips
	Contact surface smoothness and continuity	Fair	Poor
Mechanical details	Structural design concept	Exoskeletal	Exoskeletal
	Actuator location	Remote	Remote
	Actuation type	Electrical revolute motor	Electrical revolute motor (DC)
	Act. joints backdrivability	Not Found (NF)	✓
	Kind of not-actuated joints	-	-
	Type of transmission	Tendons	Tendons
	Transmission routing	Pulleys/sheaths	Pulleys/sheaths
Sensors:			
Position	Motor position sensors	✓	✓
	Joint position sensors	Potentiometers	-
Force/Torque sensors	Joint torque sensors	-	-
	Tendon tension sensors	-	✓
	Motor effort sensors	✓	-
Contact sensors	Intrinsic tactile sensors	-	Fingertip force sensors
	Tactile array sensors	-	8×8 tactile sensors array with complete coverage of the cylindrical fingertip
Additional Sensors			

Table 2.4: Main features of Utah/Mit And Belgrade/USC Hands.

Project identification	Project denomination	**Utah/Mit Hand**	**Belgrade/USC Hand**
	Reference author(s)	Jacobsen	G.A. Bekey/R. Tomovic/I. Zeljkovic
	Research institute	Utah University	University of Belgrade
	Year of presentation	1983	1988
	Reference	[6, 33, 34]	[7]
Picture		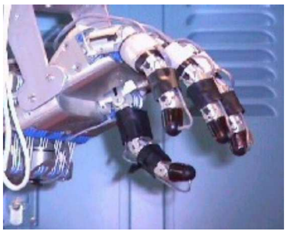	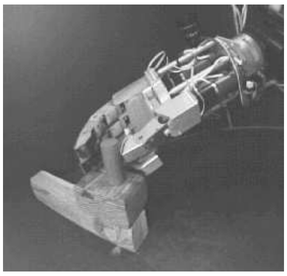
Mechanical structure:	Arm/hand Integration	IH	MH
	Main upper fingers	✓	
Kinematical scheme:	Opposable thumb	✓	✓
	Fourth finger	✓	✓
	Fifth finger	-	✓
	Palm	✓	✓
	Number of links	17	16
	Number of joints	16	18
	Number of controlled degrees of freedom	16	4 (2 thumb+2 fingers)
Morphological features:	Size w. r. to a human hand	=	=
	Surfaces apt to contact with objects	Fingertips/Phalanges/Palm	Fingertips/Phalanges/Palm
	Contact surface smoothness and continuity	Good	Fair
Mechanical details	Structural design concept	Exoskeletal	Exoskeletal
	Actuator location	Remote	Remote
	Actuation type	Pneumatic actuator	DC Motors
	Act. joints backdrivability	✓	-
	Kind of not-actuated joints	-	Rigid passive-driven joints
	Type of transmission	Tendons	Linkages
	Transmission routing	Pulleys	-
Sensors:			
Position	Motor position sensors	✓	✓
	Joint position sensors	Rotary Hall effect	Rotary potentiometers
Force/Torque sensors	Joint torque sensors	-	-
	Tendon tension sensors	✓	-
	Motor effort sensors	-	-
Contact sensors	Intrinsic tactile sensors	-	-
	Tactile array sensors	Capacitive tactile sensors covering finger segments and palm	Touch-pressure sensors (Force sensing resistor) on fingertips
Additional Sensors			

Table 2.5: Main features of Barret and UB (II) Hands.

Project identification	Project denomination	**Barret Hand**	**UB Hand II**
	Reference author(s)	W.T.Townsend	Bonivento/Melchiorri/Vassura
	Research institute	Barret Technology, Inc	Bologna University
	Year of presentation	1988	1992
	Reference	[15, 35]	[18, 19, 2]
Picture			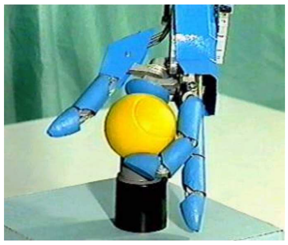
Mechanical structure:	Arm/hand Integration	MH	IH
Kinematical scheme:	Main upper fingers	✓	✓
	Opposable thumb	✓	✓
	Fourth finger	-	-
	Fifth finger	-	-
	Palm	✓	✓
	Number of links	9	14
	Number of joints	8	13
	Number of controlled degrees of freedom	4	13(2 wrist+11 hand)
Morphological features:	Size w. r. to a human hand	=	=
	Surfaces apt to contact with objects	Fingertips/Phalanges/Palm	Fingertips/Phalanges/Palm
	Contact surface smoothness and continuity	Fair	Good
Mechanical details	Structural design concept	Exoskeletal	Endoskeletal
	Actuator location	Inside the fingers	Remote
	Actuation type	Electrical revolute motors (Brushless)	Electrical revolute motors
	Act. joints backdrivability	✓	✓
	Kind of not-actuated joints	Underactuated	-
	Type of transmission	Spur and worm gear	Tendons
	Transmission routing	-	Pulleys/sheaths
Sensors:			
Position	Motor position sensors	Optical encoders	✓
	Joint position sensors	-	Hall-effect based
Force/Torque sensors	Joint torque sensors	Strain-gauges based	-
	Tendon tension sensors	-	-
	Motor effort sensors	Implicit (by means of breakaway clutches)	-
Contact sensors	Intrinsic tactile sensors	-	6-axis IT-sensors in the phalanges and the palm
	Tactile array sensors	-	-
Additional Sensors			

Table 2.6: Main features of DLR I and LMS Hands.

Project identification	Project denomination	**DLR Hand I**	**LMS Hand**
	Reference author(s)	Butterfass/Hirzinger/Knoch/Liu	Gazeau/Zeghloul/Arsicualt
	Research institute	DLR-German Aerospace Center	Université de Poities
	Year of presentation	1997	1998
	Reference	[3, 36]	[37]
Picture			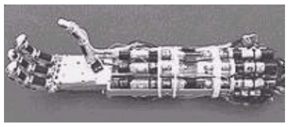
Mechanical structure:	Arm/hand Integration	MH	IH
Kinematical scheme:	Main upper fingers	✓	✓
	Opposable thumb	✓	✓
	Fourth finger	✓	✓
	Fifth finger	-	-
	Palm	✓	✓
	Number of links	17	17
	Number of joints	16	17
	Number of controlled degrees of freedom	12	16
Morphological features:	Size w. r. to a human hand	$\gg$	=
	Surfaces apt to contact with objects	Fingertips/Phalanges/Palm	Fingertips/Phalanges
	Contact surface smoothness and continuity	Good	Good
Mechanical details	Structural design concept	Exoskeletal	Exoskeletal
	Actuator location	Inside the finger	Remote
	Actuation type	Electrical revolute motors	Electrical revolute motors
	Act. joints backdrivability	✓	NF
	Kind of not-actuated joints	Adaptive passive-driven joint	-
	Type of transmission	Tendons	Tendons
	Transmission routing	Pulleys	Pulleys/Sheaths
Sensors:			
Position	Motor position sensors	✓	✓
	Joint position sensors	Optical based	Potentiometers
Force/Torque sensors	Joint torque sensors	✓	-
	Tendon tension sensors	-	Implicit (tendon elongation)
	Motor effort sensors	-	-
Contact sensors	Intrinsic tactile sensors	x-y force sensor on fingertips	-
	Tactile array sensors	Tactile sensors(Force sensing resistor)in each finger link	-
Additional Sensors		Stereo-camera in the palm and light projection diodes in the fingertip to simplify image processing	

Table 2.7: Main features of DIST and Robonaut Hands.

Project identification	Project denomination	**DIST Hand**	**Robonaut Hand**
	Reference author(s)	Cafés/Cannata/Casalino	C.S.Lovhik/M.A.Diftler
	Research institute	DIST-Universitá di Genova	NASA Johnson Space Center
	Year of presentation	1998	1999
	Reference	[38, 39]	[17, 5, 40]
Picture		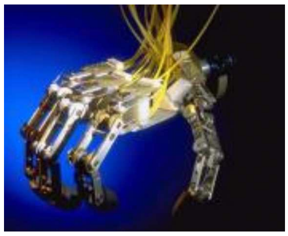	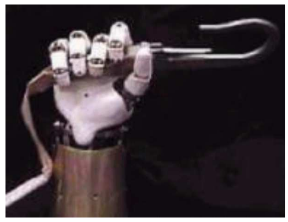
Mechanical structure:	Arm/hand Integration	MH	IH
Kinematical scheme:	Main upper fingers	✓	✓
	Opposable thumb	✓	✓
	Fourth finger	✓	✓
	Fifth finger	✓	✓
	Palm	✓	✓
	Number of links	17	22
	Number of joints	16	22 (2 wrist + 20 hand)
	Number of controlled degrees of freedom	16	14 (2 wrist + 12 hand)
Morphological features:	Size w. r. to a human hand	>	=
	Surfaces apt to contact with objects	Fingertips	Fingertips/Phalanges/Palm
	Contact surface smoothness and continuity	Poor	Very Good
Mechanical details	Structural design concept	Exoskeletal	Endoskeletal
	Actuator location	Remote	Remote
	Actuation type	Electrical revolute motors	Electrical revolute motors (Brushless)
	Act. joints backdrivability	NF	✓
	Kind of not-actuated joints	-	Adaptive Passive-driven joints
	Type of transmission	Tendons	Flex-shaft + lead screw
	Transmission routing	Pulleys/Sheaths	-
Sensors:			
Position	Motor position sensors	✓	✓
	Joint position sensors	Hall-effect based	✓
Force/Torque sensors	Joint torque sensors	-	
	Tendon tension sensors		✓
	Motor effort sensors	-	
Contact sensors	Intrinsic tactile sensors	3-axis fingertip force sensors	-
	Tactile array sensors	-	FSR (Under development)
Additional Sensors			

Table 2.8: Main features of Tokyo and DLR II Hands.

Project identification	Project denomination	**Tokyo Hand**	**DLR Hand II**
	Reference author(s)	Y.K.Lee/I.Simoyama	Butterfass/Grebestein/ Hirzinger/Liu
	Research institute	Univ.of Tokio,bunkyo-ku,J	DLR-German Aeropsace Center
	Year of presentation	1999	2000
	Reference	[41]	[4]
Picture		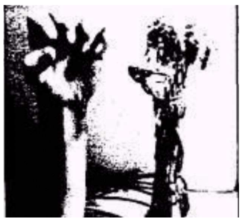	
Mechanical structure:	Arm/hand Integration	IH	MH
Kinematical scheme:	Main upper fingers	✓	✓
	Opposable thumb	✓	✓
	Fourth finger	✓	✓
	Fifth finger	✓	-
	Palm	✓	✓
	Number of links	17	18
	Number of joints	16	17
	Number of controlled degrees of freedom	12(1 wrist + 11 hand)	13
Morphological features:	Size w. r. to a human hand	=	$\gg$
	Surfaces apt to contact with objects	Fingertips/Phalanges/Palm	Fingertips/Phalanges/Palm
	Contact surface smoothness and continuity	Very good	Good
Mechanical details	Structural design concept	Endoskeletal	Endoskeletal
	Actuator location	Remote	Inside the fingers
	Actuation type	Pneumatic Mckibben artificial muscles	Electrical revolute motors
	Act. joints back-drivability	✓	✓
	Kind of not-actuated joints	Rigid passive-driven joints	Rigid passive-driven joints
	Type of transmission	NF	Harmonic drives/gears
	Transmission routing	NF	-
Sensors:			
Position	Motor position sensors	✓	✓
	Joint position sensors	-	Potentiometers
Force/Torque sensors	Joint torque sensors	-	Strain-gauges based
	Tendon tension sensors	-	-
	Motor effort sensors	✓	-
Contact sensors	Intrinsic tactile sensors	-	6-axis force sensors in the fingertips
	Tactile array sensors	Pressure sensors foreseen	-
Additional Sensors			

Table 2.9: Main features of Tuat/Karlsruhe and Ultralight Hands.

Project identification	Project denomination	**Tuat/Karlsruhe Hand**	**Ultralight Hand**
	Reference author(s)	Fukuya/Toyama/Asflur/Dillman	Schultz/Pylatiuk/Bretthaue
	Research institute	Tokyo and Karlsruhe Universities	Research center of Karlsruhe
	Year of presentation	2000	2000
	Reference	[13]	[42]
Picture			
Mechanical structure:	Arm/hand Integration	IH	IH
	Main upper fingers	✓	✓
Kinematical scheme:	Opposable thumb	✓	✓
	Fourth finger	✓	✓
	Fifth finger	✓	✓
	Palm	✓	✓
	Number of links	22	17
	Number of joints	24	18
	Number of controlled degrees of freedom	1	13 (3 wrist+ 10 fingers)
Morphological features:	Size w. r. to a human hand	=	≫
	Surfaces apt to contact with objects	Fingertips/Phalanges	Fingertips/Phalanges/Palm
	Contact surface smoothness and continuity	Poor	Good
Mechanical details	Structural design concept	Endoskletal	Exoskeletal
	Actuator location	Remote	Inside the fingers
	Actuation type	Electrical revolute motors	Pneumatic
	Act. joints backdrivability	NF	✓
	Kind of not-actuated joints	Adaptive passive-driven joints	Rigid passive-driven joints
	Type of transmission	Link mechanisms	Direct drive
	Transmission routing	-	-
Sensors:			
Position	Motor position sensors	✓	✓
	Joint position sensors	-	Bending sensors
Force/Torque sensors	Joint torque sensors	-	-
	Tendon tension sensors	-	-
	Motor effort sensors	Self-adapting mechanism	-
Contact sensors	Intrinsic tactile sensors	-	-
	Tactile array sensors	-	Pressure sensors in finger links
Additional Sensors			

Table 2.10: Main features of GIFU and Shadow Hands.

Project identification	Project denomination	**Gifu Hand**	**Shadow Hand**
	Reference author(s)	Kawasaki/Shimomura/Shimizu	
	Research institute	Gifu University	Shadow Robot Company Ltd
	Year of presentation	2001	2002
	Reference	[6, 43]	[44]
Picture			
Mechanical structure:	Arm/hand Integration	MH	IH
	Main upper fingers	✓	✓
Kinematical scheme:	Opposable thumb	✓	✓
	Fourth finger	✓	✓
	Fifth finger	✓	✓
	Palm	✓	✓
	Number of links	21	24
	Number of joints	20	23
	Number of controlled degrees of freedom	16	23 (4×4 fingers + 5 thumb + 2 wrist)
Morphological features:	Size w. r. to a human hand	=	≥
	Surfaces apt to contact with objects	Fingertips/Phalanges/Palm	Fingertips/Phalanges/Palm
	Contact surface smoothness and continuity	Good	Fair
Mechanical details	Structural design concept	Exoskeletal	Exoskeletal
	Actuator location	Inside the fingers	Remote
	Actuation type	Built-in DC Maxon servomotors	Pneumatic
	Act. joints back-drivability	-	✓
	Kind of not-actuated joints	Rigid passive-driven Joints	-
	Type of transmission	Worm gear	Tendons
	Transmission routing	-	NF
Sensors:			
Position	Motor position sensors	✓	-
	Joint position sensors		Hall-effect based
Force/Torque sensors	Joint torque sensors		
	Tendon tension sensors		
	Motor effort sensors		✓
Contact sensors	Intrinsic tactile sensors	6-axis fingertip force sensors	
	Tactile array sensors	Distributed resistive tactile sensors	
Additional Sensors			

Chapter 3

A robotic gripper for space activities

In this Chapter, a robotic gripper purposely designed for space applications is presented. Although in Ch. 2 a trend towards anthropomorphic hands has been recognized, the design of this device aims to demonstrate the effectiveness of a not-anthropomorphic structure to perform complex operations.

3.1 Space robotics: objectives and requirements

In recent years, in both the research and the industrial environments, there has been a renewed and growing interest for the planned activities in space, deriving from very important achievements such as the construction of the ISS, with all the implications of this realization, the exploration of planets or asteroids, the increasing need for satellites, and so on. These activities will obviously require the presence and the work of astronauts but, on the other hand, will also require a relevant use of automation techniques and autonomous devices. As a matter of fact, as already demonstrated in other fields, there are tasks in which it is not convenient (or even non possible) to employ human operators (the astronauts). In particular, robotic systems can be profitably used to to perform tasks, which are:

- too dangerous (e.g. because of the hostile environment)
- too difficult (e.g. because of the large masses involved, high precision and repeatability required, long duration...)
- too boring, time consuming or expensive (e.g. routine handling of experiment logistics)

If both terrestrial and spatial robots have the same aims, that is to support or replace human beings, the spatial environment has a strong impact in the robot design and requires peculiar features, which make these manipulators very different from industrial or "service" ones [55]. In table 3.1 the major constraints and their consequences on the robot design are summarized.

In the light of these constraints the solutions (concerning the mechanical structure, the sensory equipment and the control modalities) adopted in this research activity can be easily understood.

Constraint	Typical design impact
Function in vacuum	Careful material selection, brushless motors preferred, some sensing principles not applicable (e.g. acoustic)
Function in lack of gravity	Everything has to be fastened; smooth accelerations and low speeds in order to preserve micro-gravity conditions
Function under extreme radiation exposure	Shielded and hardened electronics, outdated computer performance (state-of-art computer not space compatible)
Function under extreme lighting and contrast conditions	Difficult for vision and image processing
Function in extremely remote environment (communications with the Earth very limited and expensive)	Adequate degree of autonomy
On-board mass very limited and expensive	Extremely lightweight design
On-board power/energy very limited and expensive	Very high efficiency, limited computing resources
High reliability and safety	"Inherently safe" design, problems with "non-deterministic" approaches (e.g. AI)

Table 3.1: Typical constraints in space activities and relative consequences in robots design.

3.2 Why a robotic gripper?

Although in Ch. 2 a very strong effort towards the development of dexterous robotic hands has been recognized, the choice of a "simple" gripper seems, at the moment, the most appropriate solution for space activities. As a matter of fact, the proposed end-effector tries to fill a gap between two opposite tendencies:

- the design of 2-jaw grippers, which currently are the state-of-art in the field of space robotics [56, 57];
- the development of the already mentioned dexterous robotic hands, aiming to reproduce the human hand concerning its functional capabilities as well as its structure.

If anthropomorphic robotic hands probably represent the future of space robotics (in the field of end-effectors), the limitations in terms of computational resources, power, material selection and the heavy constraints of safety and reliability (summarized in previous section) which a robotic device must satisfy in order to be qualified for space, make such complex devices not suitable for space applications yet. Conversely, the robotic end-effectors, employed in past space missions (e.g. the ROTEX gripper [56]), have very simple structure (with one or two degrees of freedom) and hence they can only perform "trivial" tasks, such as grasping small and quite regular objects; as a matter of fact, such devices have been often considered just experiments to evaluate the pro and cons of the application of robotic technologies in space.

In this frame, the design of a medium complexity robotic gripper represents an attempt to improve the capability of existing end-effectors, maintaining a structure compatible (in terms of simplicity, reliability...) with the space environment (see Fig. 3.1). In particular, this new device

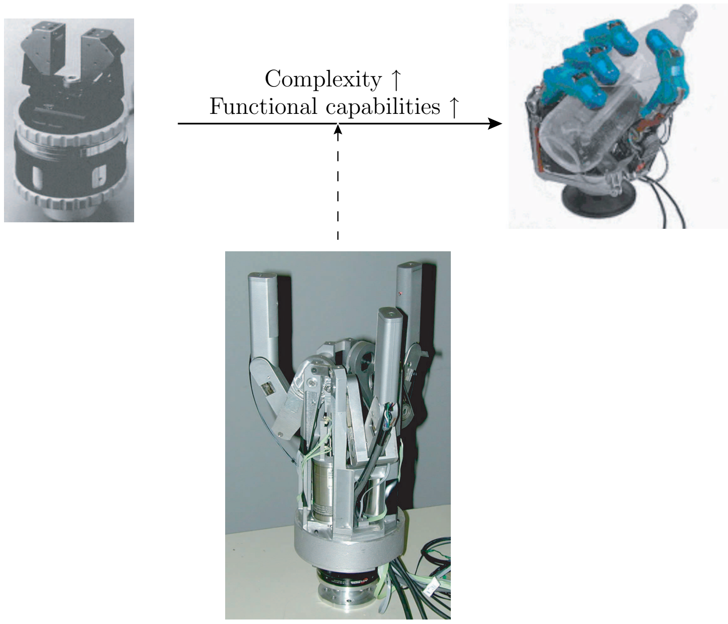

Figure 3.1: The proposed gripper as trade-off between complexity and functional capabilities.

has been purposely designed for EVA (extra-vehicular activities), where also humans, because of the thick gloves they must wear, show very poor dexterity [23]. But also considering activities performed inside spatial vehicles (the so called IVA), which could be accomplished by means of robotic systems, a not-anthropomorphic end-effector appears perfectly adequate. In fact, the required tasks are basically (see Fig. 3.2):

a) inserting a connector;

b) opening a drawer;

c) rotating a knob;

d) pushing a button.

All these "manipulation" activities can be accomplished by the gripper shown in Fig. 3.1, if a proper functional integration with the carrying arm is achieved. As a matter of fact, in this case the task that the gripper must perform is simply grasping some objects, whose shape is variable and possibly not regular.

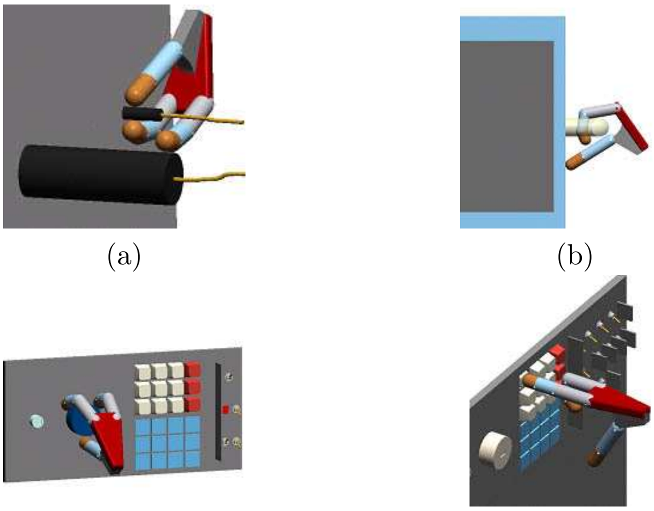

(a) (b) (c) (d)

Figure 3.2: Typical tasks performed in IVA.

3.3 A meditated minimalism as design criterium

The development of a robotic gripper, rather than a dexterous robotic hand with many degrees of freedom, results from the considerations of the previous section, and from the good old engineering principle of *minimalism*, which prescribes the choice of the simples mechanical structure, the minimum number of actuators, the simple set of sensors, that will do the desired job.
Nevertheless, the gripper is not so simple as one can think looking at Fig. 3.1. This will be immediately clear by considering both its mechanical structure and its sensory equipment.

3.3.1 Mechanical Architecture

The mechanical structure (whose design is due to the research group leaded by Prof. Vassura of DIEM [58, 59]) is the result of two basic specifications:

- the possibility of simultaneous application of the contacts;
- a limited complexity of the kinematic architecture, with not more than three controlled degrees of freedom.

The gripper shows a modular structure, characterized by three articulated fingers disposed along three intersecting lines equally spaced of 120^o. Each articulated finger has a distal phalanx, that gets in touch with the object, and two intermediate phalanxes, coupled by means of internal transmissions so that pure translation of the distal link is generated. In addition to the advantage of using only revolute pairs, this kinematic structure presents a high ratio between maximum and minimum extension, obtaining a very large workspace with respect to the size of the gripper body: the positions of the contacts can range from a diameter of 3 mm up to 195 mm, being 120 mm the external diameter of the gripper.

The actuation of each finger is provided by a linear actuator, as shown in Fig. 3.3. This linear actuator is manufactured by Wittenstein Gmbh, Germany, and is composed of a high-speed brushless motor integrated with a high-ratio, high efficiency roller-screw mechanism, that allows direct generation of linear motions.

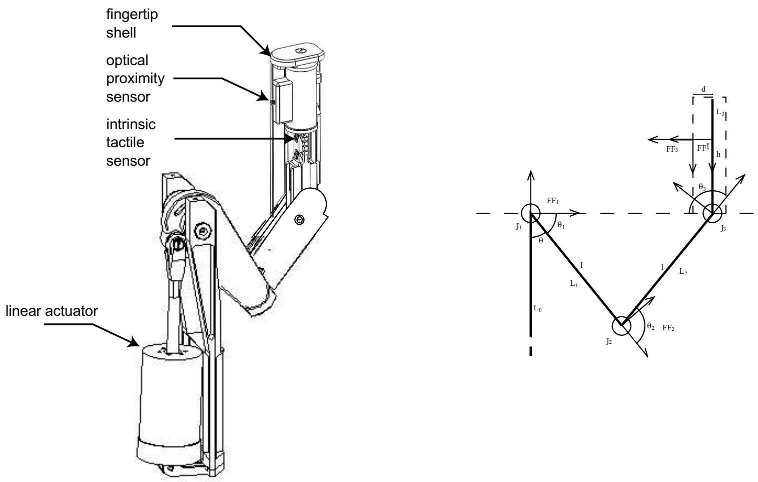

(a) (b)

Figure 3.3: Sensory equipment (a) and kinematic structure (b) of a finger of the gripper.

Since the fingers move independently, the grasping configuration may be any triangle with vertices on the approach trajectory segments. This feature allows to grasp irregular objects, even if they are not positioned in a central configuration with respect to the workspace of the gripper itself.

3.3.2 Sensory equipment

The sensory system of the gripper has been designed taking into account both the motion of the fingers and the approach and interaction phases with the grasped object. In particular, as shown in Fig. 3.3.a, each finger is equipped with:

- a Hall effect position sensor;
- a proximity sensor;
- a miniaturized (6-axis) force/torque sensor.

The proximity sensor (based on a simple light emitter-receiver) measures the distance of each finger from the object surface and allows to plan the approach motion in order to get synchronous contacts. Moreover in can be used to explore an unknown environment if other exteroceptive sensors (i.e. a camera) are not available or to improve the estimation that other sensors can provide. For example, in Fig. 3.4 a reconstruction of the shape of an object and the normal directions to the surface as computed numerically are shown. The force-torque sensor (which

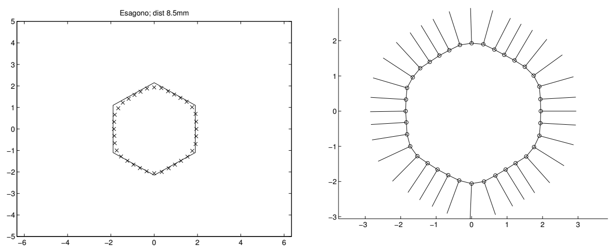

Figure 3.4: Reconstruction of an object by exploration with the proximity sensors and computation of the normal directions.

can detect the interaction forces, by measuring the deformation on the fingertip structure by means of the classical strain gauge technology) can be used for the control of grasping forces once contacts have been applied. Note that, being capable of detecting not only the intensity of contact force components but also the position of the contact centroid on the external surface of the finger, the intrinsic tactile sensor can efficiently recognize actual contact conditions, including incipient sliding [60].

3.3.3 Control of the gripper

The real time control of the gripper is based on standard HW/SW components. The control is performed with a DSP (TMS320C32) board connected to the motor drives and to an input board for the sensors. This board has been purposely designed because of the relatively high number of signals (30) to be acquired in real-time. The DSP is hosted on a PC, which provides an high-level user interface, under Linux OS, developed in order to monitor the real time control process running on the DSP board and allow the communication with the other components of the whole system (e.g.the carrying arm).
In order to cope with the main problems of the space environment (e.g. the lack of gravity) and exploit the structural features of the gripper a logic-based switching control has been designed. As a matter of fact, the different tasks are performed by the gripper according to a sequence of the following main controllers:

- position control;
- proximity control;
- stiffness control.

The position control of each finger is based on a classical PI regulator, as depicted in Fig. 3.5. At this level, a difficulty has been the compensation of nonlinearities caused by the actuation system, in particular a relevant (and non constant) dead zone and the nonlinear characteristic of the Hall effect position sensors [61].
The same structure has been exploited to accomplish the proximity control of the finger (by simply switching the feedback signal from the position sensor to the proximity one), and, in order to guarantee a smooth behavior of the finger, a proper trajectory generation has been

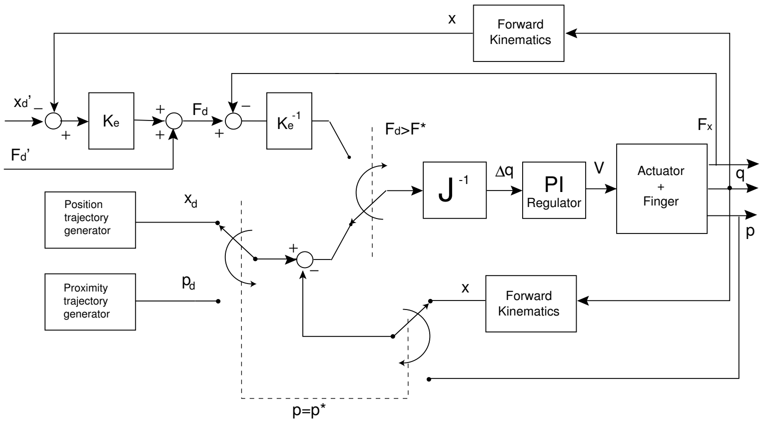

Figure 3.5: Complete control scheme of the gripper.

implemented. In this modality, it is possible to approach the fingertip to the object surface up to the desired distance and keep that constant, thus avoiding undesired interactions. An example of this procedure is reported in Fig. 3.6 where the signals from both the position and proximity sensors are shown. The finger is moved towards a moving object, plot (a), until a desired distance (10 mm) is reached and maintained, plot (b), also with the object in motion.

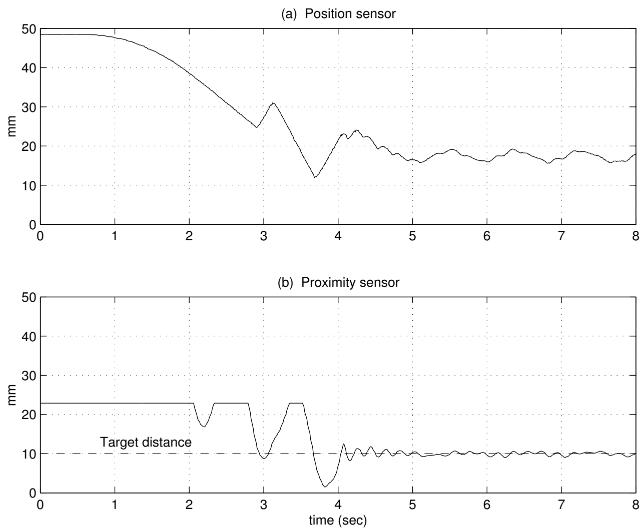

Figure 3.6: Measurements of the position (a) and proximity (b) sensor. The task is to approach a moving object and then to maintain a desired distance (10 mm) from it. The output signal of the proximity sensor is saturated at 23 mm.

When an interaction with the environment (usually an object to be grasped) is desired, the force exerted by the fingers can be regulated by means of a stiffness control [62], which in steady state assures an applied force proportional to the displacement from the desired position (x_d):

$$F = K_e(x - x_d)$$

In this way each finger behaves like a programmable spring, whose stiffness K_e can be modified according to the desired task.

Therefore, the control of the gripper can be subdivided in an hierarchical structure, in which two main levels can be considered:

- **Servo control level**, in which the basic position/proximity/force controllers for each finger are implemented;
- **Supervision level**, which coordinates the three fingers by scheduling the activation of the proper control in order to perform some basic tasks (e.g. approach to an object in the work space of the gripper or grasp with a certain force);

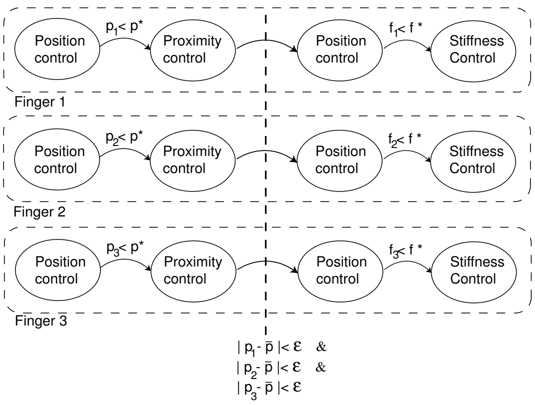

Figure 3.7: Control logic for a grasp task .

In Fig. 3.7 it is shown how a sequence of primitive controllers has been arranged in order to get a safe execution of a grasp task, that is the most critical operation the gripper must perform. First, the fingers approach the object within the gripper workspace by means of the position control, then when a distance p^* has been detected, the proximity control is activated in order to reach and maintain the desired distance $\overline{p}$ from the object surface. Once all the fingers are at distance $\overline{p}$ (sufficiently small) they are synchronously closed on the object (see Fig. 3.8). In this way it is possible to avoid undesired contacts with the object, which can cause its loss due to the lack of gravity, and assure a synchronous grasp of irregular or moving object. Finally when the forces applied by fingers become appreciable the stiffness control drives the motors to get the desired force values. In Fig. 3.9 the position and normal force for a finger, during the execution of a grasp, are shown. The object is approached under position control (phase 1), then the proximity control is switched on (2) and finally, once contact has been established, the applied force is controlled (3, 4). In this case, the reference force is changed during manipulation (from $f_d = 12\ N$ to $f_d = 15\ N$) to show the effectiveness of the force control. At the end, the object is released and the force is null (phase 5).

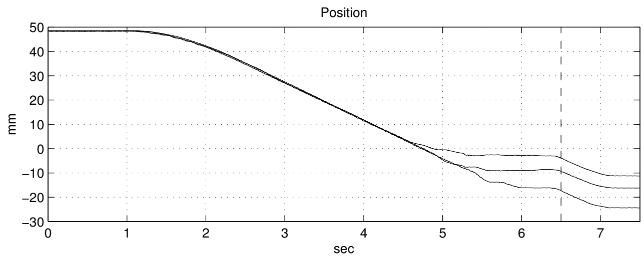

Figure 3.8: Grasp of a floating object: the fingers are moved until a given distance from the object surface is reached, then the contacts are applied synchronously.

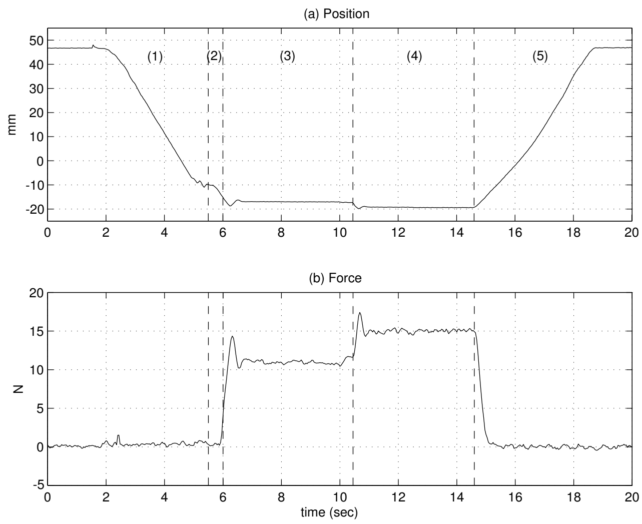

Figure 3.9: Motion of the finger (a) during an approach and a grasp and force applied on the object (b).

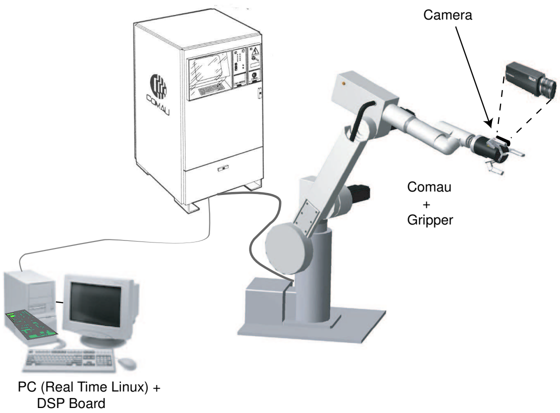

Figure 3.10: The overall system.

3.4 The overall system

As stated in Sec. 3.2, in order to accomplish complex manipulation tasks, a key role is played by the functional integration between the end-effector and the robotic arm. Therefore to validate the gripper, it has been mounted as end-effector on a Comau SMART 3-S robot arm. This is an industrial 6 degrees of freedom robot anthropomorphic manipulator with a non-spherical wrist. The robot is equipped with the standard controller C3G-9000, which drives the manipulator according to the user commands. In this setup this controller is *open*, that is it has been connected, by means of an high-speed bus, to a PC which can perform the real time control, using the controller as a simple interface towards the robot (in order to acquire the data from the encoders and drive the motors). Moreover a camera, whose images are acquired by means of a frame grabber, has been installed on the wrist of the robot arm.
The complete robotic setup is shown in Fig. 3.10.

3.4.1 Control architecture

The control of the overall arm/gripper system is based on 3 main elements: 2 standard PCs and a general purpose DSP (TMS320C32) board, as shown in Fig. 3.11. As stated in Sec. 3.3.3, this last board, devoted to the control of the robotic gripper, is hosted on a PC, which provides an high-level user interface and allows the communication with the other components of the robotic setup. In particular this PC, equipped with a real-time version of Linux Os (RTAI-Linux [63]), is the heart of the whole system. As a matter of fact, the kernel real-time running on it performs the position control of the robot arm, while a user space application (and therefore not real time) carries out the supervision of the system based on the information coming from the gripper control, the arm control, the vision system and according to the desired tasks [64]. Finally, the aim of the second PC is to process the images and to extract the features (e.g. position of the target object) necessary to drive the manipulator. Note that the functions performed by this PC can be easily hosted also on the first personal computer.

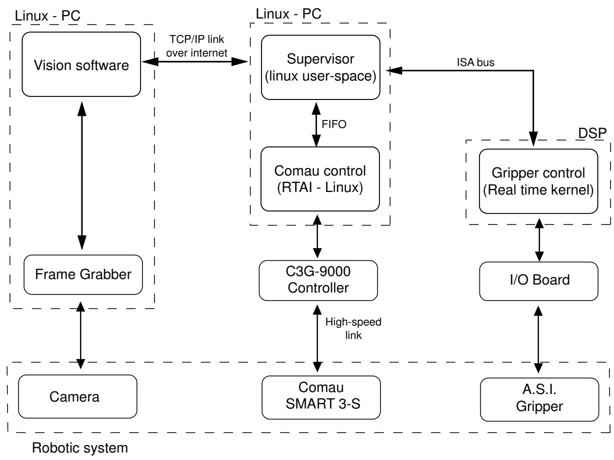

Figure 3.11: Control architecture.

3.4.2 Control of the arm and supervision

The Comau robot arm must drive the gripper in the right position in order to grasp the object. For this purpose it is used under a cartesian position control which allows to move the end-effector according to the user commands.
In this specific application an automatic grasp procedure has been implemented based on the feedback of the camera. As a matter of fact, the simple structure of the gripper and of its control system makes this device particularly suitable to perform autonomous operations, that is without any human intervention. This can very useful in space activities, where costs and difficulties (due to the distances) of communications are very crucial.
A supervision system uses the information extracted from the images to compute the distance from the target and plan the proper approach phase. Obviously, because stereo-camera is not employed, 2 images from 2 different points of view (whose relative positions are known) are necessary. Moreover the camera is used to implement a classical algorithm, based on visual feedback, of the kind *look-and-move* [65]: from the images the position set-points for the manipulator are constructed in order to bring the gravity center of the target object into the center of the image.

3.4.3 Choice of the grasp configuration

In order to deal with objects with variable and unknown shapes, a grasp synthesis algorithm has been implemented. The main theoretical foundation of this procedure is the concept of *immobility*, that is the lack of any freedom for finite movements of the immobilized object. In fact, considering a possible use of the robotic gripper in a space environment, the classical optimization processes of grasp points choice, appear not completely effective or not suitable. Aim of these algorithms is to collocate the contact points on the surface of target objects in order to maximize the external wrenches, which can be resisted by the fingertips' forces [66, 67]. But it is worth to notice that, due the lack of gravity, the magnitude of external forces in the space

environment are usually quite small. Instead the most critical problem in this context is the *stability* [68] of the grasp; as a matter of fact a small unbalanced force or a positioning error can produce the loss of the object. Therefore in this case it is necessary to find a configuration as insensitive as possible to this kind of disturbances. Moreover, also the constraints imposed by the mechanical structure of the gripper must be considered. In fact the fingers have a single degree of freedom and can behave as simple linear springs moving along the radial direction.
The implemented procedure considers 2D grasps, therefore it is suitable for relatively flat objects, or that can be treated as an extrusion of their projected silhouettes. This hypothesis is not too limiting but appears consistent with the mechanical structure of the gripper, which (considering its three parallel fingers) results particularly suitable to deal with this kind of objects.

The grasp synthesis algorithm is based on several steps aiming to identify the best triplet of contact points, [69].

Step 1: Parameterization of object contour
The presented algorithm relies on a image processing procedure and does not require any model of the object. Based on images obtained by the camera, the object shape is extracted (according to standard algorithms) and parameterized by means of circular arcs. Of each arc, the curvature (obviously infinite if straight lines are considered) and the normal vector (in the medium point) are computed.

Step 2: Equilibrium test
This stage aims at selecting all the triplets of arcs, which might be possible candidates for the grasp. In order to hold the object, a necessary condition is the equilibrium of the wrenches w_i exerted by fingers, that is:

$$\lambda_1 w_1 + \lambda_2 w_2 + \lambda_3 w_3 = 0, \quad \text{with } \lambda_i > 0$$

Besides their magnitude, the wrenches depend on geometry of the contact, therefore it is possible to find if the previous equation may admit a solution just considering the shape of the object.
Moreover, in this phase also the specific geometry of the gripper has been taken into account: in fact in order to reduce the number of possible solutions, configurations too far from the ideal case (contact forces oriented as the action line of the fingers and focus of the forces coincident with the center of the gripper) are discarded.

Step 3: Immobility
It is well-known that, in general, it is possible to achieve frictionless force-closure of almost all 2D objects by means of 4 contact points. However the effects of the curvature may allow to immobilize an object with less than 4 fingers. In order to find a grasp, that could guarantee the immobilization of the object, the so called 2^{nd} order mobility index $m^2_{q_0}$ [70, 71] is computed, for each possible (i.e. after Step 2) configuration. This index considers the admissible motions of the object (constrained by the fingers) in its configuration space taking into account the relative curvature between object and fingers. It has a simple interpretation: if $m^2_{q_0} > 0$ there exist accelerations such that the object can break away from the 3 fingers.

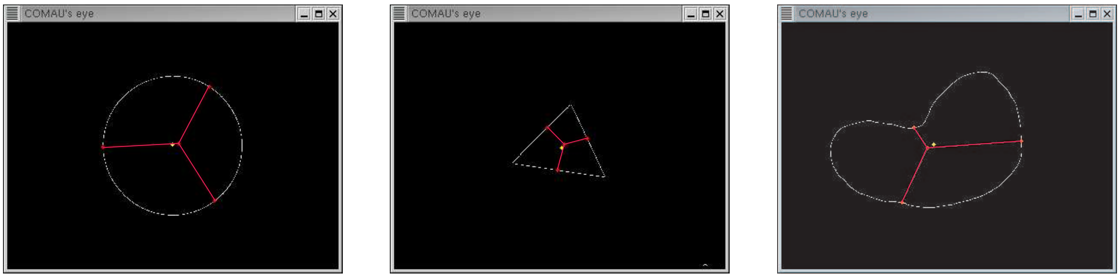

(a) (b) (c)

Figure 3.12: Grasp points selection considering a circle (a), a triangle (b), a "potato" (c).

Step 4: Optimal grasp

Among the configurations with the lower 2^{nd} order mobility index (possibly 0, that is the object is immobilized), a further optimization process is performed in order to choose the "best" grasp. This last step considers the reaction forces (exerted by fingers) to an angular displacement α imposed around the focus of the contact normals, and tries to maximize these quantities.
Also in this choice the curvatures of the object and the fingers play a central role. In fact the momentum of the finger reaction force is

$$m_i = \frac{1}{2} k_i^2 \alpha^3$$

where

$$k_i = \frac{(\rho_i - r_{\mathcal{O}_i})(\rho_i + r_{\mathcal{F}_i})}{r_{\mathcal{F}_i} + r_{\mathcal{O}_i}}$$

and ρ_i , $r_{\mathcal{O}_i}$ and $r_{\mathcal{F}_i}$ are respectively the distance of the contact point from the rotational axis, the radii of curvature of the object and of the finger in the considered point. The purpose of this procedure is therefore to obtain the maximum value of

$$\sum_{i=1}^{3} k_i^2$$

.

Finally, the criteria used to find a suitable grasp configuration lead to the intuitive results, shown in Fig. 3.12 where a circle, a triangle and an irregular object are considered.

3.4.4 Experimental activity

In order to test the effectiveness of the robot arm/gripper system together with the control strategies and the grasp planner introduced in previous Sections, a completely autonomous procedure has been developed. The desired task is to grasp an unknown object placed within the manipulator workspace and selected by the user, see Fig. 3.13.

The procedure is composed by 6 main steps:

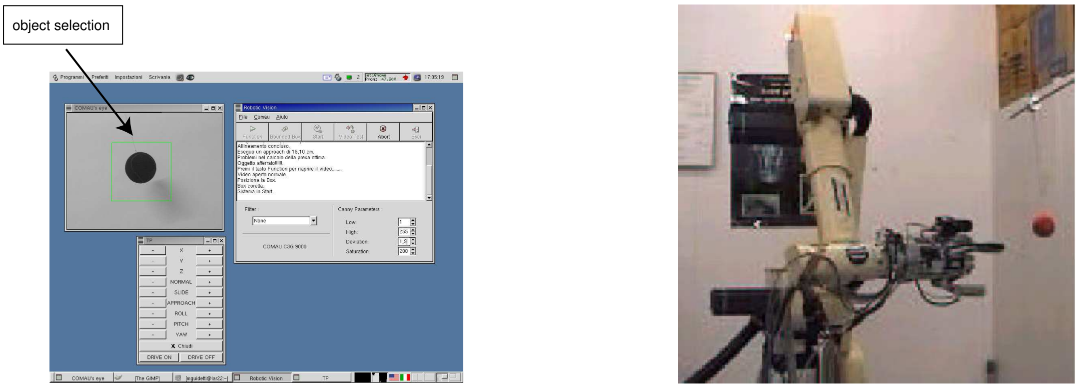

(a) (b)

Figure 3.13: Screen-shot of the object selection (a), and robotic system in action (b).

(1) The user moves the robot end-effector by means of the keyboard, the mouse or a joystick until the vision system points to the object to be grasped. Because we are currently using a single camera and considering a two dimensional model of the object, with this operation the user implicitly chooses the approach direction to the target.

(2) At this step the vision system moves the robot arm in order to align the center of the camera with the object. The vision algorithm can also deal with moving objects.

(3) Since the current vision system is not stereo, the distance from the target can not be estimated from a single image. Therefore the robot is moving along the camera-object direction in order to take two picture of the object and then compute the distance by means of simple geometric considerations.

(4) Using previous estimation, the robot is moved in order to reach a given distance from the object.

(5) The grasp planner selects the contact points on the object according to the criteria mentioned in Sec. 3.4.3 and computes the proper position trajectory for the end-effector in order to reach this configuration.

(6) Finally, the robot is moved according the planned trajectory and the grasp performed by the gripper, as shown in Section 3.3.3.

3.5 Conclusions

In this chapter the development and the validation of a robotic gripper for space activities have been reported. Its kinematic configuration with three independent one-dof fingers allows to deal with irregular and quite variable in size objects. On the other hand, its simple structure and its high-level sensing apparatus (which includes proximity and force/torque sensors) make this robotic device particularly suitable to perform grasp and manipulation operations in an autonomous way. In fact, the simplicity of the mechanical configuration allows to adopt simple but very reliable control strategies (by means of position, proximity and force sensors). In particular, it may be easily implemented an on-line planner to automatically choose the grasp points, and also the coordination with the robot arm results immediate. The gripper must be leaded in a position, with the target objects within its work-space, and then it can perform the grasp based on its own sensors (e.g. proximity sensors, force sensors).

Chapter 4

A novel sensor for mechanical stress measurement

This Chapter describes a research activity on a new sensing element for mechanical "strain" aiming to validate its use in the robotic field. In particular, this new transducer (directly built on a deformable substrate) could replace traditional strain-gauge technology in force/torque sensors manufacturing, encouraging a deeper integration between mechanical and electronic part. The final result will be a general simplification and a considerable reduction of the dimensions of force sensors, which could be easily integrated in those structures where the available room is very narrow, such as the fingers of a robotic hand.

As mentioned in previous Chapters, force and/or tactile sensing is one of the most basic requirements for any manipulator interacting physically with the environment in a non-conventional or non-structured manner. Also in the case of the "simple" gripper, shown in Ch. 3, the use of Intrinsic Tactile (IT) sensors installed in each fingertip, greatly contributes to its overall dexterity. As a matter of fact if the shape and the size of an object are unknown, a position control is absolutely inadequate to grasp it and it can produce unacceptable contact forces, which can damage the object and the gripper itself. Conversely, by means of direct measurements of the forces applied on the contacted objects, it is possible to control the interaction and apply control strategies in order to accomplish complex tasks in autonomous or semi-autonomous way. Other sensory equipments can provide only generic information on the interaction between the manipulator and the environment. For example vision systems, that cannot give precise and local information on the contact state, are often used in the planning phase, and not exploited for regulation purposes. For these reasons, the design of tactile/force sensors (installed directly on the fingertips) and the development of techniques to exploit their information are considered relevant research areas for the robotic community.

4.1 An introduction to force sensing

As briefly summarized in Sec. 2.3 the technologies current available to get information about the contact with the external environment are basically:

- force/torque sensors;
- intrinsic tactile sensors;
- tactile array sensors.

The last sensors are still characterized by severe problems in terms of reliability and functional capabilities because of the large number of electrical connections they require, the nonlinear phenomena (such as hysteresis) which affected their measurements. Moreover the data they provides can be hardly used in real time tasks, because of the very large number of the sensing elements and the related signals. Therefore, force and IT sensors are usually preferred. This kind of sensors are commonly based on the well settled technology of strain gauges (i.e. electrical resistances whose value change because of a mechanical stress) [72]:

- forces/torques are measured by means of the induced mechanical strains on flexible parts of their mechanical structure;
- the mechanical strains are transduced into electrical signals by strain gauges, properly glued on the structure, that change their resistance according to local deformations, see a schematic drawing in Fig. 4.1.a.

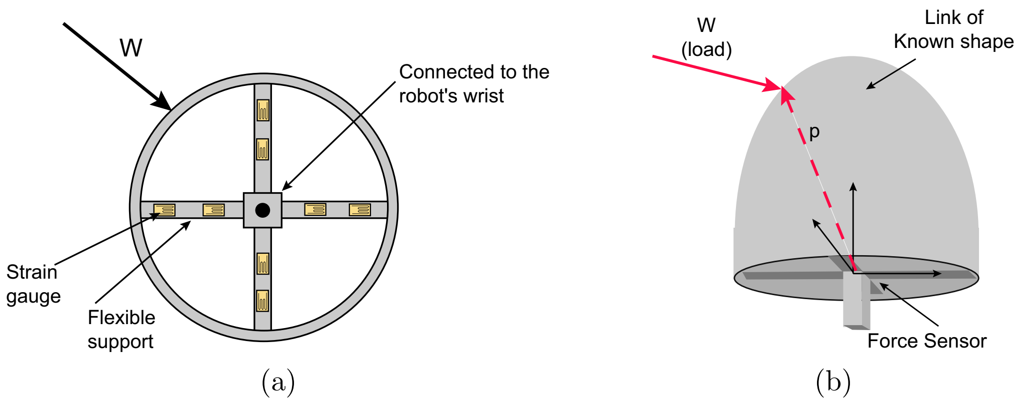

Figure 4.1: Conceptual scheme of a force/torque sensor (a) and a sensor connected to a link of known shape (b).

In order to derive the actual values of the applied forces/torques, a linear mapping between the readings of the strain gauges, collected in a vector $\mathbf{s} \in \mathbb{R}^n$, and the applied wrench $\mathbf{w} = [\mathbf{f}^T, \mathbf{m}^T]^T \in \mathbb{R}^6$ is commonly assumed. This linear mapping is expressed by a matrix, called the *calibration matrix* $\mathbf{C} \in \mathbb{R}^{6\times n}$:

$$\mathbf{w} = \mathbf{C}\,\mathbf{s} \tag{4.1}$$

Based on force/torque sensors, Intrinsic Tactile sensors are able to provide not only the estimation of the wrench vector **w** applied during the interaction with the object/environment, but also the position of the *contact centroid*. Obviously some hypotheses are needed. In particular the knowledge of the shape of the external shell, rigidly connected to the force sensor (and which physically is involved in the interaction), and the a unique contact point are required. The basic idea of the IT principle is illustrated in Fig. 4.1.b. Despite the limitations which characterize this kind of sensor, in particular as regard the impossibility of detecting when multiple contacts occur (and also the size and shape of the contact area), IT sensors are widespread in the field of dexterous robotic manipulation (as shown in Ch.2). The key of such a success is the relatively low complexity (if compared with force array sensors) of this type of sensor, which can be integrated also in very small structures, such as the phalanges of a robotic hand. Nevertheless some problems (mainly technological) remain: as a matter of fact, as shown by eq. (4.1) the amount of required strain gauges is clearly proportional to the number of wrench components which one want obtain and if the magnitude of all the six components of wrench are desired must be $n \geq 6$, that is at least six different information from the strain gauges are necessary. In the practice, a higher number is commonly used to reduce the effects on force estimation of electrical noise and other possible measurement errors. For example, in the gripper for space applications shown in Ch. 3 intrinsic tactile sensors have been obtained by means of eight independent strain gauges installed on the structure of each fingertip. In this case the strain gauges have been arranged in a serial configuration (with a constant current) and an extra sensor is used to compensate for the resistance drift due to the temperature variations. In more general situations the strain gauges are disposed in half- or full- bridge configurations, thus their number considerably grows. Furthermore, in order to reduce the effects of electro-magnetic disturbances, the electronics for signal conditioning (in particular for the amplification) must be placed as near as possible to strain gauges'outputs. Therefore (IT) force sensors are highly integrated systems (see, for example, Fig. 4.2) with very small dimensions, and with typical problems of reliability and high costs.

To this drawbacks it is necessary to add the basic problems deriving from the use of strain gauge technology:

- in some application (e.g. miniaturized force/torque sensors for robotic finger) the area of the strain gauges is not negligible with respect the dimensions of the other involved elements and therefore they impose strong constraints on the design of the overall sensor;
- the operations needed to glue the strain gauges to the deformable structure are time consuming and quite tricky. In order to make the manufacturing process easier, the design of the force sensor is further constrained. Moreover the final result can be not-satisfactory, e.g. because of a not perfect placement of the strain gauges;
- the layer of glue may reduce the sensitivity of strain gauges to mechanical deformations and produce nonlinear phenomena, e.g. hysteresis.

The development of an innovative transducer, aiming to replace strain gauges in force/torque sensors and thus overcoming the related drawbacks, is presented in the following. This sensing

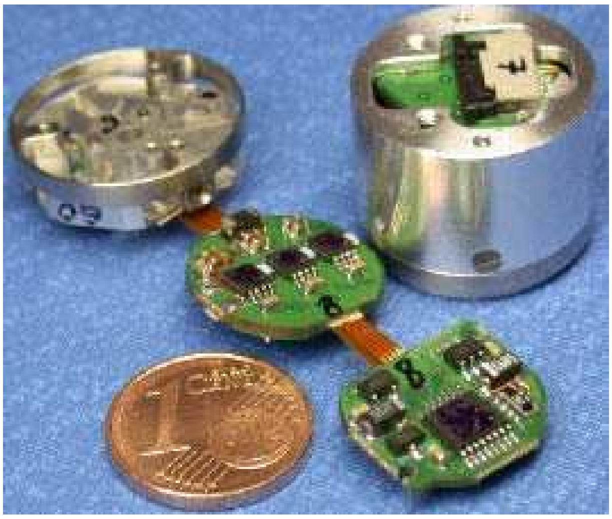

Figure 4.2: Miniaturized 6-dof (fingertip) force/torque sensor with full digital output realized at DLR [73].

element, capable to detect mechanical “strain”, was originally designed considering its integration in microelectronic circuits in order to measure the stress induced by plastic packaging [74]. Tacking into account, on the one hand, its features and, on the other hand, the needs of dexterous manipulation an activity to validate the employment of this transducer in the robotic field has been performed.
This new device, based on amorphous silicon technology, is particularly promising to obtain a great simplification of the present force sensors. As a matter of fact, it can be easily constructed by directly depositing the electronics of the sensor on the flexible part subject to mechanical deformations. This allows the realization of a very small and high-sensitive sensors.

4.2 Structure and physical principle of the sensor

As mentioned in previous section, the sensor is based on silicon technology. In fact, silicon is an excellent piezoresistive material, with good mechanical properties and hence it is particularly suitable to convert mechanical deformations into electrical signals. Therefore, silicon is widely used in sensors for mechanical stresses, such as pressures, forces and flows. In this context, while mono-crystalline silicon is well known and commonly used, the behavior of the amorphous silicon has not been deeply investigated yet.
The basic structure of the sensor consists of a thin layer acting as sensitive area, with size $300 \times 300 \mu m$, grown on a bed of a-silicon, previously deposed on the mechanical substrate. Four metallic contacts, that can be of different geometries and sizes, provide the connections with the other electronic components: two of these metallic contacts are used to apply a voltage or a current to the sensing element, while the other two, orthogonal to the previous ones (Fig. 4.3), provide as output a voltage proportional to the mechanical stress.

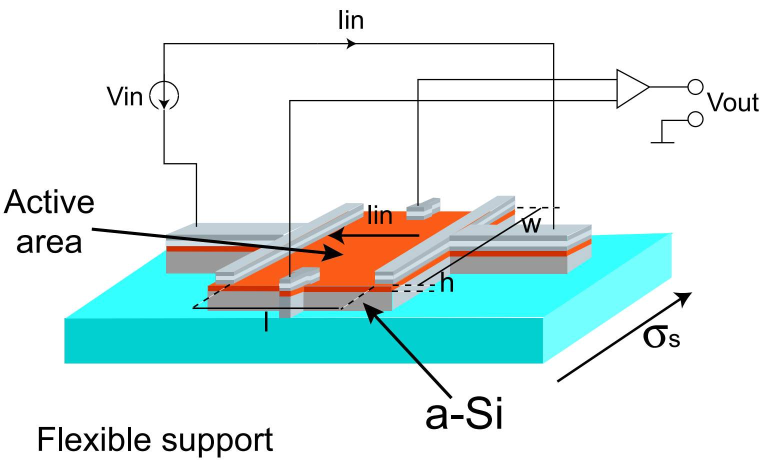

Figure 4.3: Structure of the sensing element and shear stress σ_s.

The active area, which is formed by a compound of amorphous silicon, behaves in such a way as, when mechanical stress is applied, an anisotropic modification of resistivity occurs [75]. As a matter of fact, theoretical considerations and experimental tests (reported in the following) suggest that in this device the electric field $E_\perp$ perpendicular to the current density $|\vec{J}|$ can be written as:

$$E_\perp = \rho\ \gamma_s\ \sigma_s|\vec{J}| \tag{4.2}$$

where ρ refers to the resistivity of the active layer, γ_s and σ_s to the shear piezo coefficient and to the shear stress respectively, see Fig. 4.3. By simply integrating (4.2), the dependance of output voltage V_{out} on the input V_{in} can be written as:

$$V_{out} = V_{in} \cdot \frac{w}{l \cdot h} \cdot \int_h \gamma_s(z) \cdot \sigma_s(z) dz$$

or with reference to the input current I_{in}:

$$V_{out} = I_{in} \cdot \rho \cdot \frac{1}{h^2} \cdot \int_h \gamma_s(z) \cdot \sigma_s(z) dz$$

where l e w respectively are the length and the width of the active area and the integral has been done over the whole depth h of the layer itself (see Fig. 4.3). By applying, for example, a fixed current to the sensor, when a mechanical stress occurs, because of the variation of σ_s, the value of $E_\perp$ changes according to 4.2 and V_{out} can be measured with standard electronics.

Amorphous silicon has been deposited by PECVD (Plasma Enhanced Chemical Vapor Deposition) in high vacuum deposition system, at temperature ranging from 200 to 250 ^oC. A multi-layered thin film metalization $(15 + 100 + 15\ nm)$ of chromium-aluminum-chromium has been used to reduce aluminum penetration into amorphous silicon layer. The active layer is a

"side effect" of the metalization process and therefore does not require further steps.
Since the PECVD does not need special substrates (like for instance the epitaxy which needs a crystalline substrate) and since the deposition process can be made at relatively low temperatures ($200 \div 250\ ^oC$), several materials can be used as mechanical substrate, such as for example plastics. Thus, this possibility makes the sensor suitable for special requirements and, in particular, low cost applications. In fact, the sensing elements can be directly integrated on the material that must be monitored. Moreover, the sensing element is intrinsically insulated from the electrical point of view because of the underlying a-silicon layer and can be directly deposed on metallic substrates. This makes the range of possible applications of the proposed sensor very wide.

4.3 Basic Properties

A prototype of the sensor described in the previous section has been constructed by depositing amorphous silicon on a mechanical support consisting of a glass beam, with dimensions $100 \times 50 \times 1.2\ mm$. Note that neither the material (standard glass) nor the dimensions of the beam are of particular relevance for the sensor properties. Several sensing elements have been deposited on this support, with different orientations, in order to test the measuring capabilities of the transducer when mounted in different configurations, see Fig. 4.4.

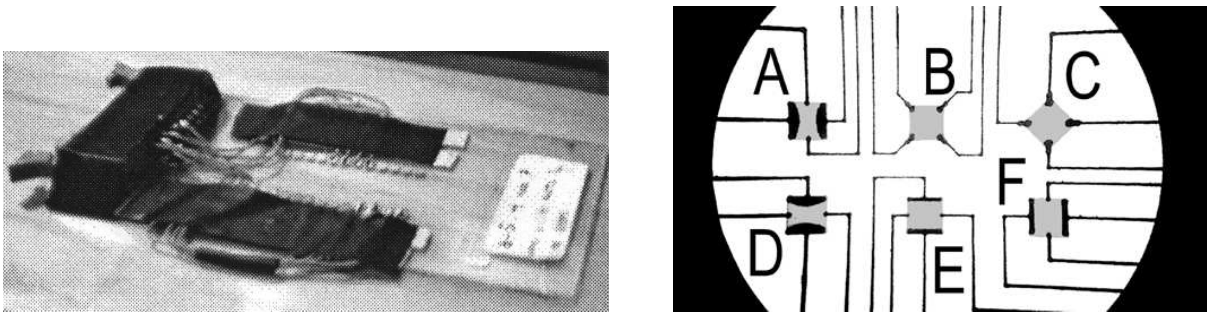

(a) (b)

Figure 4.4: Prototype of the sensor (a) and Micrograph showing the different designs and placements of the sensing elements(b).

In fact, considering the principle on which the sensor is based, it is clear that the reciprocal orientation between the current $\vec{J}$ and the applied stress σ_x affects the measure [74], see Fig. 4.5.

In particular, for the first sensor in Fig. 4.5 the applied strain is parallel to the current direction and therefore the output voltage is zero. Instead, the second sensor is capable to detect σ_s, the component of σ_x that is orthogonal to the current, while the third sensor is the most sensitive to the mechanical stress σ_x.

From an electrical point of view, each sensing element can be considered as a simple resistance if the relationship between the input voltage V_{in} and input current I_{in} is considered, see Fig. 4.3.

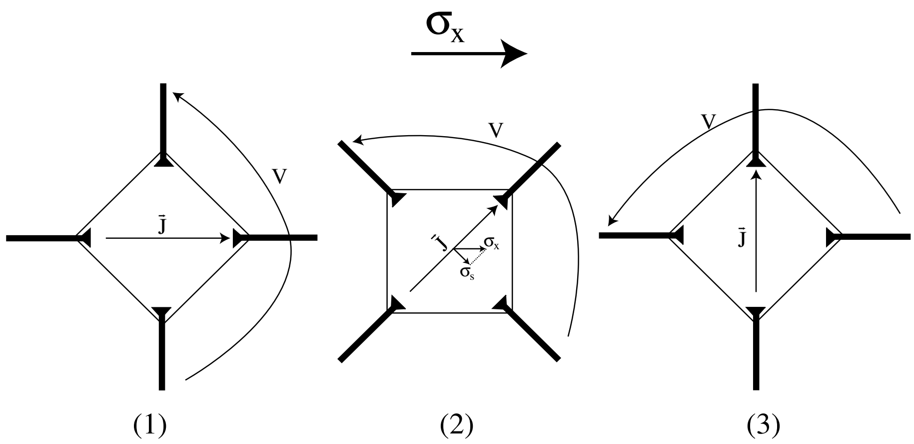

Figure 4.5: The angle between current and mechanical stress affects the measurement.

In Fig. 4.6 the input voltages V_{in} corresponding to several input currents I_{in} are shown. The resistance value of the sensing element is in this case $R_{in} = 7.5\ k\Omega$.

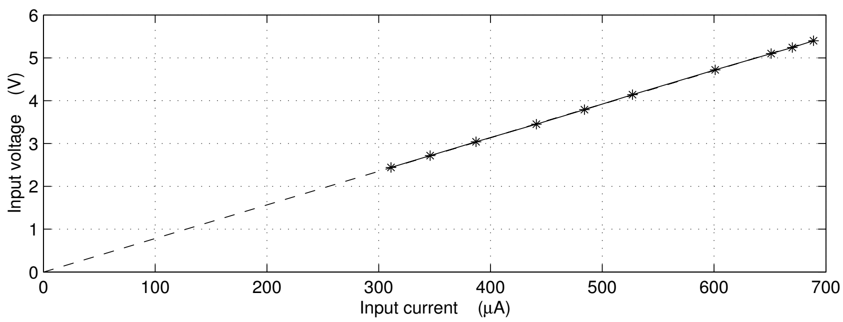

Figure 4.6: The sensor, considering the input voltage and current, can be considered as a resistance.

Note that, for the tests described in the following, a fixed bias current has been applied to the sensing elements. A fixed current, rather than a fixed bias voltage, has been chosen in order to try a first compensation of several undesired effects, such as temperature drift and photo-sensitivity variations. In particular, in order to avoid problems of auto-heating that could damage the sensor, a current of 1 mA has been applied, with a input voltage of about 7.5 V. In this manner, the power flowing to the sensing element is very low, about 7.5 mW.

Several tests have been performed on this prototype concerning the gauge factor and the linearity, which are the preeminent properties of a sensor for mechanical stress. Moreover some additional features of the sensor have been tested, such as the variation of the output with the temperature and the influence of EM fields.

4.3.1 Linearity

A first, basic, feature of the sensor is the linearity of its output signal as regard to the mechanical deformation. In order to test this property, the beam has been subjected to a bending momentum, by fixing a side with a clamp and by applying a vertical force at the other end, as shown in Fig. 4.7. In Fig. 4.8 typical responses are reported.

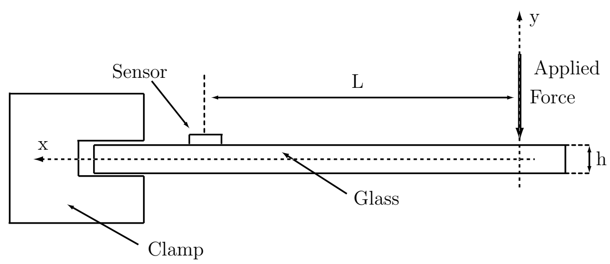

Figure 4.7: Scheme of the experimental setup (L=7cm).

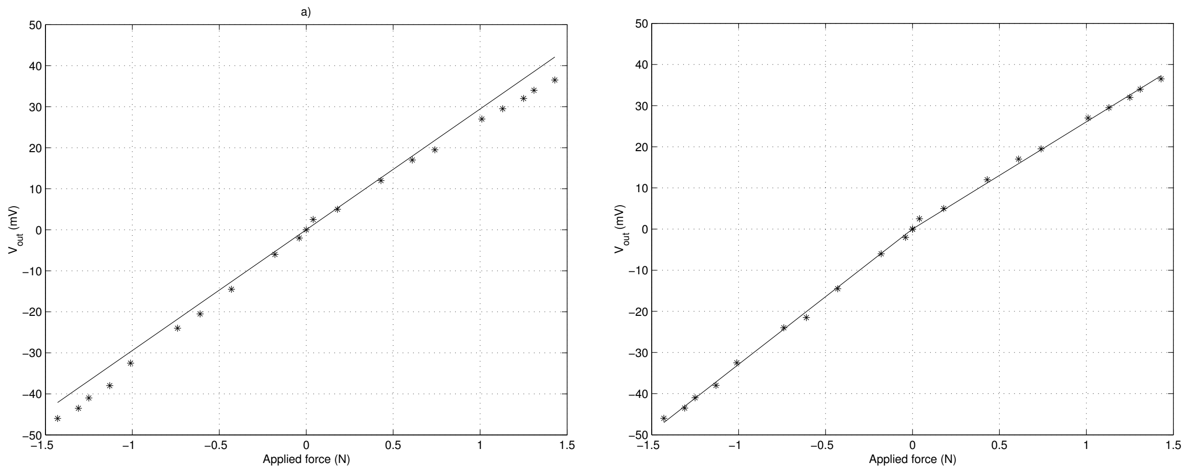

(a) (b)

Figure 4.8: Linearity properties of the sensor: one interpolating line (a), two interpolating lines (b).

In particular, in Fig. 4.8.a the output of a sensing element (more precisely the element "B", see Fig. 4.4) is shown as a function of the load applied to the glass beam, along with the linear interpolation of the data. In Fig. 4.8.b two interpolating lines are used, one for the positive loads and one for the negative ones. In this manner, a better approximation is obtained, with a typical linearity error of 1%. Note that this different behavior between positive and negative values is due to the fact that the sensing elements have been deposited only on one side of the beam, and therefore, there is an asymmetry between its positive and negative deformations.

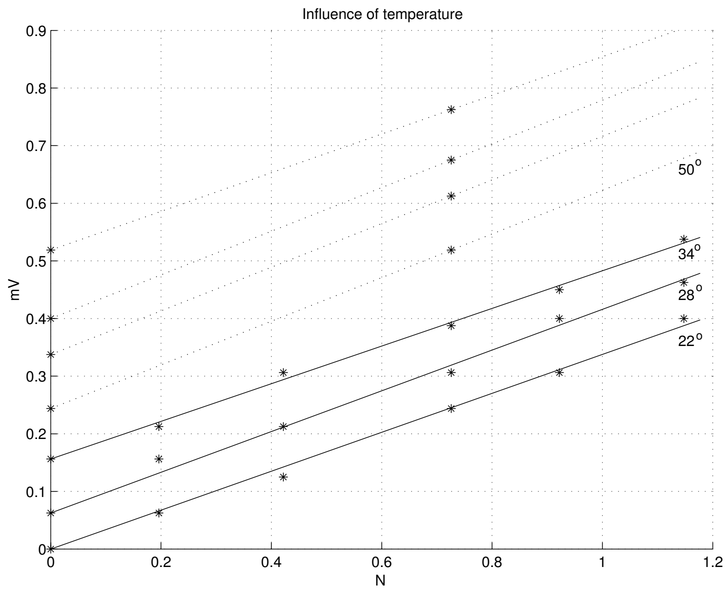

Figure 4.9: Variation with temperature of the sensor's output.

The gain of the sensor (mV/N) in the implemented configuration is $G = 0.37$ considering only one interpolating line and $G_- = 0.41, G_+ = 0.33$ with two interpolating lines. The weights applied to the beam are $w = \pm[4, 18, 43, 61, 74, 101, 113, 125, 131, 143]\ g$. Obviously, the loads have been limited to these values in order not to break the glass support.

4.3.2 Influence of temperature

A second important feature is the influence of the temperature on the sensor output and on its gain. These properties are summarized in Fig. 4.9, where the sensor has been loaded with constant weights ($w = [20, 43, 74, 94, 117]\ g$) at different temperatures. Note that the linearity and the gauge factor of the sensor are basically constant, while a bias output value, function of the temperature, appears. This phenomenon can be removed by means of proper hardware or software compensation which simply add an offset depending on external temperature.

4.3.3 Dynamic behavior and electromagnetic sensitivity

In Fig. 4.10 the output of the sensor is shown when a coin is dropped on the beam. This shows the capability of the sensor to measure impulsive forces and not only static forces. In Fig. 4.10.a the output of sensor is shown, while in Fig. 4.10.b the filtered signal is reported. One can note that the data of the sensor are rather satisfactory, considering the low value of the load. Obviously this test gives only a qualitative idea of the capacity of the sensing element to follow the changes of the applied stresses, and a more quantitative characterization of its dynamic properties is necessary. However, if it is important to notice that those properties are function of both the sensing element and the mechanical support and hence a characterization

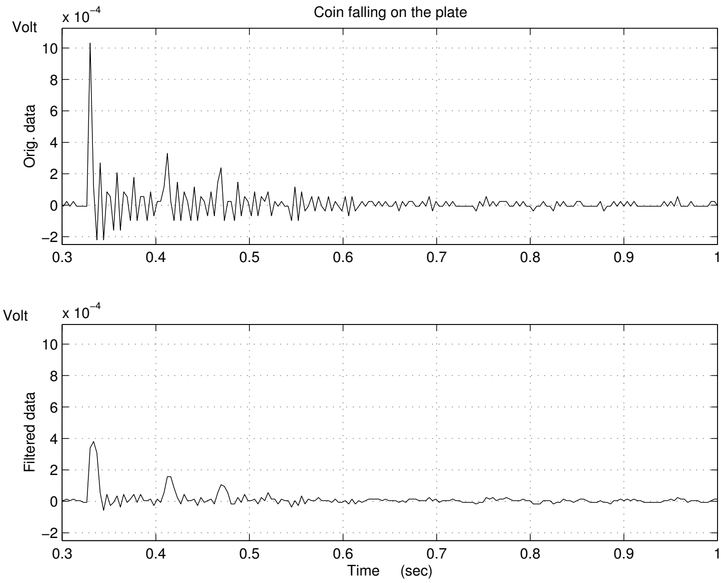

Figure 4.10: Detection of a falling coin.

of the transducer alone is in practice impossible but requires the definition of the complete force sensor. A consideration can be done at this level: the proposed technology does not need glue but is directly built on the mechanical support and hence, without any "filtering" intermediate layer, will be very sensitive to the imposed deformations and to their variations.

Another aspect that can be of some relevance for the use of the sensor is its sensitivity to EM fields. Although the new sensing element has a physical structure quite similar to Hall-effect sensors, its sensitivity to the external electro-magnetic fields appears good. In particular, some "empirical" tests have been performed by generating an EM disturbance (by means of a DC-Brushless motor). Fig. 4.11 shows the behavior of the new sensor and of a strain-gauge when the motor is switched on and off at a distance of 2 *cm* from the sensor. In order to estimate the disturbance, its magnitude has been compared with the response of the sensor to the strain caused by a force of 0.19 N acting on the glass (as shown previously). From these measures it appears clear that the proposed sensor has a standard behavior, and it does not require special precautions if compared to a standard strain-gauge sensor.

4.4 Comparison with strain-gauge sensors

As shown in the previous Section, the behavior of the sensor under development appears quite promising for the proposed use, that is as transducer of mechanical stress in force/torque sensors for robotics. However, in order to understand its real performances, an analysis aiming to compare it with the technologies current available appears necessary.

As stated in Sec. 4.1, strain-gauges, installed on some flexible mechanical element, are the

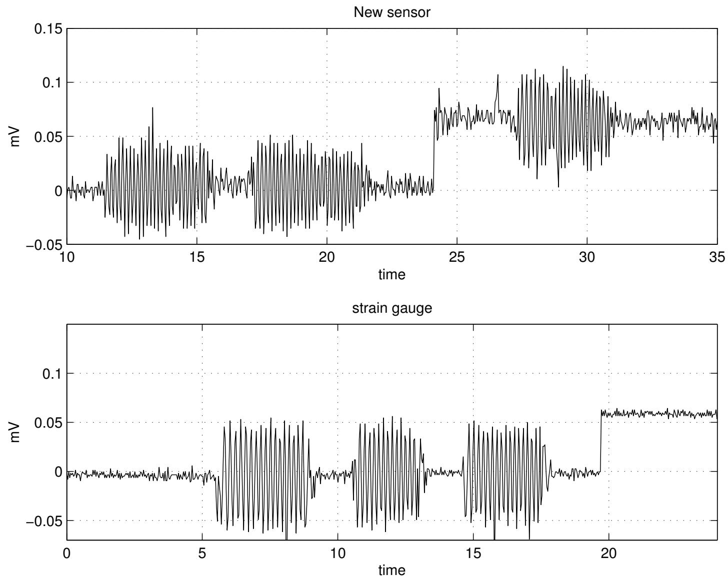

Figure 4.11: Electro-magnetic sensitivity of new sensing element compared with that of traditional strain gauges.

standard solution for force/torque sensing. They are simple electrical resistances whose value changes according to the relation:

$$\frac{\Delta R}{R} = G_F \frac{\Delta L}{L} = G_F \ \varepsilon$$

where $\frac{\Delta L}{L} = \varepsilon$ is the relative deformation (or strain) and G_F is the so called gage-factor. Strain-gauges can be of two main type:

- semiconductor;
- metallic.

Semiconductor strain gauges have gauges factors approximately 50 times greater than metallic ones, and moreover their dimensions are smaller. However, they have a high temperature coefficient of resistance and a higher nonlinearity. Thus, semiconductor strain gauges are employed where it is desirable to use a simple amplification electronics, or for elastic elements of small size. Metal-foil strain gauges seem to be more general purpose. They are appropriate for sensors without constraint on dimensions, including force sensors with small nominal strain in the elastic element. Low temperature coefficient and substantially lower level of thermal noise in these strain gauges compensate for their lower gauge factor.

A first difference between this new sensor and the standard technology is the fact that the linearity and hysteresis properties can be noticeably improved because there is no need of adhesive resin to fix the sensor elements. As a matter of fact, the deposition process used to realize the sensor ensures the lowest non-linearity error and low hysteresis.

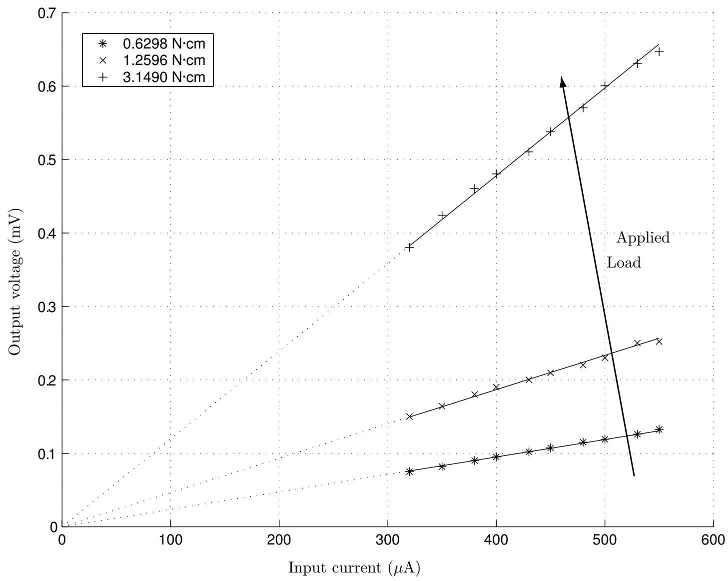

Figure 4.12: Sensor's output with different input currents and loads.

A second important aspect concerns the gauge factor. With this respect, the sensor has been compared with a classical full-bridge configuration of strain gauges. In this case, the relation between the applied strain and the output is

$$\frac{V_{out}}{V_{in}} = G_{Fs}\ \varepsilon \tag{4.3}$$

where V_{in} is the input voltage of the bridge, G_{Fs} the gauge factor and ϵ the strain. A similar relation can be determined for the new sensor, which implements a kind of implicit bridge configuration (see Fig. 4.13), whose differential output voltage V_{out} is a linear function of both the input voltage V_{in} (or current I_{in}, see Fig. 4.6) and the strain ε[1]. In particular, the sensor tested in these experiments has a gauge-factor $G_{Fn} = 0.98$.

In Fig. 4.14.a the comparison (with respect to the sensitivity to imposed strains) between the two sensing technologies is shown. For the strain-gauges, different values of gauge factor (2 and 50) and input voltage ($3 - 10\ V$) have been considered. It is possible to notice that the gain of the new sensor is similar to that of metallic strain-gauges, but it is also important to underline

[1]In Fig. 4.8 the dependence of V_{out} on the external force is reported, but, as well known, it exists a linear relation between the loads applied to the glass beam and the produced strains. Such a relation depends on mechanical parameters of the glass substrate, according the following formulas:

$$\sigma = \varepsilon \cdot E \tag{4.4}$$

and

$$\sigma = \frac{M_b \cdot y}{J} \tag{4.5}$$

where E is the elastic modulus of the glass, M_b the applied bending momentum, J the inertia momentum of the glass beam, $y = \frac{h}{2}$ with h height of the glass substrate.

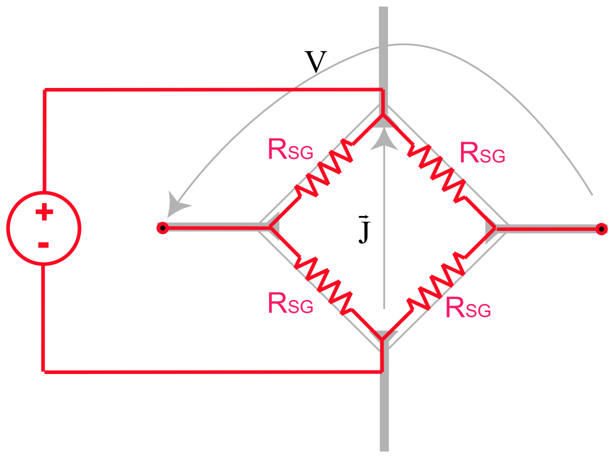

Figure 4.13: The structure of new sensor as full bridge.

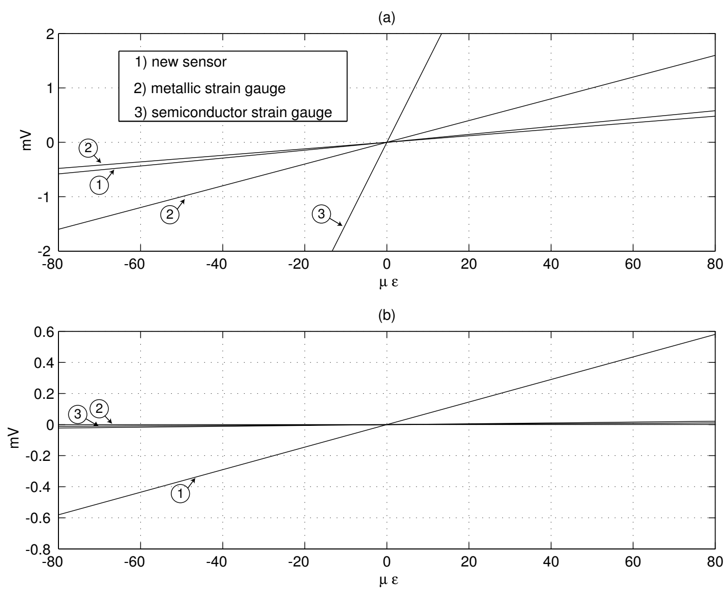

Figure 4.14: Comparison with standard strain-gauges sensors. The strain ϵ has been computed considering the glass substrate and the loads of Fig. 4.8.

that the power required is considerably less than that necessary with standard technology. As a matter of fact, the power coming in a strain-gauge bridge is

$$P_{in} = V_{in} \cdot I_{in} = R_{SG} \cdot I_{in}^2 = \frac{V_{in}^2}{R_{SG}}$$

where R_{SG} is the resistance of strain-gauges; if, for instance, typical values are considered, such as $V_{in} = 3V$ and $R_{SG} = 120\Omega$, P_{in} is $75mW$ ($\gg 7.5mW$ required by the new sensor). Therefore, seeing that, as shown by eq. (4.3), the output of the bridge is a linear function of strain through V_{in} (and hence P_{in}) as well as the gauge-factor, the comparison of sensitivity has been done considering the same coming power. In Fig. 4.14.b the results are reported, and can be noted that the new sensor shows the best performances. That suggests two immediate considerations:

- the new sensing technology is particular suitable for those applications which require very low power (e.g. space applications);
- the sensitivity (to imposed strains) of the new sensor can be improved if higher current/voltage values (at the moment constrained by problems of auto-heating) are used. That could be simply obtained by increasing the dimensions of the sensing element, by connecting in parallel several elements, or with different geometries.

4.5 Achieved results

The results so far achieved shows that this new transducer for the mechanical stress can be particularly suitable for robotic applications, and can lead to a general simplification of force/torque sensors. As a matter of fact the possibility to directly build the sensing elements on the stressed mechanical structure and its very small dimensions may abate design and manufacturing problems, and the side effects intrinsically tied to strain gauges technology (non-linear behavior, wrong placement, low sensitivity). In particular, this new technology will allow a reduction of the dimensions of the final force sensor for its integration in devices where the available room is very narrow, i.e. the fingers of a robotic hand or a manipulator for MIS (Minimum Invasive Surgery) [76]. Furthermore the manufacturing process allows to use almost every kind of substrate: plastic and metallic. Finally the sensing element can be easily integrated with the electronics needed for signal conditioning and amplification, possibly printed in the same substrate, with a noticeable reduction of the wires necessary for data transmission.
The final result of this research activity has been the definition of a *data sheet* of the proposed sensing element, whose the main characteristics are summarized in Tab. 4.1.

Parameter	**Min**	**Typ**	**Max**	**Units**
Current excitation	500		1500	μA
Null offset		80	190	mV
Linearity		± 1		% Span
Strain sensitivity	1,0		2,8	$\mu V/\mu\varepsilon$
Input resistance	7,5K		27,0K	Ω
Resistance shift 20 to 50$°C$		0.027		$\%/°C$
Null shift 20 to 50$°C$	90		270	$\mu V/°C$
Power consumption	3,75		40,5	mW

Table 4.1: Performance characteristics of the new sensor at 25$°C$.

Chapter 5

Control of complex systems physically interacting with the environment

This chapter presents the development of a controller able to drive a complex robotic system, such as a multifingered robotic hand, during the interaction with the environment in order to perform grasp and manipulation tasks. In particular a suitable strategy has been recognized in the impedance controller approach, which has been adapted to solve the specific problems of dexterous robotic end-effectors. The achieved control algorithm has been implemented and experimentally validated on the DLR Hand II [4].

5.1 A paradigm for advanced robotic hands: The DLR Hand II

One of the most advanced robotic hands developed up to now is certainly the so called "DLR Hand II", the second generation of robotic hands designed at the Institute for Robotics and Mechatronics of DLR (the German Space Agency)[4, 77]. The hand (see Fig. 5.1) shows a modular structure, characterized by four identical fingers arranged in a human-like way, that is three upper fingers and an opposable thumb. This modular approach allowed to greatly simplify the design and the manufacturing process of the whole hand, which is however an extremely complex systems, as it is clear by tacking into account the features of the single fingers.

The fingers have an anthropomorphic kinematic structure, with three phalanges, and three joints:

- the proximal joint has 2 degrees of freedom; one is for the curling motion and another is for abduction/adduction;

Figure 5.1: DLR's Hand II.

- the motions of the middle phalange and the distal phalange are not individually controllable but the relative base joints are rigidly coupled (by means of a belt) in a such way as to accomplish a motion similar to those of human fingers during grasping; therefore they are actuated by one motor and the coupling ratio is with a good approximation one to one.

The three independent joints are actuated by means of brushless DC-motors (integrated in the modular structure of each finger), whose motion is transmitted by tooth belts, harmonic drive gear and, in the base joint, bevel gears.
Furthermore, in the finger structure are hosted several sensors (and the relative electronics for signal conditioning and amplification) which provide information about the configuration of the hand and the state of the interaction with the environment/object; in particular, besides the Hall-effect position sensors integrated in the motors:

- each joint is equipped with strain gauge based torque sensors and specially designed potentiometers, which yield a direct measure of the joint position;

- in the fingertip is located a tiny force/torque sensor (depicted in Fig. 4.2), able to detect all the six components of the wrench vector exchanged during a contact with the external environment, as shown in Sec. 4.1.

This schematic description of the main characteristics of the DLR Hand II, gives an insight into the complexity of a such device; complexity which is a common features of the generality of articulated robotic hands. Moreover, as will be shown in the following, the DLR Hand exhibits some drawbacks (quite important for control purposes), which are also widespread in the field of robotic manipulation. Therefore it can be considered as a paradigmatic example of dexterous robotic device and the development of control strategies suitable for this specific case has a more general meaning and more general applications.

5.2 Hierarchical control structure for multifingered robotic hands

The controller of a multifingered robotic hand, although conceptually simple, is made particularly difficult by the complexity of the system to be controlled. As a matter of fact, it must be able to deal with a device with many degrees of freedom (thirteen in the case of DLR Hand II[1]), large amount of sensory information, and multiple control objectives which are necessary for manipulation.
A natural way to dominate such a complexity is the adoption of the classical principle *divide et impera*, that is splitting the (control) problem in subproblems, which can be easily solved. The same approach has been followed in the design of the hand itself, which has been developed by joining the single modular fingers. And also the nature seems exploiting the same concept: in the biological control of the human hand, for example, it is possible to recognized different control levels, with different degrees of complexity and capabilities.
In particular, as shown in Fig. 5.2, it has been proved that in the human case there are 2 main control loops:

- the external one (and therefore the highest level in this hierarchical structure) is accomplished by the brain that perceives the sensory information and originates the conscious motor commands (by means of sensory and motor cortex) which are in turn coordinated and sent down the spinal cord (by brainstem and cerebellar structures); one of the main characteristics of this loop is the high delay between the brain and the muscles (variable between 150 and 250 ms), which demonstrates the existence of a "local muscle control";
- the low-level is the so called "spinal reflex loop", performed by the muscles and the sensory organs of each finger; in particular, *muscle spindles*, directly "integrated" in the muscles, have afferent nerves, which besides sending information up the spinal column, make excitatory connection onto the nerves that send motors command out to the muscles themselves; in this way a stimulation of a muscle spindle produces the contraction of the corresponding muscle with a delay of 25/30 ms (and this is the fastest feedback system in the human body). In addition to this control mechanism, Golgi tendon organ makes a feedback connection via the spinal cord to the muscle it is in, but in this case the action is inhibitory (that is tending to turn off the muscles). The combination of these (force, position and velocity) feedbacks works in such a way as to modulate the muscle's impedance (that is the dynamic behavior of the muscle).

Probably inspired by the solution adopted by nature and according to the criterium of simplicity above mentioned, the systems which actually implement the control of complex robot hands have a similar structure [78], as shown in Fig. 5.3. In particular in these control architectures two

[1]Four fingers with three degrees of freedom each one, as stated in Sec. 5.1 and an additional dof to change the position of the opposable thumb.

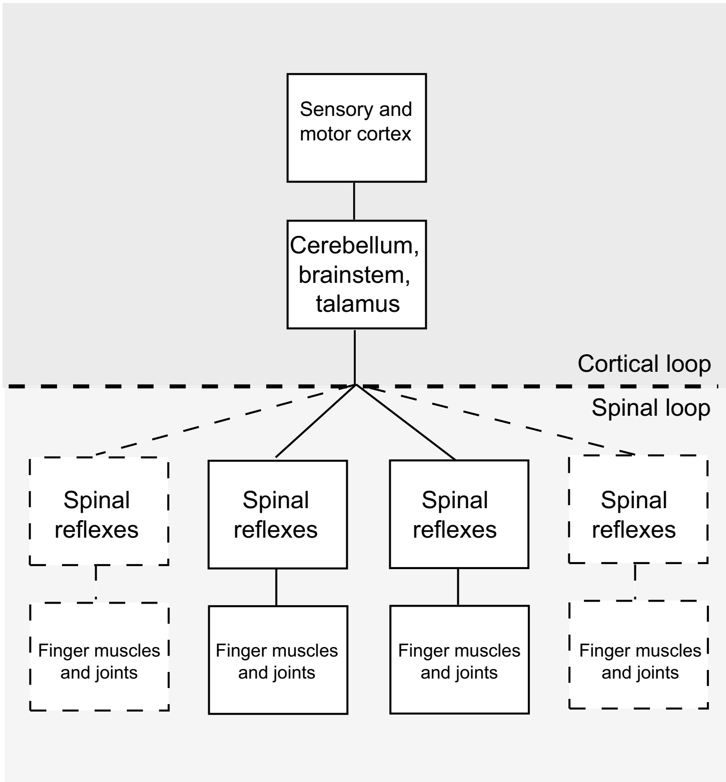

Figure 5.2: Hierarchical control scheme of human fingers.

main parts, which play a complementary role, can be recognized:

- a *deliberative* module, which takes care of planning the tasks to be performed, by means of reasoning and learning capabilities (and thus can be compared with the human brain).

- a (underlying) *reactive* layer, which accomplishes reflex-based activities, that ensure the safety, adaptability and autonomy of the overall system.

This last layer can be further subdivided: the control of the hand, and therefore the control of the operations aiming to grasp and manipulate a some object, is usually founded on the control of the single fingers, that finally is an atomic operation.
The control of a very complex systems, such as a dexterous robotic hand, may therefore reduced to the control of a set of "simple" manipulators, which, during manipulation operations, are coupled to each other and to the grasped object by velocity/force constraints and must be properly steered in order to carry out the desired tasks (e.g. changing the orientation of the object).
In the following, the attention will be focussed on the single robotic finger, which is the basic element of the overall system.

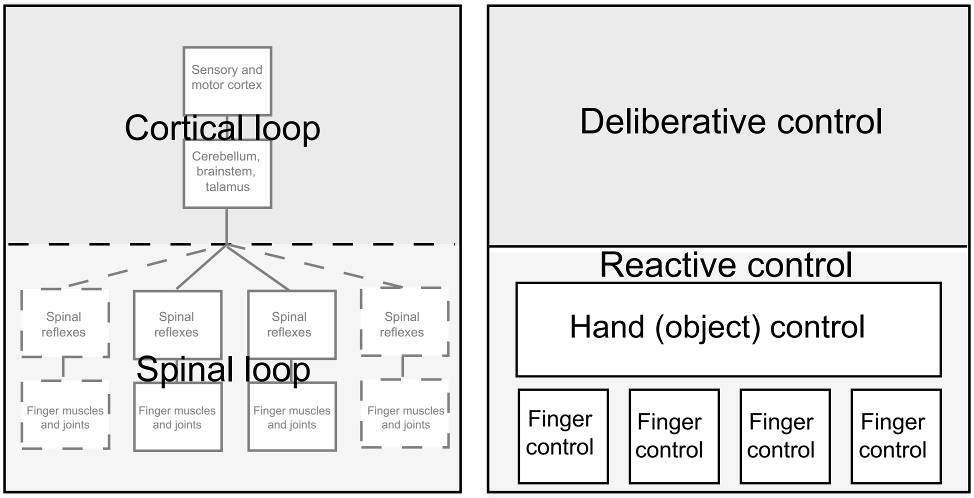

Figure 5.3: Analogy robots/humans control.

5.3 A natural controller for physical interactions

Robotic manipulation fundamentally requires a physical interaction with the object(s) being manipulated; in other words the robot manipulator, during the execution of the planned tasks, encounters some constraints and hence the interaction forces are not negligible. Obviously, in this case the robot hand can not be treated as an isolated system and the control strategies must explicitly consider this issue.
In the literature a number of controllers, which face the problem of interaction with the environment, have been proposed:

- force control strategies [79];
- hybrid approaches, where position and force controllers are joined in order to achieve desired behaviors in different directions of the robot work-space or in different phases of the task to be performed [79];
- impedance controllers [80].

At this point, it is worth to notice that all the strategies involving explicit force controls are inadequate in the case of a robot hand. As a matter of fact the tasks, a such device must perform, involve the interaction with environments and objects whose dynamics is unknown or only partially known. Furthermore, they require not only the application of desired forces but also the capability to perform precise positioning in free space and tracking of planned trajectories (and obviously in this case a force control does not make sense since, in free space, it is not possible apply forces different from zero). Finally, manipulation tasks often need the simultaneous application of desired forces and position displacements and they contemplate also the transition between no-contact and contact conditions.
More suitable to accomplish manipulation and grasp operations appears an *impedance controller*,

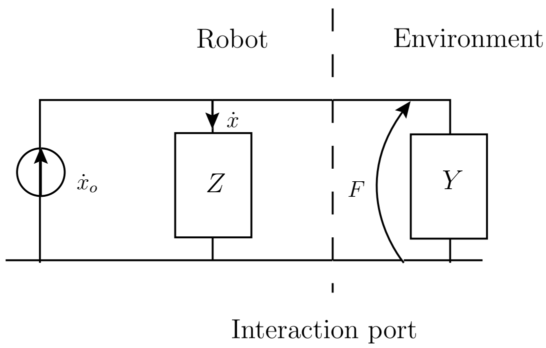

Figure 5.4: Description of the robot/environment interaction with a network.

whose target is to modulate and control the dynamic behavior of the manipulator, rather than a vector quantity such as force, position and velocity.
The basic idea is quite simple and has a clear physical meaning. When a robotic system interacts with the environment an exchange of energy occurs through this *interaction port*; in order to characterize the power flow between the manipulator and the environment the system must be described on one hand by means of forces/moments (more generally, *efforts*) and on the other hand by velocities/angular rates (more generally, *flows*). The *interaction port behavior*, that is the dynamic behavior at this energetic port, depends on the existing relation between these port variables. Borrowing terms original of electrical network theory, it has been defined *impedance* the dynamic operator that map an input motion time function $\dot{x}(t)$ into an output force time function $F(t)$:

$$\begin{cases} \dot{z} = Z_r(z, \dot{x}, t) \\ F = Z_o(z, \dot{x}, t) \end{cases} \tag{5.1}$$

where z is a finite-dimension state vector and $Z_r()$ and $Z_o()$ are algebraic functions. The admittance (characterized by $Y_r()$ and $Y_o()$) is the dual operator relating $F(t)$ to $\dot{x}(t)$. In general, a robot is described by an impedance and the environment by an admittance (see Fig. 5.4). As a matter of fact, the environment is composed by inertial elements which accept effort (force) inputs and yield flow (velocity) outputs. As a consequence the robot manipulator (coupled to the environment) is an impedance which accepts motions and determines the interaction forces.

Aim of this control approach is to modulate the impedance of the robot (and hence its dynamics behavior) at the port of the interaction with the environment. Therefore, given a generic manipulator which can be described in work-space coordinates x as

$$\tilde{\mathbf{M}}(\theta)\ddot{x} + \tilde{\mathbf{C}}(\dot{\theta}, \theta)\dot{x} + \tilde{\mathbf{G}}(\theta) = F_c + F \tag{5.2}$$

where $\tilde{\mathbf{M}}(\theta)$, $\tilde{\mathbf{C}}(\dot{\theta}, \theta)$, $\tilde{\mathbf{G}}(\theta)$ are the dynamic parameters of the system as viewed from the work-space variables, F_c and F are respectively the forces applied to the manipulator by the control (through the actuators) and the environment, the goal of this control approach is to transform, by using a feedback controller, its structural behavior described by eq. (5.2) into a new desired one (i.e. that described by eq. (5.3)). In this way, as shown in Fig. 5.5, by means of control

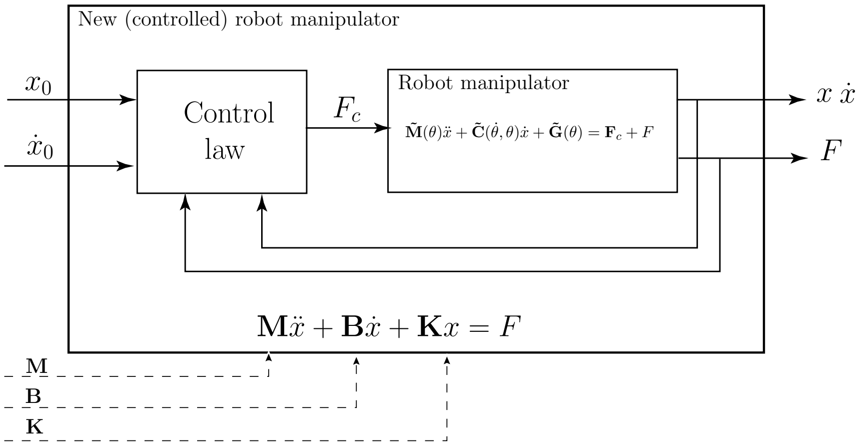

Figure 5.5: Physical equivalence of a robot and the relative (impedance) controller.

it is possible to define a new equivalent robot, characterized by a dynamic relation between velocities(/positions) and forces, which, for sake of simplicity, is commonly assumed to be linear

$$F = \mathbf{M}\ \ddot{x} + \mathbf{B}\ \dot{x} + \mathbf{K}\ x \tag{5.3}$$

Therefore, it is possible to use the classical tools of the linear analysis, and write the impedance as:

$$\frac{\mathbf{F(s)}}{s\mathbf{X}(s)} = \mathbf{Z(s)} = s\mathbf{M} + \mathbf{B} + \frac{\mathbf{K}}{s} \tag{5.4}$$

As a result of this approach, the robotic system (or more precisely its end-point, if cartesian coordinates are considered) appears like a pure mechanical system with mass (matrix) **M**, damping **B** and stiffness **K** arbitrary chosen.

It is clear that in order to accomplish a stable positioning of the robot, the impedance (defined as a dynamic map between velocity and force) must include a static relation between force and position, which is given by the spring of stiffness **K**. In this sense, the impedance can be thought as a dynamic generalization of the stiffness. Stiffness(/impedance) at a point is a system property independent of any objects it may contact, and hence the meaning of impedance controller becomes clear: it is an attempt to determine the interactive behavior of a manipulator that is *unaffected* by contact with environment. The only constraint remains a properly choice of the impedance parameters to perform a particular task and this is the a duty of the supervisor built over this basic controller (see Fig. 5.6) [62]. As the physical intuition suggests, in those directions where a contact is expected the values of **M** must be high in order to limit the dynamics of the robot, and the stiffness low enough to keep the contact forces small. Conversely along the "position controlled" directions (where a physical contact is not foreseen) an high stiffness value can guarantee an accurate positioning. Finally the terms of **B** affect the dissipation of the kinetic energy and therefore their value must be high enough to damp the response of the system.

In the title of the section this control approach has been defined "natural". Two are the main

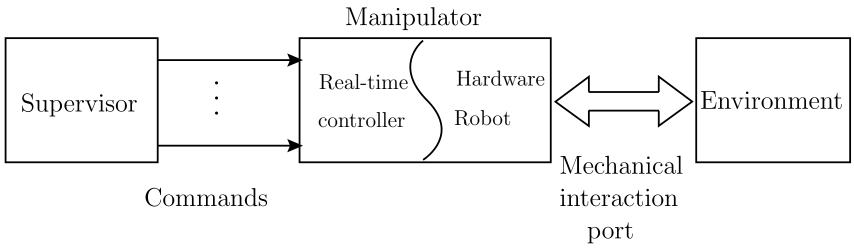

Figure 5.6: Schematic diagram of the overall control structure of a finger.

reasons: firstly, as already stated, impedance controller appears as the most immediate (and conceptually simple) solution to the problem of physical interaction; furthermore, the same mechanism is "implemented" in the human body, where the effects of the choice of impedance parameters (in particular, the stiffness) are evident: when we explore an unknown environment (typically by means of hands) the stiffness of the arm/hand muscles is set to a small value in order to apply small forces during a possible interaction, conversely when we want follow a some trajectory our supervisor, that is our brain, makes the muscles very stiff.

5.4 An impedance controller for dexterous robotic hands

As pointed out in Sec 5.1 a dexterous robotic hand is a extremely complex system and (on the basis of the previous considerations) the impedance control can be considered the key element to manage such a complexity. As a matter of fact, this control strategy is not only the mean to explicitly face the problem of the physical interaction, but also an important way to achieve a great simplification of the overall system; in particular it allows to mask the structural behavior of a robot manipulator, which is strongly nonlinear with couplings between the different directions of work-space and several non idelities (e.g. static friction), and to choose the desired (linear, uncoupled) dynamics. That considerably simplifies the job of the supervision system. It is not an accident that in the fields of grasp choice and task planning (i.e. manipulation of an object) the trend is to use quite simple models, basically mass-spring-damper systems (or simply springs, considering only static conditions). For example, Asada, in one of the earliest works about prehension and handling by means of robotic hands [81], assumes elastic fingers moving along a linear trajectory with a single degree of freedom. More recently Nguyen [82] addresses the stability of three-dimensional objects grasped by *virtual springs*, corresponding to the interactions between the object surface and the fingertips.

The aims and the reasons of the adoption of an impedance controller for robotic manipulation and in particular for robotic hands have been outlined but no hints about its actual implementation has been given: as a matter of fact the terms impedance controller defines the goal of this approach (that is to change the dynamic behavior of a system according to the constraints imposed by the task to be performed), while a number of alternative ways to achieve this goal are available.
The implementation of a specific regulator must take into account the characteristics of the physical systems: mechanical architecture, sensory equipment... In particular, if the fingers of

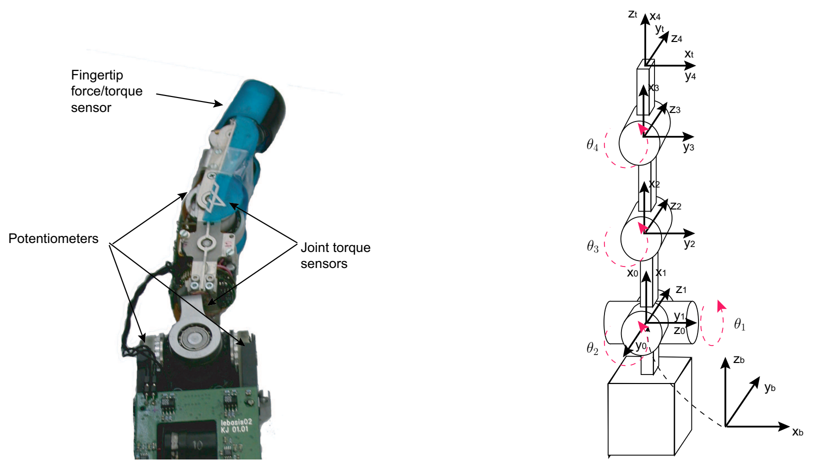

(a) (b)

Figure 5.7: The modular finger (a) and its kinematic structure (b).

a robotic hands, like the DLR Hand, are considered the control must cope with the drawbacks that such devices present and exploit their peculiar features.

5.4.1 Model of the robotic finger

To construct any controller for a robotic device the natural starting point are the equations describing its dynamic behavior; furthermore in order to implement such a controller, some tools, tied to kinematic structure of the manipulator, are needed, namely:

- direct ($\mathbf{L}$) and inverse kinematics ($\mathbf{L}^{-1}$);
- Jacobian $\mathbf{J}$ (and its transposed).

Therefore in the section the kinematic and dynamic model of robotic finger structure described in Sec. 5.1 are deduced and discussed.
Fig. 5.7 shows the modular finger and the corresponding kinematic chain, with the reference frames associated to each link.

According to the Denavit-Hartemberg notation, the four parameters which synthetically describe the kinematic transformation between two contiguous frames are reported, for each link, in Tab. 5.1. By means of well known homogeneous transformations, the relation between the joint variables $\theta = [\theta_1 \ \theta_2 \ \theta_3 \ \theta_4]^T$ and the position/orientation of the fingertip frame (t-subscript) in the base frame (b-subscript) is

$$\begin{aligned} {}^b\mathbf{H}_t &= {}^b\mathbf{H}_0 \ {}^0\mathbf{H}_1 \ {}^1\mathbf{H}_2 \ {}^2\mathbf{H}_3 \ {}^3\mathbf{H}_4 \ {}^4\mathbf{H}_t \\ &= \begin{pmatrix} C_{234} & 0 & S_{234} & l_2S_2 + l_3S_{23} + l_4S_{234} \\ S_1S_{234} & C_1 & -S_1C_{234} & -(l_2C_2 + l_3C_{23} + l_4C_{234})S_1 \\ -C_1S_{234} & S_1 & C_1C_{234} & (l_2C_2 + l_3C_{23} + l_4C_{234})C_1 \\ 0 & 0 & 0 & 1 \end{pmatrix} \end{aligned}$$

	d	θ	a	α
L_1	0	$\theta 1$	0	$\frac{\pi}{2}$
L_2	0	$\theta 2$	l_2	0
L_3	0	$\theta 3$	l_3	0
L_4	0	$\theta 4$	l_4	0

Table 5.1: Denavit-Hartemberg parameters of the DLR Hand's finger.

where

$$\begin{aligned} S_{ijk} &= \sin(\theta_i + \theta_j + \theta_k) \\ C_{ijk} &= \cos(\theta_i + \theta_j + \theta_k) \end{aligned}$$

In the matrix ${}^b\mathbf{H}_t$ one can recognize a part (${}^b\mathbf{R}_t$) related to the orientation of the fingertip and a component which provides the position of the tip frame origin. By taking into account that, because of the mechanical coupling between the two last joints of the finger, is

$$\theta_3 = \theta_4$$

the orientation of the of the end-frame can be expressed as

$${}^b\mathbf{R}_t = \begin{pmatrix} C_{233} & 0 & S_{233} \\ S_1 S_{233} & C_1 & -S_1 C_{233} \\ -C_1 S_{233} & S_1 & C_1 C_{233} \end{pmatrix}$$

while the position of the fingertip is given by

$$\begin{pmatrix} x \\ y \\ z \end{pmatrix} = \mathbf{L}\left(\begin{pmatrix} \theta_1 \\ \theta_2 \\ \theta_3 \end{pmatrix}\right) = \begin{pmatrix} l_2\, S_2 + l_3\, S_{23} + l_4\, S_{233} \\ -(l_2\, C_2 + l_3\, C_{23} + l_4\, C_{233})\, S_1 \\ (l_2\, C_2 + l_3\, C_{23} + l_4\, C_{233})\, C_1 \end{pmatrix} \tag{5.5}$$

Since the finger has a total of three degrees of freedom, the controller will deal only with its position in the workspace (neglecting the orientation); concerning the speeds, only the linear ones will be obviously considered. Therefore the kinematic relation between joint and task-space velocities can be obtained by simply differentiating (5.5) with respect to θ. This leads to the relation

$$\begin{pmatrix} \dot{x} \\ \dot{y} \\ \dot{z} \end{pmatrix} = \mathbf{J}(\theta) \begin{pmatrix} \dot{\theta}_1 \\ \dot{\theta}_2 \\ \dot{\theta}_3 \end{pmatrix} \tag{5.6}$$

where the Jacobian $\mathbf{J}(\theta)$ of the robotic finger is

$$\mathbf{J}(\theta) = \begin{pmatrix} 0 & l_2C_2 + l_3C_{23} + l_4C_{233} & l_3C_{23} + 2l_4C_{233} \\ -C_1(l_2C_2 + l_3C_{23} + l_4C_{233}) & S_1(l_2S_2 + l_3S_{23} + l_4S_{233}) & S_1(l_3S_{23} + 2l_4S_{233}) \\ -S_1(l_2C_2 + l_3C_{23} + l_4C_{233}) & -C_1(l_2S_2 + l_3S_{23} + l_4S_{233}) & -C_1(l_3S_{23} + 2l_4S_{233}) \end{pmatrix}$$

From the last expression, it is possible to compute the singular configurations for the kinematic structure under analysis. As well known in these configurations (where Jacobian matrix is no

link #	length
l_2	75
l_3	40
l_4	29.5

(a)

θ_i	θ_{min}	θ_{max}
1	-0.52	0.52
2	-0.5	0.7
3	0	1.4

(b)

Table 5.2: a - Length of the finger-links (mm); b - Range of the joint angles (rad).

longer full-rank) the robot exhibits a pathological behavior (i.e. it "loses" degrees of freedom, that is it can not generate speeds in some directions). The following equation provides the analytical values of such positions:

$$det(\mathbf{J}(\theta)) = -(l_3(l_2 + l_4) + 4l_2 l_4 C_3)(l_2 C_2 + l_3 C_{23} + l_4 C_{233}) S_3 = 0$$

Note in particular that $\theta_3 = 0$ is one of such conditions: that means that when it is upright, the finger is in singularity; nevertheless this configuration is frequently used in manipulation tasks (as we can observe in our everyday life, by looking at our hand). Instead the other singular configurations can not be physically reached because of the limits on the joint angles (see Tab. 5.2);

Finally, the relation between the positions in the task-space x and the configuration of joint θ, can be obtained for the robotic finger in a close form by means of simple geometrical considerations (and thanks to the fact that $\theta_3 = \theta_4$). The inverse kinematics

$$\begin{pmatrix} \theta_1 \\ \theta_2 \\ \theta_3 \end{pmatrix} = \mathbf{L}^{-1} \left(\begin{pmatrix} x \\ y \\ z \end{pmatrix} \right)$$

is expressed by the following equations

$$\begin{cases} \theta_1 = \mathrm{atan2}(-y, x); \\ \qquad z_p = -\frac{z}{\cos(\theta_1)}; \\ \qquad l = \sqrt{x^2 + z_p^2}; \\ \theta_3 = \arccos\left(1/8\ \frac{-2\ l_2\ l_3 - 2\ l_3\ l_4 + 2\sqrt{l_3^2\ l_2^2 - 2\ l_3^2\ l_2\ l_4 + l_3^2\ l_4^2 - 4\ l_4\ l_2^3 - 4\ l_4^3\ l_2 + 4\ l^2\ l_4\ l_2 + 8\ l_2^2\ l_4^2}}{l_4\ l_2}\right); \\ \theta_2 = \mathrm{atan2}(z_p, x) + \arcsin\left(\frac{l_3\ (l_2 - l_4) + (l_2^2 - l_4^2 + l^2)\ \cos(\theta_3)}{l\ (l_3 + 2\ l_2\ \cos(\theta 3))}\right); \end{cases}$$

and leads, within the feasibile work-space, to a unique solution.

Concerning the dynamic behavior of the finger, it can be described by means of the familiar Lagrangian formulation, as

$$\mathbf{M}(\theta)\ddot{\theta} + \mathbf{C}(\theta, \dot{\theta})\dot{\theta} + \mathbf{g}(\theta) = \tau_{act} + \mathbf{J}^T(\theta)\mathbf{F}_{ext} \tag{5.7}$$

where $\mathbf{M}(\theta)$ is the inertia matrix, $\mathbf{C}(\theta, \dot{\theta})\dot{\theta}$ represents the centrifugal and coriolis forces, $\mathbf{g}(\theta)$ the gravitational forces, τ_{act} are the torques supplied to the joints by the actuators, and $\mathbf{F}_{ext}$ the external forces impressed at the fingertip. However, to this set of dynamic terms theoretically computed, must be added an important (and troublesome) contribution (some times neglected in theoretical analysis and control synthesis), that is the friction. As a matter of fact the friction is one of the main problems on manipulation by means of robot hands in particular for small motions or when an interaction with the environment occurs. In fact the main efforts in robotics have been devoted to compensation of friction in tracking problems (see for example [83]) but few researches address the problem of compensating for it when the robot exchanges forces with the environment. In particular friction does not allow to control such forces in a fine way, and makes the manipulation of small or fragile objects prohibitive.
According to the classical model, in frictional phenomena several components can be recognized. Each of them takes care of certain aspects of friction forces. In particular the main contributions are:

- *coulomb friction*, taking into account the forces that oppose the motion and whose magnitude is independent from speed and contact area;
- *viscous friction*, which considers the friction component proportional to the velocity;
- *stiction*, describing the friction force at rest.

The superposition of all these effects leads to the following behavior:

$$\tau_{fric} = \begin{cases} \tau_{CV}(\dot{\theta}) & \text{if } \dot{\theta} \neq 0 \\ \tau_e & \text{if } \dot{\theta} = 0 \text{ and } |\tau_e| < \tau_S^{max} \\ \tau_S^{max} sgn(\tau_e) & \text{otherwise} \end{cases} \tag{5.8}$$

where τ_e is the external torque acting on the joints and $\tau(\dot{\theta})$ is a function of the speed $\dot{\theta}$ as shown in Fig. 5.8, where two models are introduced, according to different levels of detail.

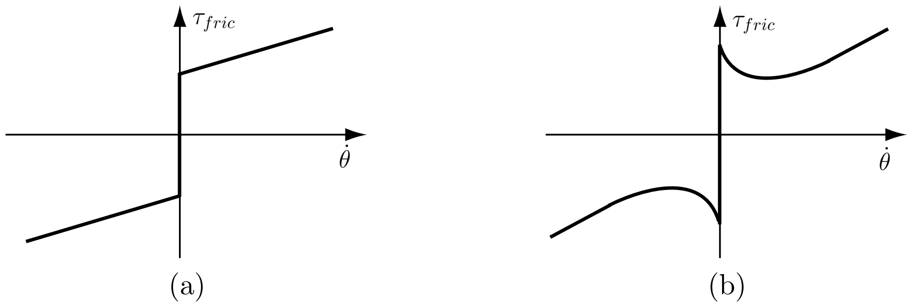

Figure 5.8: Examples of static friction models. Figure a) shows Coulomb plus viscous friction, figure b) shows how the friction force decrease continuously from the static friction level.

Due to the use of harmonic drive the friction in the joints heavily affects the dynamic behavior of the fingers of DLR Hand II and a terms such as (5.8) must be added to (5.7); in particular the breakaway torque, that is the torque needed to overcome the stiction while the motion of the joints starts, is about 10% of the maximum torque that actuators can supply (that is 0.4 Nm). Moreover its value is different for each joint and for each finger because of small variations on mechanical manufacturing and assembly, and also considering the same joint it is not constant but depending on the configuration, with a not negligible stochastic component. On the other side, because both the physical characteristics (length and weight of each link) of the robotic finger and the required speeds are small, the effects of Coriolis and centrifugal forces can be neglected (in particular, if compared with friction terms). In Fig. 5.9 the contributions of the different dynamic terms, which describe the behavior of the finger, are reported (considering different configurations, velocities and accelerations). This simulation has been done on the base of the theoretical model (5.7), with the values of the mechanical parameters given by the CAD program used to design the finger. By a simple comparison, the heavy effect of the stiction on robot behavior appears clear.

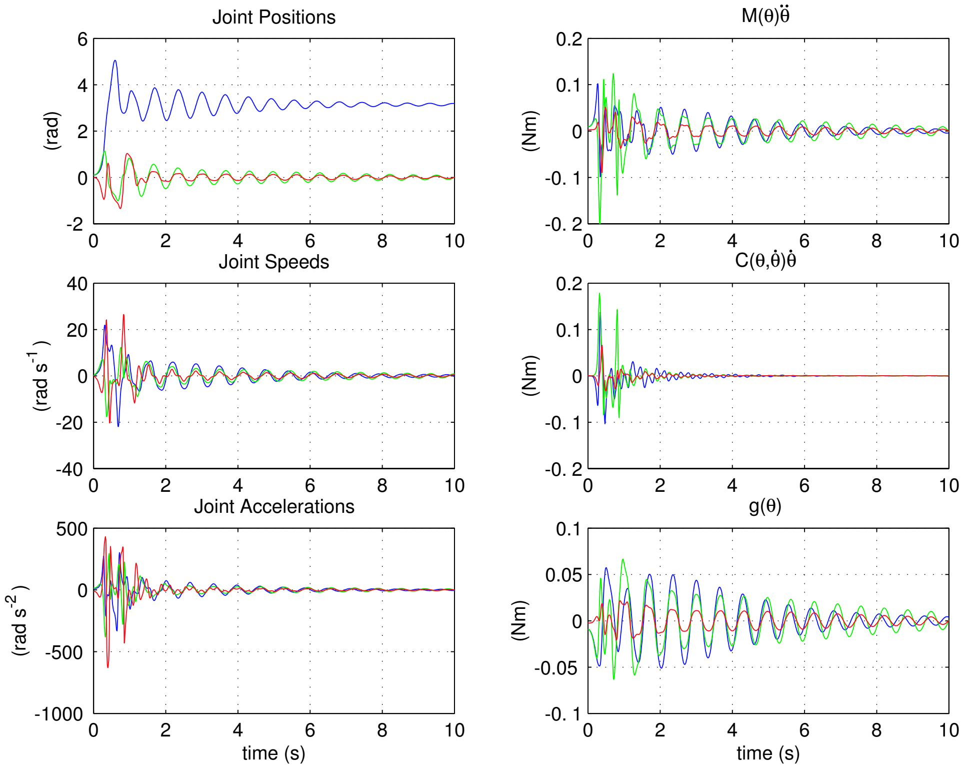

Figure 5.9: Dynamic terms of the finger behavior.

5.5 A passivity-based approach to the impedance control

Tacking into account the possible applications of a robot hand, it is obvious that the main goal of the controller to be implemented must be the stability of the system during the interaction with objects and environment. In particular an hand must be capable to deal with a set as large as

possible of objects, whose dynamics may be unknown and considerably complex. To guarantee such robustness properties, the best starting point for the implementation of an impedance controller is the so called passivity-based approach.
Aim of this approach is to impose to the robot manipulator an impedance with the following form:

$$\mathbf{F}_z = \mathbf{K}(x_z - x_0) + \mathbf{B}(\dot{x}_z) \tag{5.9}$$

where $\mathbf{K}()$ and $\mathbf{B}()$ are generic function defining the relation force/displacement and force/velocity and x_0 is the vector of equilibrium positions for the target impedance (and therefore for the manipulator) when it is isolated from the environment. The behavior described by (5.9) is defined as a *simple impedance* if:

1. $\mathbf{K}(x_z - x_0)$ is the gradient of a positive-definite nondecreasing function of the displacement $(x_z - x_0)$;
2. $\dot{x}^T\mathbf{B}(\dot{x}) > 0 \ \forall \dot{x} \neq 0$

It is possible to prove that when a simple impedance is coupled with an environment of arbitrary dynamic complexity, provided that the environment was stable in isolation, the overall system is still stable [84]. Therefore, if it is possible to impose to the fingers of a robotic hand the behavior of a simple impedance, they will be stable during the interaction with generic objects (with the only condition of their stability in isolation).
An immediate solution to the implementation of this kind of controller may be achieved by coupling the robot manipulator with the model of impedance so far introduced: the basic idea is to consider the robot and the controller as two interacting dynamic systems. A typical realization of the impedance (5.9) with the two cited conditions is achieved by means of:

$$\mathbf{K}(x_z - x_0) = \mathbf{K} \cdot (x_z - x_0) \ \text{ and } \ \mathbf{B}(\dot{x}) = \mathbf{B} \cdot \dot{x}$$

where $\mathbf{K}$ and $\mathbf{B}$ are positive-definite matrices.
Considering the usual Lagrangian formulation of the robot finger dynamics, expressed by (5.7), the coupling with the target impedance is expressed by

$$\begin{cases} \mathbf{M}(\theta)\ddot{\theta} + \mathbf{C}(\theta,\dot{\theta})\dot{\theta} + \mathbf{g}(\theta) + \tau_{fric} = \tau_{act} + \mathbf{J}^T(\theta)\mathbf{F}_{ext} \\ \tau_{act} = \tau_g - \mathbf{J}^T(\theta)\mathbf{F}_z \end{cases} \tag{5.10}$$

where the the further term $\tau_g = \mathbf{g}(\theta)$ has been added to compensate for the gravity, $\mathbf{J}^T(\theta)$ is the transposed Jacobian of the finger (which maps task-space forces into joint torques) and $\mathbf{F}_z$ is given by (5.9). It is worth to notice that when the target impedance and the manipulator are coupled (in the work-space) their position and velocity variables are the same and hence they are related to the generalized coordinated of the robotic finger (θ) by the usual kinematic transformations (5.5) and (5.6). The dynamic equation describing the overall system is therefore

$$\mathbf{M}(\theta)\ddot{\theta} + \mathbf{C}(\theta,\dot{\theta})\dot{\theta} + \tau_{fric} = \mathbf{J}^T\mathbf{K}(x_0 - x) - \mathbf{J}^T\mathbf{B}\dot{x} + \mathbf{J}^T(\theta)\mathbf{F}_{ext} \tag{5.11}$$

and the complete control scheme is reported in Fig. 5.10.
In the case that no interactions with the external environment occur ($\mathbf{F}_{ext} = 0$) and if the

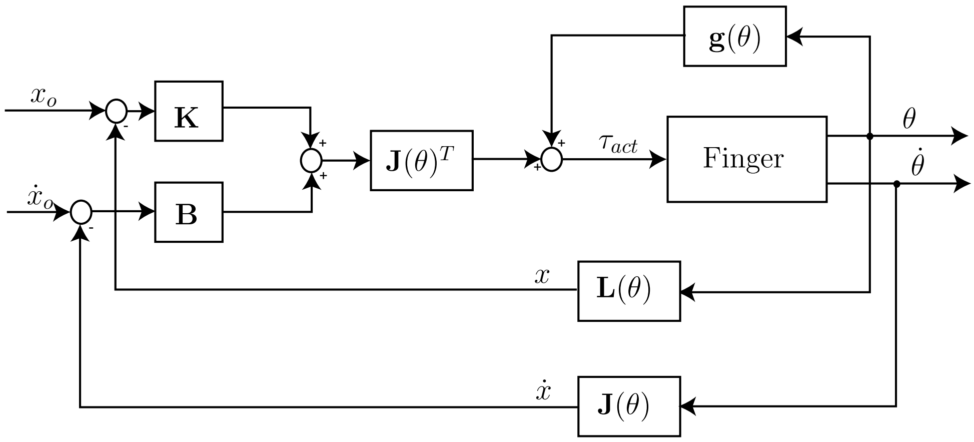

Figure 5.10: Complete control scheme for the robotic finger based on passivity approach.

generalized forces due to the friction are neglected the global stability of the system for ($\dot{x} = 0$, $\Delta x = 0$)[2] can be easily proved. In the same way can be shown the stability if friction phenomena are considered, but in this case the position error Δx will not converge asymptotically to zero. In order to prove the stability of the system in this last case, the following Lyapunov function can be chosen:

$$V(\theta, \Delta x) = \frac{1}{2}\dot{\theta}^T \mathbf{M}(\theta)\dot{\theta} + \frac{1}{2}\Delta x^T \mathbf{K} \Delta x > 0 \qquad \forall \dot{\theta}, \Delta x \neq 0 \tag{5.12}$$

where, by the assumption of a simple impedance, $\mathbf{K}$ is symmetric and positive-definite. The derivative of this Lyapunov function is

$$\dot{V} = \dot{\theta}^T \mathbf{M}(\theta)\ddot{\theta} + \frac{1}{2}\dot{\theta}^T \dot{\mathbf{M}}(\theta)\dot{\theta} + \dot{\Delta x}^T \mathbf{K} \Delta x$$

which computed along the trajectories of the system (5.11) leads to the expression

$$\dot{V} = \dot{\theta}^T(-\mathbf{C}(\theta, \dot{\theta})\dot{\theta} - \tau_{fric} + \mathbf{J}^T \mathbf{K} \Delta x - \mathbf{J}^T \mathbf{B} \Delta \dot{x}) + \frac{1}{2}\dot{\theta}^T \dot{\mathbf{M}}(\theta)\dot{\theta} + \dot{\Delta x}^T \mathbf{K} \Delta x \tag{5.13}$$

Since

$$\dot{\Delta x} = -\mathbf{J}(\theta)\dot{\theta}$$

and $(\mathbf{M}(\theta) - 2\mathbf{C}(\theta, \dot{\theta}))$ is, as well known, a skew-symmetric matrix and therefore

$$\dot{\theta}^T(\mathbf{M}(\theta) - 2\mathbf{C}(\theta, \dot{\theta}))\dot{\theta} = 0$$

equation (5.13) can be reduced to

$$\dot{V} = -\dot{\theta}^T \mathbf{J}^T \mathbf{B} \mathbf{J} \dot{\theta} - \dot{\theta}^T \tau_{fric} \tag{5.14}$$

[2] $\Delta x = x_0 - x$

If we consider the model of friction (5.8), shown in previous section, we can write

$$\tau_{fric} = \tau_S + \tau_{CV}(\dot{\theta}) \tag{5.15}$$

where τ_S and $\tau_{CV}(\dot{\theta})$ are respectively the contribution of the stiction and of coulomb/viscous friction. In particular it must be noticed that, according to the adopted static model, the two terms affect the system in different phases. Considering the vector components, for each joint is

$$\begin{cases} \tau_{Si} = 0 & \text{if} \quad \dot{\theta}_i \neq 0 \\ \tau_{CVi} = 0 & \text{if} \quad \dot{\theta}_i = 0 \end{cases}$$

Furthermore, since $\tau_{CVi}(\theta_i)$, as depicted in Fig. 5.8, belongs to the first and third quadrant

$$\dot{\theta}_i \cdot \tau_{CVi}(\dot{\theta}_i) \geq 0 \quad \forall \theta_i \tag{5.16}$$

while

$$\dot{\theta}_i \cdot \tau_{Si} = 0 \tag{5.17}$$

By substituting (5.15) into (5.14), from considerations (5.16) and (5.17) and under the hypothesis that $\mathbf{B}$ is definite positive (simple impedance) immediately follows that

$$\dot{V} \leq 0$$

and, in particular

$$\dot{V} = 0 \quad \text{for} \quad \dot{\theta} = 0$$

Therefore the function $V(\dot{\theta}, \Delta x)$ decreases until $\dot{\theta} \neq 0$. In this case the dynamic equation of the system (5.11) becomes

$$\mathbf{J}^T \mathbf{K} \Delta x = \tau_S \tag{5.18}$$

To show the effects of of the friction (and in particular of the stiction), it is worth to map the friction torques into the equivalent forces in the work-space, according to

$$\mathbf{F}_S = \mathbf{J}^{-T} \tau_S \tag{5.19}$$

Since the components of $\mathbf{F}_S$ are a linear combination of τ_{Si}, which are limited from above, as reported in (5.8), if the finger is not in a singularity condition, follows that

$$|\tau_{Si}| < \tau_{Si}^{max} \ \ \forall i \qquad \rightarrow \qquad |F_{Sj}| < F_{Sj}^{max} \ \ \forall j$$

Taking into account the case, quite common in the practice, of a diagonal matrix $\mathbf{K}$ (that means uncoupled stiffness on different directions of work-space), it holds the inequality

$$|\Delta x_i| < \frac{F_{S\ i}^{max}}{K_{ii}}$$

that is

$$x_i \in (x_{i0} - \frac{F_{fric\ i}^{max}}{K_{ii}}, x_{i0} + \frac{F_{fric\ i}^{max}}{K_{ii}}) \tag{5.20}$$

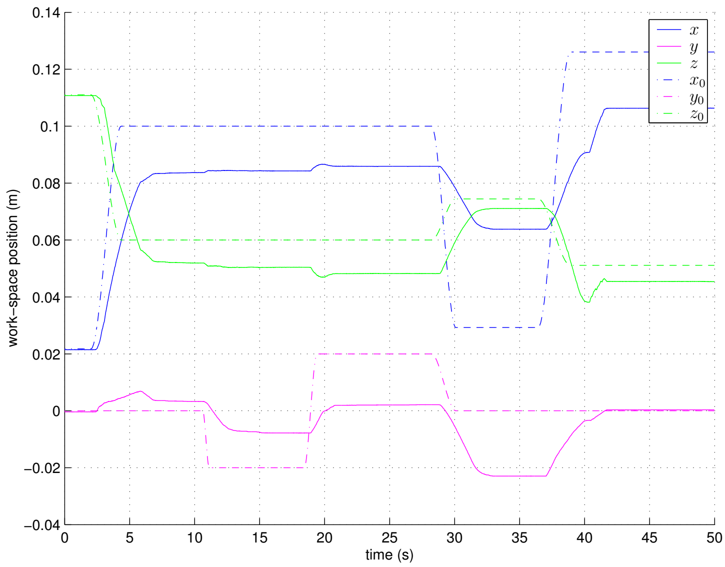

Figure 5.11: Tracking of a desired trajectory (x_0) by means of a passive impedance controller ($K_{ii} = 50\ Nm^{-1}$).

This reflect the fact that, with uncompensated stiction, the fingertip will stop within a dead zone around the desired position x_0. The width of such a dead zone is inversely proportional to the "gain" K_{ii} and depends also by the finger configuration (through $\mathbf{J}^{-T}(\theta)$).
The approach followed to point out the stability properties of the controller (5.9) considers only the position tracking problem and is particularly suitable to highlight the (heavy) effects of friction on the system's performances (as shown in Fig. 5.11, where the fingertip position x and the set point x_0 are displayed). But, if an interaction with the external environment is considered (and hence F_{ext} can be no longer neglected) a different analysis based on Hamiltonian formalism seems preferable. By defining the Hamiltonian of the controller (that is the target impedance corresponding to a mechanical spring/damper system) and of the robot finger, impedance control assumes a clear physical meaning. To this end one must remember that:

- the Hamiltonian of a system corresponds with its total energy:

$$\mathbf{H}(\mathbf{p}, \mathbf{q}) = \mathbf{E_k}(\mathbf{p}, \mathbf{q}) + \mathbf{E_p}(\mathbf{q})$$

  where $\mathbf{E_k}(\mathbf{p}, \mathbf{q})$ and $\mathbf{E_p}(\mathbf{q})$ are respectively the kinetic energy and the potential energy, which are function of the generalized momenta p and of the generalized coordinates q ($= \theta$ for the robot finger) describing the system;

- the dynamic interaction between two physical system is isenergetic, that is involving a power exchange without loss, storage or generation of energy;

- a robot manipulator is a passive system from the input τ_{act} to the output $\dot{\theta}$ (with reference to the symbol used in (5.7)), that is its total energy has a bounded minimum.

The coupling of the controller (5.9) and the manipulator leads to a controlled system which may be described by an equivalent physical system, whose Hamiltonian $\mathbf{H}_C(p,q)$ (and therefore the energy) is the sum of Hamiltonians for the uncontrolled system ($\mathbf{H}_F(p,q)$) and the impedance ($\mathbf{H}_Z(p,q)$):

$$\mathbf{H}_C(p,q) = \mathbf{H}_F(p,q) + \mathbf{H}_Z(p,q) \tag{5.21}$$

where (p,q) refers to the robot finger. Therefore if the goal is to drive the robot finger in a desired position x_0, that can be achieved by shifting, through the controller, the energy minimum of the overall system in such position. That is exactly the procedure followed with the control approach above described: the potential energy of the robot (due to the gravity) has been compensated and a new elastic potential

$$U_k = \frac{1}{2}(x - x_0)^T \mathbf{K}(x - x_0)$$

whose minimum is in x_0 has been added. In this way, if the system is stable it will move towards such energy minimum.
Formally, given a system described by the following equations:

$$\dot{q} = \frac{\partial \mathbf{H}(p,q)}{\partial p} \tag{5.22}$$

$$\dot{p} = -\frac{\partial \mathbf{H}(p,q)}{\partial q} - \mathbf{D}(p,q) + \mathbf{P}(t) \tag{5.23}$$

where $\mathbf{D}(p,q)$ are the generalized non conservative forces and $\mathbf{P}(t)$ the generalized (external) forces, if, as usual, the kinetic and potential energy are positive-definite, non decreasing functions respectively of the momenta p and the generalized displacements q (and therefore at equilibrium $p = 0$ and $q = 0$), the Hamiltonian may be used as Lyapunov function for the analysis of stability. In particular, it is sufficient to show that:

$$\frac{d\mathbf{H}(p,q)}{dt} < 0 \tag{5.24}$$

to prove the stability of the equilibrium point $(p = 0, q = 0)$.
The Hamiltonian of the overall system robot finger/impedance model $\mathbf{H}_C(p,q)$ has a rate of change

$$\frac{d\mathbf{H}_C}{dt} = -\dot{\theta}^T \tau_{fric} - \dot{x}^T \mathbf{B}\dot{x} + \dot{x}^T \mathbf{F}_{ext} \tag{5.25}$$

Considering $\mathbf{F}_{ext} = 0$, by a simple inspection (see (5.13)), results that

$$\frac{d\mathbf{H}_C}{dt} = \dot{V}$$

and therefore it is possible to reach the same conclusions. If finally, an interaction with the environment occurs, the total energy for the coupled system is still the sum of the two systems in isolation

$$\mathbf{H}_T(p_t, q_t) = \mathbf{H}_C(p,q) + \mathbf{H}_E(p_e, q_e) \tag{5.26}$$

where $\mathbf{H}_E(p_e, q_e)$ is the hamiltonian of the environment. The temporal derivative of the overall energy is therefore

$$\frac{d\mathbf{H}_T}{dt} = -\dot{q}_e^T \mathbf{D}_e + \dot{x}_e^T \mathbf{F}_e - \dot{\theta}^T \tau_{fric} - \dot{x}^T \mathbf{B}\dot{x} + \dot{x}^T \mathbf{F}_{ext} \tag{5.27}$$

with q_e and $\mathbf{F}_e$ generalized coordinates and generalized forces of the environment (which because of the physical interaction are related to robotic finger variables according to (5.5) and (5.6)) and $\mathbf{D}_e$ dissipative forces.
Since the coupling can not generate power

$$\dot{x}_e^T \mathbf{F}_e + \dot{x}^T \mathbf{F}_{ext} = 0 \tag{5.28}$$

and hence

$$\frac{d\mathbf{H}_T}{dt} = -\dot{q}_e^T \mathbf{D}_e + -\dot{\theta}^T \tau_{fric} - \dot{x}^T \mathbf{B}\dot{x} \tag{5.29}$$

From the last equation can be easily inferred that sufficient conditions for the asymptotic stability of the overall system are the stability of the robot system (5.25) and the environment ($\dot{q}_e^T \mathbf{D}_e > 0 \ \ \forall \dot{q}_e \neq 0$) when they are decoupled. As a result, the finger is able to deal with a large class of objects, which are stable in isolation.
In Fig. 5.12 the interaction of the robotic finger (steered by the controller so far introduced, assuming a diagonal stiffness matrix whose elements are $K_{ii} = 50\ Nm^{-1}$) with an obstacle disposed in $x_b = 0.045\ m$ (see Fig. 5.19) is reported. Despite the intrinsic properties of robustness of this approach, its poor performances are also evident: the force F_x is quite different from the ideal value given by $K_{11} \cdot \Delta x$ ($= 1.75\ N$), and above all there are strong (undesired) couplings in the different directions of the work-space (in particular along z direction, where no constraints exist, the value of the force should be identically equal to 0). The reason of this behavior is again the friction on the joints, which makes this control approach not suitable for the considered test-bed, that is the DLR Hand.

5.6 Practical issues on the implementation of an impedance controller

The two main constraints to the implementation of the controller described in Sec. 5.5 are:

1. co-location of sensors;
2. friction on the joints.

According to the former condition, position sensors (which are the only required by the controller (5.10)) must be placed in the location where the interaction between the robot and the controller occurs. This point (previously called "interaction port") is obviously on the motors which provide the torques commanded by the control algorithm. In this way the port is described by two power consistent variables (position/speed $\theta_m/\dot{\theta}_m$ and torque τ_m of the actuator) whose product provides the power flow and hence the energetic considerations made in previous section are valid. Conversely, if torques and speeds refer to different sections, such considerations are

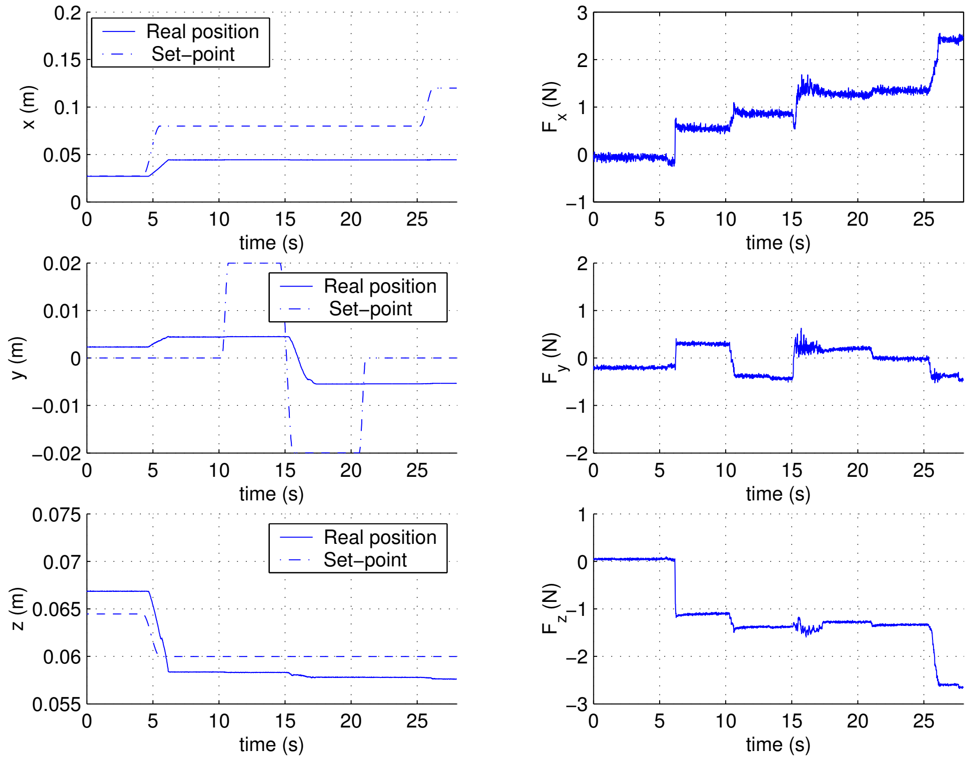

Figure 5.12: Interaction of the robotic finger (driven by the impedance controller based on passivity) with a wall placed in x_b =const.

no longer true.
The problem of *co-location* of the sensor is a quite general problem, which affects force control of robotic system and it is not limited to energetic approaches. In general when actuator and sensor are physically located at different points, in the closed loop system are introduced dynamic modes which can be instable (e.g. when flexible structures are considered) [85].
In the practice it is often supposed that the mechanical transmission is ideal and therefore torques/positions are the same at the initial and final sections of the kinematic chain; however this assumption is quite far from the reality if tendons or (like in this case) belts, which unavoidably introduce dynamic effects, are used.
Therefore, the implementation of the controller (5.10) on the robotic finger should be based on the hall position sensors directly integrated in the motors; this solution seems ideal, considering that, thanks to the high reduction ratio of the mechanical transmission, these sensors allow very high resolutions. Unfortunately they yield a relative position information which must be integrated with the position measure made by special potentiometers directly located on the joints (in this case absolute but not as precise as the one provide by hall sensors).
The target is to find a trade off between:

- a precise and absolute estimation of the joint position;

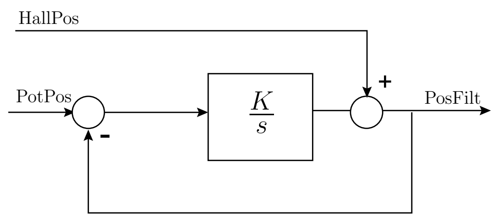

Figure 5.13: Filter for the fusion of the position information coming from motor (hall effect) sensors and joint potentiometers.

- a position information “in phase” with motor motion.

A possible solution is reported in Fig. 5.13: it is a simple low-pass filter on the signal coming from the potentiometer (PotPos), whose cut-off frequency is proportional to the gain K. In addition a feed-forward term given by the hall sensor's signal has been introduced at the output of the integrator. In this way (as shown by simulation reported in Fig. 5.14, where a sinusoidal motion with a frequency of 0.1 Hz is supposed) if K is sufficiently small (in the example $K = 0.1$) there is no delay between the hall sensor's signal (conveniently translated to make a clear comparison) and the filtered position (see Fig. 5.14.b). On the other hand, since, as shown in Fig. 5.14.a, there may be an initial error and a drift between hall sensor data and the real position of joints (directly measured), the feed-back loop guarantee that the filtered position asymptotically converge to the real value. By changing the value of K it is possible to make the filtered position more similar to the Hall sensor's measure or to the potentiometer's estimation: in the present application the sensors integrated in the actuators have been privileged (for the above mentioned constraint of co-location).

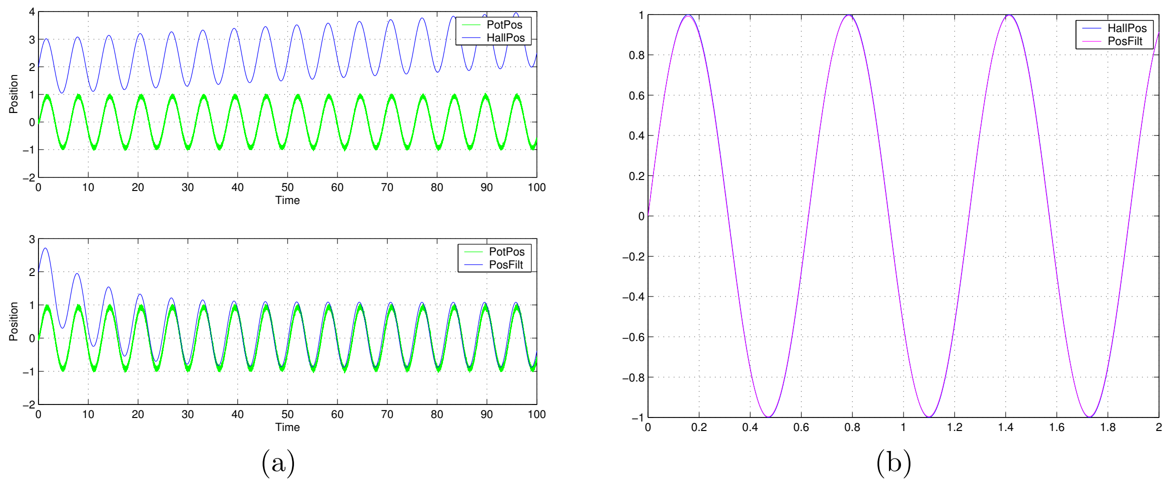

Figure 5.14: Performances of the filter for position measurement: tracking of the joint position (a) phase delay with respect to hall sensor signal (b).

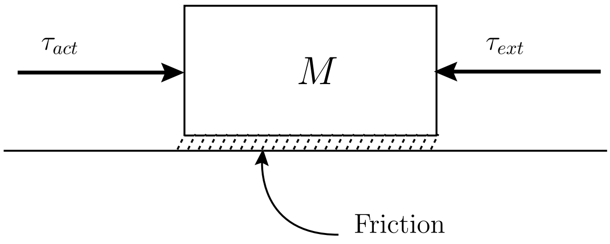

Figure 5.15: 1-dof robot manipulator.

As claimed at the beginning of this section, a second important problem in the experimental implementation of an impedance controller concerns the friction. Frictional phenomena on the joints and in particular "stiction", as widely substantiated in the previous section, prejudices the performances of the system in terms of both position tracking capabilities and application of desired forces. Therefore its compensation appears absolutely necessary.
A first way (very often adopted in practice) to achieve such compensation is adding to the control input a feed-forward term equal and opposite to the friction torque contribution. But, on the contrary to the standard robot applications, where the goal is to follow a desired trajectory with an error as small as possible, in the case of a robot hand also the interaction with the external environment must be taken into account.
Considering the friction model reported in (5.8) and the simple (1-dof) robot depicted in Fig. 5.15 (which can be used to model a single finger joint), where τ_{act} is the force applied by the actuator (and computed on the base of the implemented controller), and τ_{ext} a possible external force, an additive term able to erase the stiction effects is:

$$\tau'_{act} = \tau_S^{max} sgn(\tau_e) \quad \text{if} \quad \dot{\theta} = 0 \tag{5.30}$$

where τ_S^{max} is the maximum value of the static friction, $\dot{\theta}$ the speed of the robot and τ_e is the total force acting on the mass M:

$$\tau_e = \tau_{act} - \tau_{ext}$$

At this point some considerations are necessary:

- in order to estimate the value of τ_e, sensors on the joints able to detect the applied external torques are needed. Therefore the basic control strategy which does not require in principle force/torque transducers, can be enhanced by adding in the robot structure such kind of sensing technology. In the case of the DLR Hand torque sensors are actually integrated in the fingers' joints, and a compensation for the stiction can be implemented;

- besides additional force sensors, the friction compensation requires the estimation of the joint speed $\dot{\theta}$, which is usually achieved by differentiating the position signal; therefore the measure of the position must have a resolution as high as possible but unavoidably the velocity signal will be affected by noise (amplified by differentiation operation). The real implementation of the compensation term (5.30) will be:

$$\tau'_{act} = \tau_S^{max} sgn(\tau_e) \quad \text{if} \quad |\dot{\theta}| < \varepsilon$$

where ε is a parameter experimental chosen to discriminate when the speed is "practically" null;

- from the physical point of view, the effect of the additive term (5.30) it to inject energy in the system (composed by both the mechanical structure of the robot finger and the adopted controller); in order to preserve its stability it must be assured that the amount of this energy is smaller than the energy dissipated by frictional phenomena, and hence must be:

$$\begin{cases} \tau'_{act} = \tau^*_S sgn(\tau_e) \quad \text{if} \quad |\dot{\theta}| < \varepsilon \\ \tau^*_S = \min(\tau^{max}_S) \end{cases} \tag{5.31}$$

As a matter of fact the magnitude of the stiction components τ^{max}_S is, as reported in Sec.5.4.1 is extremely variable, therefore to avoid an overcompensation (which can lead to the instability) in every operative condition the choice of the coefficient of compensation term must be conservative and assume the minimum value of τ^{max}_S. Conversely, a real-time estimation of such term is not conceivable because its rate of change is comparable with the typical frequencies of the robot finger.

When the motion of the finger starts (that is $|\dot{\theta}| > \varepsilon$) a partial compensation of the dynamic friction is also performed; as a matter of fact, as shown in (5.25) dissipative terms make the system (robot, control and object) stable; nevertheless in order to avoid an an excessive loss of energy (especially for small velocities) and a discontinuous behavior of the finger when the speed is different from zero (and therefore the additive term for the stiction compensation vanishes) the coulomb friction term has been also compensated, by simply adding a constant torque contribution, whose sign depends from speed direction. Also in this case hold the same considerations previously done with respect to the stiction (in particular concerning the great variability of the parameters' values in different devices and in different conditions), therefore in order to avoid an overcompensation the additive term is

$$\begin{cases} \tau'_{act} = \tau^*_C sgn(\theta) \quad \text{if} \quad |\dot{\theta}| > \varepsilon \\ \tau^*_C = \min(\tau_C) \end{cases} \tag{5.32}$$

where τ^*_C is a term certainly lower than the real magnitude of the coulomb friction τ_C.

As a result of the extremely conservative estimates of the parameters τ^*_S and τ^*_C, the final compensation of the friction is quite rough and the performances of the impedance controller remain unacceptable, in particular for small values of the stiffnesses/gains K_{ii}. Otherwise, if bigger K_{ii} are assumed, the position tracking capabilities (when no interactions occur) are improved but the interaction forces will be too large to perform grasp and manipulation tasks. In particular in Fig. 5.16 the system (whose stiffness parameters K_{ii} are set to 1000 Nm^{-1}) is shown while tracks a position set-point: the performances in terms of error and coupling between the different direction of the work-space are in this case satisfactory.

Beside the friction, other elements makes the implementation of the controller shown in Sec. 5.5 quite different from the ideal target. As a matter of fact by simply coupling the target impedance (5.9) with the robot system, the overall system dynamics will be the sum of the two component dynamics as shown by eq. (5.11). In particular it is worth to notice that, even if in

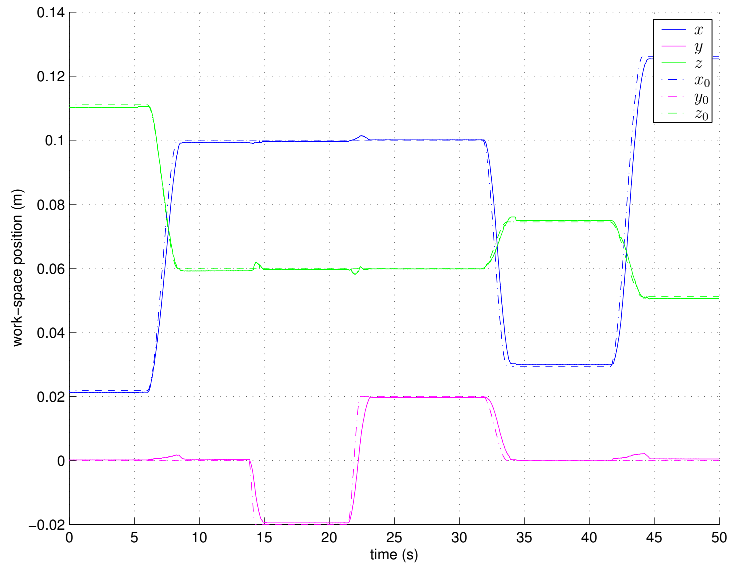

Figure 5.16: Tracking of a desired trajectory (x_0) by means of a passive impedance controller ($K_{ii} = 1000\ Nm^{-1}$).

the case of the DLR Hand fingers the term $\mathbf{C}(\theta, \dot{\theta})\dot{\theta}$ may be neglected, and the gravity has been explicitly compensated, nevertheless the inertia matrix $\mathbf{M}(\theta)$ of the robot remains and leads to a behavior of the system which depends on the specific configuration and is coupled along the different directions of the work-space.
In order to overcome these problems in the standard control approach, before imposing the desired impedance model, a compensation for the non-linear robot dynamics is performed [86]. Starting from task-space dynamics of the robot finger

$$\tilde{\mathbf{M}}(\theta)\ddot{x} + \tilde{\mathbf{C}}(\theta, \dot{\theta})\dot{x} + \tilde{\mathbf{G}}(\theta) + \tilde{\mathbf{F}}_{fric} = \mathbf{J}^{-T}\tau_{act} + \mathbf{F}_{ext} \tag{5.33}$$

which can be easily deduced from (5.7), the first step concerns the achievement of the dynamics behavior

$$\ddot{x} = u \tag{5.34}$$

by means of the controller

$$\mathbf{J}^{-T}\tau_{act} = \tilde{\mathbf{M}}(\theta)u + \tilde{\mathbf{C}}(\theta, \dot{\theta})\dot{x} + \tilde{\mathbf{G}}(\theta) + \tilde{\mathbf{F}}_{fric} - \mathbf{F}_{ext} \tag{5.35}$$

where u is an auxiliary input. Afterwards a target impedance, i.e. (5.3), can be directly imposed through

$$u = \ddot{x}_0 - \mathbf{M}^{-1}(\mathbf{B}(\dot{x} - \dot{x}_0) + \mathbf{K}(x - x_0) + \mathbf{F}_{ext}) \tag{5.36}$$

where $\ddot{x}_0$, $\ddot{x}_0$, x_0 are the desired task-space accelerations, velocities, and positions. In this case, as can be seen substituting (5.36) in (5.34),in ideal conditions, the target impedance behavior can be perfectly reproduced. But if the robot dynamics is not exactly known, the inverse task-space dynamics given by (5.35) will be corrupted by uncertainties and the final result will be quite far from the ideal one.

To reduce the effects of unmodeled dynamics and improve the capability of exerting desired (small) forces on the environment, the implementation of a cartesian impedance controller on the DLR Hand's finger must proceed in a different way and can not leave aside force sensing.

In particular two are the alternative approaches to the implementation of such a controller which exploit the force/torque sensors integrated in the fingertip and in the joints:

1. by constructing the controller over an explicit torque loop, see Fig. 5.17.a;
2. by basing the impedance controller on an inner position control loop, see Fig. 5.17.a.

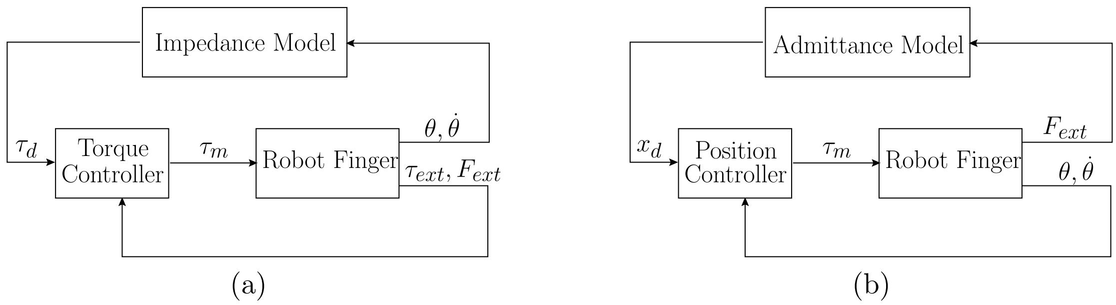

Figure 5.17: Impedance controller based on a inner torque loop (a) and on a inner position loop (b).

5.7 Torque-based impedance control

The so called passivity-based approach to the implementation of an impedance controller (shown in Sec. 5.5) is founded on the assumption that the robot (finger) can be adequately modelled as a rigid-body kinematic mechanism driven by controllable force actuators. This hypothesis, valid for direct-drive robot, is not true for the robot hand, object of this research activity: as shown in Sec. 5.4.1 the mechanisms adopted to perform the motion transmission (from the actuators to the joints) cause strong frictional phenomena which dissipate a considerable portion of the energy provided by motors. The results are those shown in previous section, with poor performances on position tracking as well as on the application of desired forces. To obtain good results and overcome the friction disturbance a possible solution is the implementation of a (high -gain) joint torque controller, on which the impedance model is constructed.
The conceptual steps of this approach are:

1. given the position/velocity inputs $x, \dot{x}$ (derived from the joint variables $\theta, \dot{\theta}$ by means of (5.5) and (5.6)) from the impedance model, e.g. (5.9), one achieves the corresponding forces $\mathbf{F}_z$;

2. the torques τ_d related to $\mathbf{F}_z$ can be obtained as:

$$\tau_d = -\mathbf{J}^T(\theta)\mathbf{F}_z \tag{5.37}$$

3. τ_d are used as set-point for the torque control loop, which generates the torque motor commands τ_m;

In the specific case of the DLR Hand, the torque controller has been obtained with a simple proportional (high) gain and an additive term (positive-definite) function of the speed which damps the system

$$\tau_m = \mathbf{K}_\tau(\tau_d - \tau_{ext}) - \mathbf{B}_\theta\dot{\theta} \tag{5.38}$$

The torque set-point is then computed according to the impedance model

$$\mathbf{F}_z = \mathbf{K}(x - x_0) + \mathbf{B}(\dot{x} - \dot{x}_0) \tag{5.39}$$

where the variables x_0 and $\dot{x}_0$ are the virtual (because if an interaction with the environment occurs they can not be reached) positions and speeds and $\mathbf{K}$, $\mathbf{B}$ are assumed definite-positive and symmetric. In particular, as already mentioned, in the performed experimental tests this matrices have been considered diagonal; this does not prejudge the generality of the control, as a matter of fact, considering only linear displacements (as in the current application), the system which plans the motions (and therefore provides the values of x_0 and $\dot{x}_0$) certainly will choose the desired value of stiffness/damping along the different directions of the work-space according to the task to be performed, without any coupling between displacements along a particular direction and forces exerted in another one. In the general case these directions will be not coincident with those of the base frame associated to the finger (but they will be aligned with the frame normal to the surface at the desired point of contact) and hence $\mathbf{K}$ (and in the same manner $\mathbf{B}$) must be defined (by means of a singular value decomposition) as:

$$\mathbf{K} = \mathbf{R}\ \mathbf{K}'\ \mathbf{R}^T$$

where $\mathbf{R} = [r_1\ r_2\ r_3]$ is an orthonormal matrix representing the principal axis of stiffness (in the base frame) and $\mathbf{K}'$ a diagonal matrix, whose elements define the magnitude of stiffness along the directions r_i. By taking $\mathbf{K}$ and $\mathbf{B}$ diagonal, implicitly it is assumed that $\mathbf{R}$ is equal to the identity matrix.

The overall scheme of the impedance controller based on an inner torque loop, is reported in Fig. 5.18 while Fig. 5.19 shows a meaningful experimental test: the robot finger interacts with an obstacle placed along the x_b direction; in particular the metallic case of a PC, whose dynamic behavior is quite stiff but not very well damped, has been used as test-bed.
Despite the robotic finger, steered by this controller (whose stiffness parameters K_{ii} have been set to 50 Nm^{-1} and the damping terms B_{ii} to 5 Nsm^{-1}), is able to follows position trajectories with small errors, when interacts with the environment shows some instability phenomena. During the transition between unconstrained and constrained motion some oscillations occur and make the behavior of the finger absolutely unacceptable. The cause is probably the high gain of

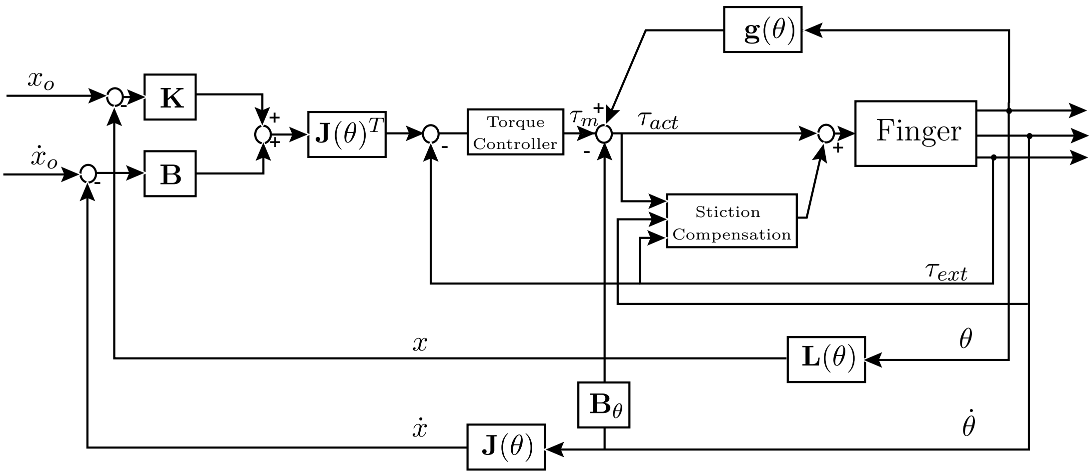

Figure 5.18: Impedance controller constructed over an explicit torque loop.

the torque controller which reduces the effects of the friction and of the other uncompensated dynamics terms, but on the other hand tends to destabilize the controller itself and to amplifies the measurement noise. In particular, force and torque sensors based on strain gauges are usually characterized by a considerable electric disturbance overlapping the signal of interest, and however a (heavy) filtering is not conceivable, since the stability of the overall system depends on the bandwidth of the basic torque control (especially if big value of K_{ii} are considered). Due to the same reason, is not possible to reduce the gain $\mathbf{K}_\tau$ of the controller under a certain value or add more damping.

Another important drawback of this control strategy is that the control signal (and therefore the behavior of the finger) strongly depends from the finger configuration, and in particular near to singularities the system exhibits a behavior quite far from the desired one; the following example can be explanatory: because of the relation (5.37) from task-space forces to joint torques (which also maps control forces into desired torques) when the robotic finger is upright (that is in the singular configuration given by $\theta_3 = 0$), it is infinitely rigid along its axis and the control in the same direction (i.e. a virtual displacement Δx is imposed in this direction) is null; as a matter of fact, in this condition, the Jacobian is no more full rank and

$$\mathbf{K}\Delta x \quad \in \quad \mathrm{Ker}(\mathbf{J}(\theta)^T)$$

Therefore

$$\mathbf{J}(\theta)^T\mathbf{K}\Delta x = 0$$

and no motion can happen along this direction even if an external force acts on the system or a position set-point is given, despite the goal is to have in each position of the cartesian space the equivalent of a spring/damper/mass system. In the practical cases, singularities are not a simple set of points, but rather a set of regions where the behavior of the manipulator is critical. By using this control approach (which exploit the transposed Jacobian) the stiffness (and more generally the impedance) of the finger is similar to that programmed, only if its configuration

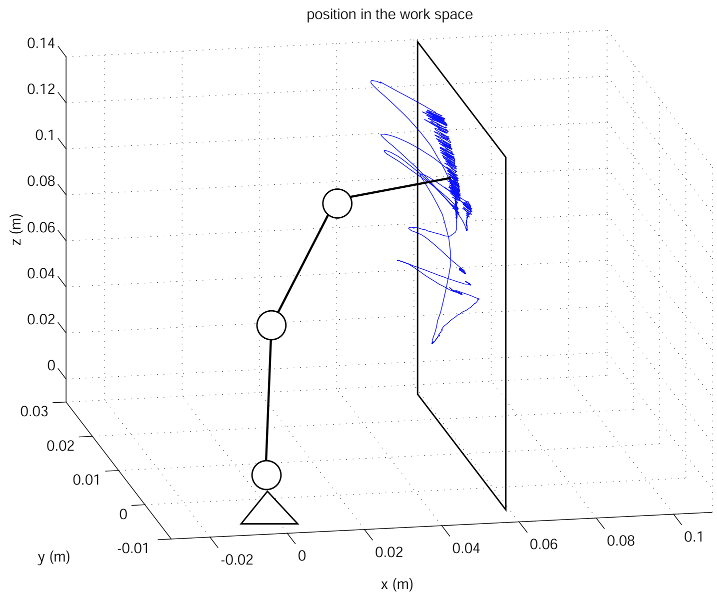

Figure 5.19: Interaction of the robotic finger with a wall placed in x_b =const (with an impedance controller based on a inner torque loop).

is far enough from a singularity. Conversely, the goal is to achieve a behavior as uniform as possible in each point of the work-space.

5.8 Position-based impedance control

An alternative solution for the implementation of a cartesian impedance controller exploits an underlying position loop. According to this approach the robot receives as input a force and gives as output a position; for this reason this control approach is usually pointed out as "admittance control". However, it is worth to notice that the causality (mentioned in Sec. 5.3) between the behavior of the robot manipulator and that of the environment is not lost: as a matter of fact the environment obviously remains an admittance (which therefore determines the position/velocity of the interaction port), the robot becomes also an admittance, but, interposed between them, there is the force sensor which can be modelled as an impedance (and in particular a spring). In this case the conceptual steps are:

1. given the force inputs $\mathbf{F}_{ext}$ (directly measured by means of the sensor collocated at the finger end-point) from the desired admittance model one achieves the corresponding positions/speeds ($x_z/\dot{x}_z$).

2. the position $x_z(t)$ is employed as set-point for the position control loop, which generates the torque motor commands τ_m;

As in the case of the auxiliary torque loop, also in this approach the high gain position controller is able to compensate for friction (and more generally for unmodelled dynamics), but equally

instability problems can arise, in particular for low desired stiffness and damping, for which the bandwidth of the external (admittance) loop approaches the position bandwidth. A further drawback found in the practical implementation of this controller is in the vicinity of singularities, where fast and destabilizing movements can occur [87].
In the following a specific implementation of this general approach is presented. At first an impedance target is chosen; as in previous cases has been adopted the linear model

$$\mathbf{F}_{ext} = \mathbf{M}\ \ddot{x}_z + \mathbf{B}\ (\dot{x}_z - \dot{x}_0) + \mathbf{K}\ (x_z - x_0) \tag{5.40}$$

where x_0 is the virtual point position, and $\mathbf{M}$ $\mathbf{B}$, $\mathbf{K}$ are definite positive matrices which can be written as:

$$\mathbf{T} = \mathbf{R}\ \mathbf{T}'\ \mathbf{R}^T$$

with $\mathbf{R} = [r_1\ r_2\ r_3]$ orthonormal matrix and $\mathbf{T}'$ diagonal. Given the external force $\mathbf{F}_{ext}$ measured by the fingertip force/torque sensor and expressed in the base frame [3], and the two inputs x_0 and $\dot{x}_0$ which allow to define desired position and velocity trajectories, the solution of the differential equation (5.40) provides in each instant the position (and speed) of a system with the desired behavior (and with the real force affecting the robotic finger as input). At this point, it is enough to impose this behavior (in terms of positions/velocities) to the manipulator, that is to assure that all the time

$$x\ \equiv\ x_z$$

An immediate solution is to couple the output of the impedance model with the passive controller described in Sec. 5.5 (and reported in Fig. 5.10)

$$\tau_{act} = \mathbf{K}_x(x_d - x) + \mathbf{B}_x(\dot{x}_d - \dot{x}) \tag{5.41}$$

that for high gains ($\mathbf{K}_x$) assures good position tracking capabilities and very nice properties of robustness.
The overall complete scheme, where the terms for stiction and gravity compensations are also reported, is shown in Fig. 5.20. As already stated, this scheme makes use of the force/torque sensors installed in the fingertips of DLR Hand (and which often are part of the standard sensory equipment of a robotic hand), where the interaction is expected; therefore the measure is certainly betters than that provided by torque sensors placed on the joints and is not affected by the configurations of the finger (i.e. singularities).
This force measure is transformed into a position by means of the impedance model, which can be rewritten (without the inputs x_0, $\dot{x}_0$) as

$$\frac{\mathbf{X}(s)}{\mathbf{F(s)}} = \frac{1}{s^2\ \mathbf{M} + s\ \mathbf{B} + \mathbf{K}} \tag{5.42}$$

Hence the force signal is implicitly filtered by a low-pass filter whose cutoff frequency depends on the impedance parameters. Moreover the high-gain loop is based on position signals, which are characterized by very low level of electrical noise; as a matter of fact the Hall effect sensors

[3] $\mathbf{F}_{ext} =\ {}^b\mathbf{R}_t\ \mathbf{F}_s$, with $\mathbf{F}_s = [F_{sx}\ F_{sy}\ F_{sz}]^T$ vector of the force components provided by the force sensor, and ${}^b\mathbf{R}_t$ rotational matrix from the fingertip frame (coincident with the sensor frame) to the base frame

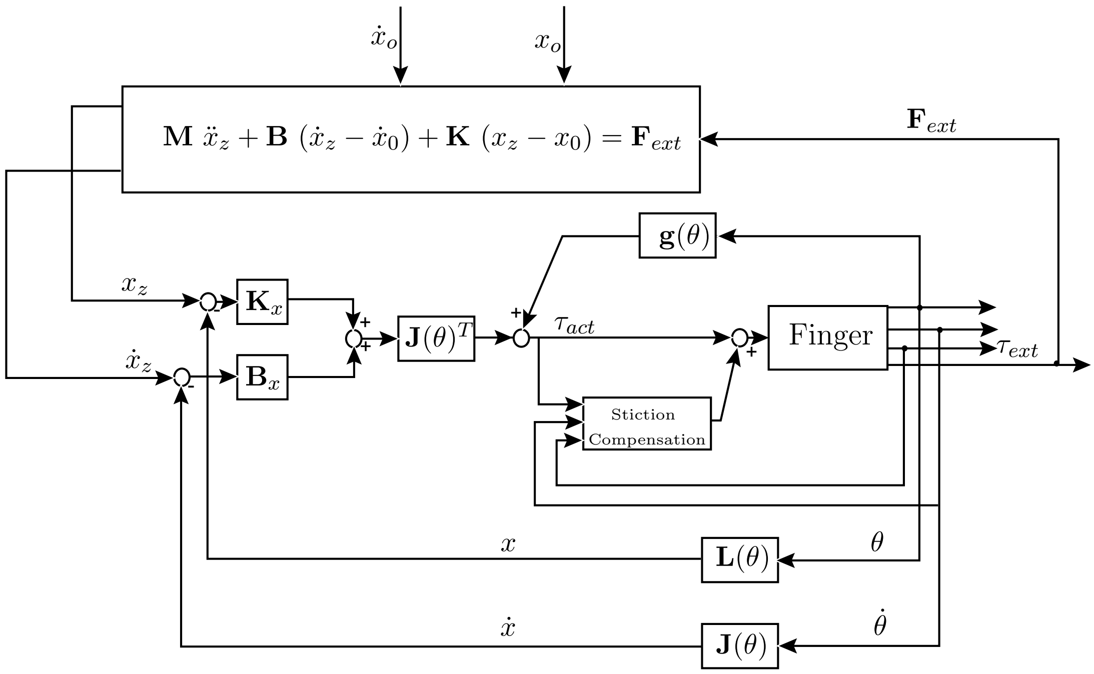

Figure 5.20: Impedance controller constructed over an inner cartesian position control.

placed on the motor provide a signal with a very high resolution, because of the mechanical reduction of the motion, and the ratio signal/noise is very favorable.
As a consequence, electrical disturbances have only a little influence on this control scheme, and the behavior of its real implementation is similar to the ideal case.

Nevertheless some important drawbacks occur:

- the performances of the position control loop depends on the finger configuration; as a matter of fact this controller is nothing but a PD controller, whose proportional gain is given by $\mathbf{K}_x\mathbf{J}(\theta)^T$ and hence is depending on the joint position θ through the transposed Jacobian. As for the controller based on the inner torque loop reported in Sec.5.7, in this case the same problems arise near to singularity conditions, where the robotic finger "loses" a degrees of freedom. In these configurations the force sensor (which is directly placed on the tip) is able to detect the forces exchanged with the environment, the impedance model provides the corresponding displacements in the task-space but the position controlled robot cannot follows these trajectories. The solution usually adopted to overcome this drawback is to avoid that a singularity occurs by properly planning the desired trajectories. This is not possible in the case of a robotic hand driven by an impedance controller, for a number of reasons.
  First the singular configuration corresponding to $\theta_3 = 0$ (that is upright finger) is usually the starting point for any grasp/manipulation task; and also in our everyday life we can observe that hand configurations with some extended fingers are very important and fre-

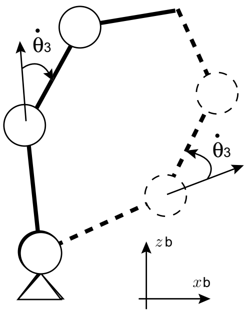

Figure 5.21: Joint configurations of the robotic finger corresponding to the same end-point.

quently employed.
Furthermore, even if the planned trajectory are far enough from a singularity, the actual position of the robotic finger depends also on external environment (through $\mathbf{F}_{ext}$) which can steers the manipulator into (or simply near) a "forbidden" configuration.

- As shown in Sec. 5.5 the position control based on transposed Jacobian assures the stability of the robot finger in the task-space and the convergence to the equilibrium point $x = x_z$, but not the stability of the configuration of the manipulator. In the case of the DLR Hand fingers there are not extra degrees of freedom (but to the three task-space variables x, y, z correspond exactly three joint variables θ_i) and therefore the stability of x implies that of θ. Anyway in joint space is not possible stated the global asymptotical stability of the system: if for simplicity we consider the planar manipulator obtained by blocking the adduction/abduction joint, without limit in the joint motion, it can reach any end-point position (not in the boundary of its workspace) at two joint configurations (the "left-hand" and the "right-hand" solutions of the inverse kinematic equation), as shown in Fig. 5.21.
 Indeed, the joint motions are limited (in particular $\theta_3 \geq 0$) therefore only a configuration is really allowed; nevertheless, by means of the controller based on the transposed Jacobian it is not possible take into account these constraints, and in some case happens that is depicted in Fig. 5.22: give a some virtual point x_0, the finger moves towards the "wrong" configuration (see Fig. 5.22.b), but clearly the joint position θ_3 remains equal to zero. At the end, the finger remains in a singularity configuration where the magnitude of the control is null or too small to overcome the uncompensated friction phenomena (Fig. 5.22.c) and the desired set-point is not reached, even if no interaction occurs.
 Also in this case, an immediate solution consists in a proper planning of the virtual point trajectory but unfortunately the real set-point x_z also depends on the external forces $\mathbf{F}_{ext}$ (which are unknown and not controllable).

To solve the above mentioned drawbacks, preserving at the same time the positive properties of the controller so far constructed (smooth behavior in the neighborhood of a singularity, robustness, use of transposed Jacobian and not of its inverse) a further control term in the position loop is added.
The criteria which leading to its choice is clear if we consider the potential energy of the overall system (robot + position control) expressed in the joint variable space. As a matter of fact,

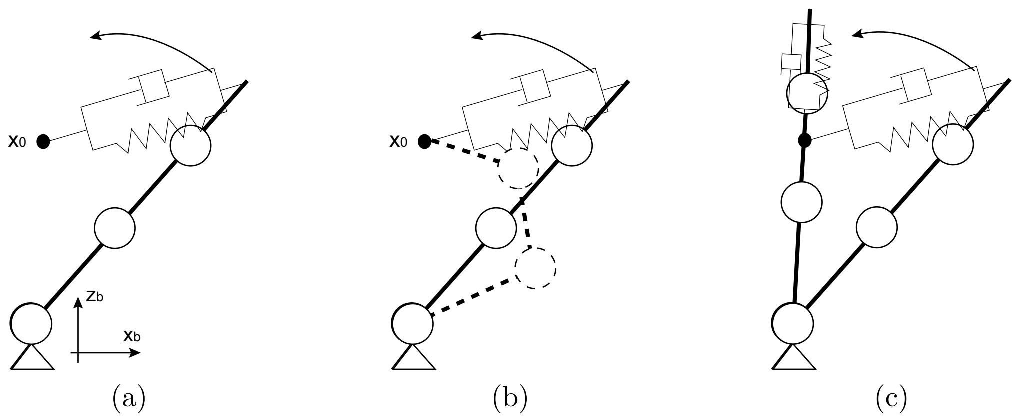

Figure 5.22: Motion of the robotic finger under the impedance control based on task-space position loop: effect of joint limits.

as reported in Sec. 5.5, the position controller has been achieved by reshaping the potential energy of the physical robotic system, by compensating the potential associated to gravity field and adding an elastic potential whose minimum corresponds with the desired set-point x_0. As already stated, if the total potential energy is reported in the joint space, there is not a unique minimum but two configurations of minimum energy exist, see Fig. 5.23.a. In order to drive the

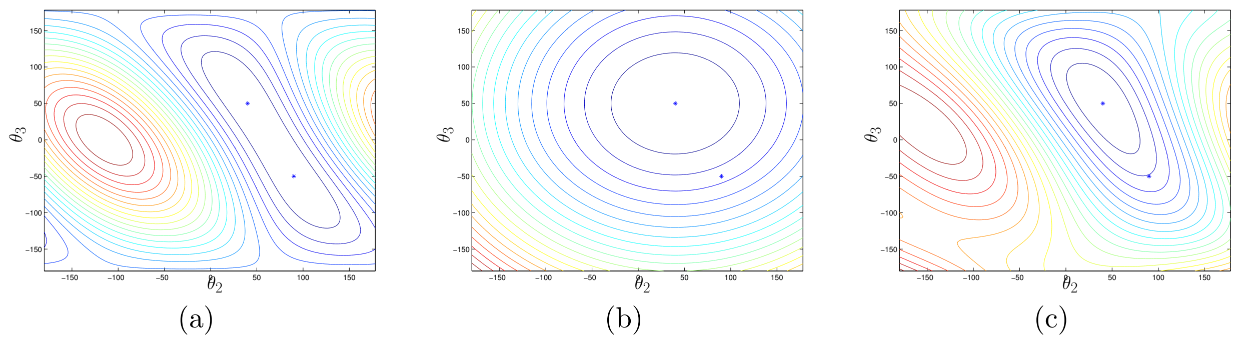

Figure 5.23: Iso-potential contours of the energy (expressed in the joint space) associated to the elastic term $\mathbf{K}_x \, \Delta x$ (a), to the elastic term $\mathbf{K}_\theta \, \Delta\theta$ (b), and to their sum (c).

system towards the (unique) desired configuration the principle of *superposition of impedances*[4] can be exploited: as a matter of fact, the dynamic behavior of the manipular is given by the simple addition of the component impedances.
According to this principle it has been added a potential contribution whose minimum coincides with the feasible configuration

$$\theta_d = \mathbf{L}^{-1}(x_d) \quad \text{with} \quad \theta_{d3} \geq 0$$

[4]the position controller is nothing but an impedance controller with very high stiffness values.

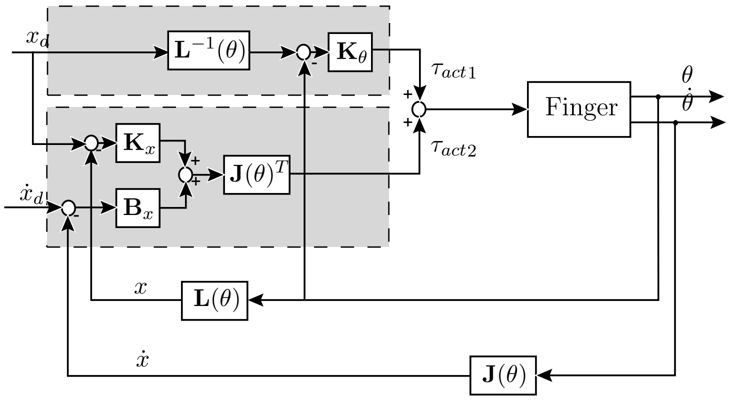

Figure 5.24: Basic position control.

that is the elastic potential

$$U_k = \frac{1}{2}(\theta - \theta_d)^T \mathbf{K}_\theta (\theta - \theta_d) \tag{5.43}$$

with $\mathbf{K}_\theta$ positive-definite diagonal matrix.
The overall potential energy given by the contribution of the virtual spring in the work-space and of that in the joint-space is depicted in Fig. 5.23.c: in this case a unique minimum exists and coincides with the desired position. Therefore the system will move towards this configuration. In terms of forces/torques acting on the system, the new potential means an additional control term

$$\tau_{act} = -\tau_{K_\theta} = \mathbf{K}_\theta(\theta_d - \theta) \tag{5.44}$$

which corresponds to an elastic torque acting on the joints and whose stiffness is $\mathbf{K}_\theta$. The choice of this last parameter is particularly crucial. In fact (5.44) is a (proportional) controller in the joint space which can be adopted alone to accomplish the position servo loop. But it is also the cause of that "nervous" behavior of robot system in the neighborhood of singularities which has been experimentally observed [87].

By recalling that the variation of the joints' configuration due to a variation of the end-point position can be approximated as

$$\Delta\theta \;\simeq\; \mathbf{J}^{-1}(\theta)\Delta x \tag{5.45}$$

the terms (5.41) and (5.44) can be described with the following mappings:

$$\Delta x \;\xrightarrow{\mathbf{K}_x}\; F_{act} \;\xrightarrow{\mathbf{J}^T}\; \tau_{act} \tag{5.46}$$

$$\Delta x \;\xrightarrow{\mathbf{J}^{-1}}\; \Delta\theta \;\xrightarrow{\mathbf{K}_\theta}\; \tau_{act} \tag{5.47}$$

For the sake of simplicity, only the static relations between Δx and τ_{act} are considered. This means that the derivative parts of (5.41) is neglected, but this does not prejudice the validity of the overall analysis. Since, in particular, we want to consider the effects of the Jacobian on the control action, a further simplification is performed, that is the stiffness matrices are considered identity. This leads to

$$\mathbf{K}_x = \mathbf{I}_2 \quad \Rightarrow \quad \Delta x \quad \xrightarrow{\mathbf{J}^T} \quad \tau_{act} \tag{5.48}$$

and

$$\mathbf{K}_\theta = \mathbf{I}_2 \quad \Rightarrow \quad \Delta x \quad \xrightarrow{\mathbf{J}^{-1}} \quad \tau_{act} \tag{5.49}$$

Therefore, the relations between a displacement Δx and the resulting torque control are given by $\mathbf{J}^T$ and $\mathbf{J}^{-1}$. Obviously these relations have only a numerical (and not physical) meaning; as a matter of fact in (5.48) Δx is a linear force (expressed in N) numerically identical to the corresponding displacement.

To understand the effects of these two relations, we have defined a tool similar to the "manipulability ellipsoids", which show how velocities and torques are transmitted from joint-space to the task-space by a particular robotic structure in a specific configuration [88]. In this case the converse operation has been done, that is we have defined two ellipsoids which represent how a displacement, with amplitude one, is mapped into the space of the control torques by (5.48) and (5.49).

The two ellipsoids, which display the *sensitivity of the control* to a variation of the set-point, are defined by

$$\Delta x^T \Delta x = 1 \Rightarrow \tau_{act}^T \mathbf{J}\mathbf{J}^T \tau_{act} = 1 \tag{5.50}$$

and

$$\Delta x^T \Delta x = 1 \Rightarrow \tau_{act}^T (\mathbf{J}\mathbf{J}^T)^{-1} \tau_{act} = 1 \tag{5.51}$$

They are depicted in Fig. 5.25, where for sake of clarity the 2-dof planar robot, obtained

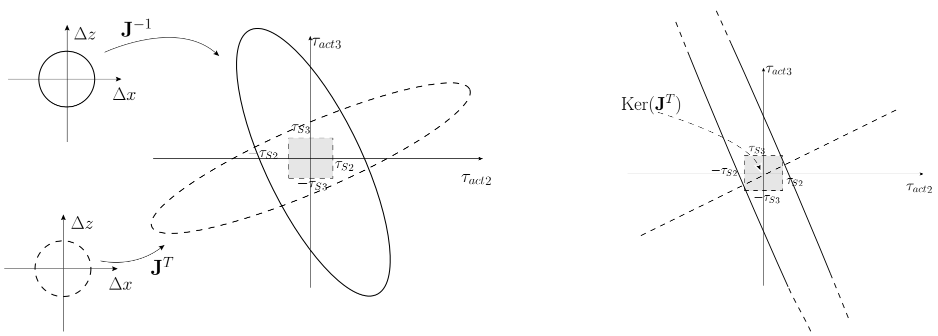

(a) (b)

Figure 5.25: Sensitivity of the control to variations of Δx considering a configuration of the robotic finger far from (a) and close to (b) a singularity.

by blocking the adduction/abduction joint of the finger, is considered. As a matter of fact, the reachable singular configurations depend only by θ_3, while the the first joint (θ_1) does not play any role. As for standard position/force manipulability ellipsoids, the principal directions of (5.50) and (5.51) are the same, while the lengths of axis are inversely proportional. This

suggests that in those directions (of workspace) where the control approach (5.41) gives the smallest contribution with respect to a position displacement Δx, (5.44) produces the largest control torques and *viceversa*.
In particular if the singular condition $\theta_3 = 0$ is taken into account (as reported in Fig. 5.25.b) there are some task-space directions, where torques corresponding to (possibly large) position variations, computed by means of the control approach exploiting the transposed Jacobian (that is (5.46)), are null ($\Delta x \in Ker(\mathbf{J}^T(\theta))$). In this case the finger can not follow any trajectory along these directions. In practice it is necessary to consider not only the point $\tau_{act} = 0$ but also a region which depends on the static friction magnitude τ_S (see Fig. 5.25.b). If the control torques belong to this region, the robotic finger keeps still.
Conversely, the control approach (5.47) provides, along these directions, a theoretically infinite contribution. As already stated, (5.45) is only an approximation, and the actual torque computed on the basis of (5.44) will be limited ($(\theta - \mathbf{L}^{-1}(x_d))$ is certainly bounded), nevertheless the corresponding ellipsoid gives an insight into the behavior of this class of controllers: when the robot (finger) is close to a singularity there are some directions where the control torques are very large because of small variation of Δx. In this way it is possible to explain that "nervous" behavior that robots, position controlled in the joint space, exhibit near to a singularity, and the great sensitivity to the noise of the sensors.
The use of matrices $\mathbf{K}_x$, $\mathbf{K}_\theta \neq \mathbf{I}_2$ does not change the results. As a matter of fact, these matrices are usually taken diagonal and with the same (or similar) values[5], and therefore their effect is to amplify the ellipsoids, without changing their shape.
If controller different from simple gains are adopted, the considerations so far reported give anyway a qualitative idea of the final result: by directly implementing a controller in the task-space there will be tracking problems near to a singularity, conversely if the controller is carried out in joint-space it will be extremely sensitive to small variations of the position error Δx (due to variations of the set-point or the noise on position measure).

By combining the two position control approaches, in the work-space and in the joint-space, which are shown in Fig. 5.24 it is possible to assure good performances in every configuration. To avoid that the control (through (5.44)) could be too sensitive to small variations of x_d in singularity configuration, the components of $\mathbf{K}_\theta$ are kept as small as possible: (5.44) must assure the tracking of a generic position trajectory only in the neighborhood of the singularity, while when the finger is far enough by a singular configuration the main control action is provided by (5.41).

In Fig. 5.26 the complete control scheme is reported with:

- the terms for the compensation of the gravity and of the stiction;
- the overall position loop;
- the differential equation which represents the impedance model and which must be solved in real-time.

[5]there is no reason to have different "gain" along different directions in a position controller.

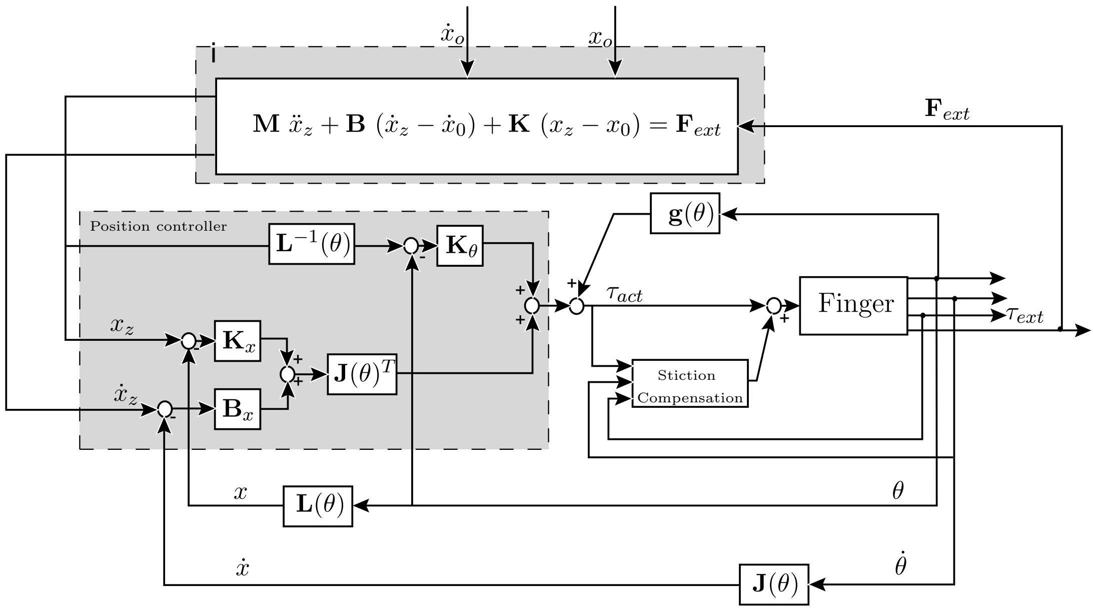

Figure 5.26: Impedance controller constructed over an inner cartesian/joint position control.

It must be noticed that this scheme does not make use of the inverse Jacobian and therefore no computational problems arise. The work-space positions (coming by the target impedance model) are directly transformed into motor torques (by means of $\mathbf{J}(\theta)^T$) or into feasible joint positions (through the inverse kinematics which for the finger is available in the closed form). The position loop in joint-space exploits the natural damping (viscous friction) of the robot and hence does not require any damping injection.

In the Fig. 5.27 the performances of the impedance controller are shown, when no interaction with the environment occurs. In particular the adopted parameters are reported in Tab.5.3.

Despite the very small values of stiffness and the unavoidable (small) errors on force measurement, the system is able to follow desired trajectories with acceptable errors, i.e. 1 mm, (the goal of a robot hand is the interaction with the environment more than the absolute precision in positioning) and also the couplings between the different directions are negligible. Obviously

K_{ii}	50	Nm^{-1}
M_{ii}	0.1	Kg
B_{ii}	4.5	Nsm^{-1}
K_{xii}	500	Nm^{-1}
B_{xii}	25	Nsm^{-1}
$K_{\theta ii}$	1	$NmRad^{-1}$

Table 5.3: Parameters of the overall impedance controller based on a position loop.

if better performances are required, it is sufficient rising the stiffness values.

When an interaction happens (in this case $K_{11} = 50$ along x, while in y and z directions of the

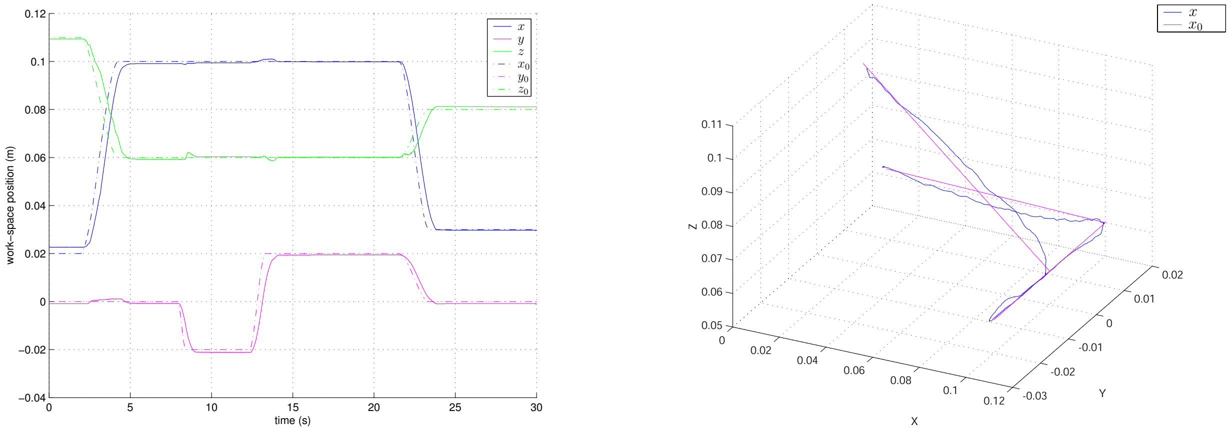

(a) (b)

Figure 5.27: Performances of the position based impedance controller in joint-space (a) and in work-space (b).

workspace $K_{ii} = 200$) the system maintains a stable behavior, as shown in Fig. 5.28, where the finger meets an obstacle along the x_b direction. In this case the finger behaves almost like an ideal (decoupled in the work-space directions) spring; as a matter of fact $F_x = K_{11}(x_0 - x)$ with good approximation while F_y and F_z are quite small despite the high stiffness values and the coupling due to the friction of the contact; moreover, during the contact phase, the virtual point is moved in y and z directions (where no constraints exist) and the fingertip is able to follow this set-point. It is worth to notice that when the z position of the finger changes also the x moves: the reason is the fact that the adopted model considers a punctual fingertip, indeed the finger end point has a precise shape, and due to its rotation the tip frame position (and therefore the x position) changes.

Finally in Fig. 5.29 a motion of the finger starting from a singularity configuration is reported: the tracking error is quite large, but it is possible to improve the performance of the controller by acting on $\mathbf{K}_\theta$ (by taking a higher gain this error can be reduced but the behavior of the finger will be probably less smooth in critical configurations).

5.9 Conclusions

A cartesian impedance controller has been realized. This strategy which “transforms” the fingertips of the DLR Hand II (used for fine manipulation tasks) into mass-spring-damper systems (whose parameters can be arbitrarily chosen) allows to greatly simplify task planning operations. The proposed solution exploits the overall sensor equipment of the hand (motor position sensors and joint potentiometers, joint torque sensors and the fingertip force/torque transducer) to achieve a controller robust with respect to:

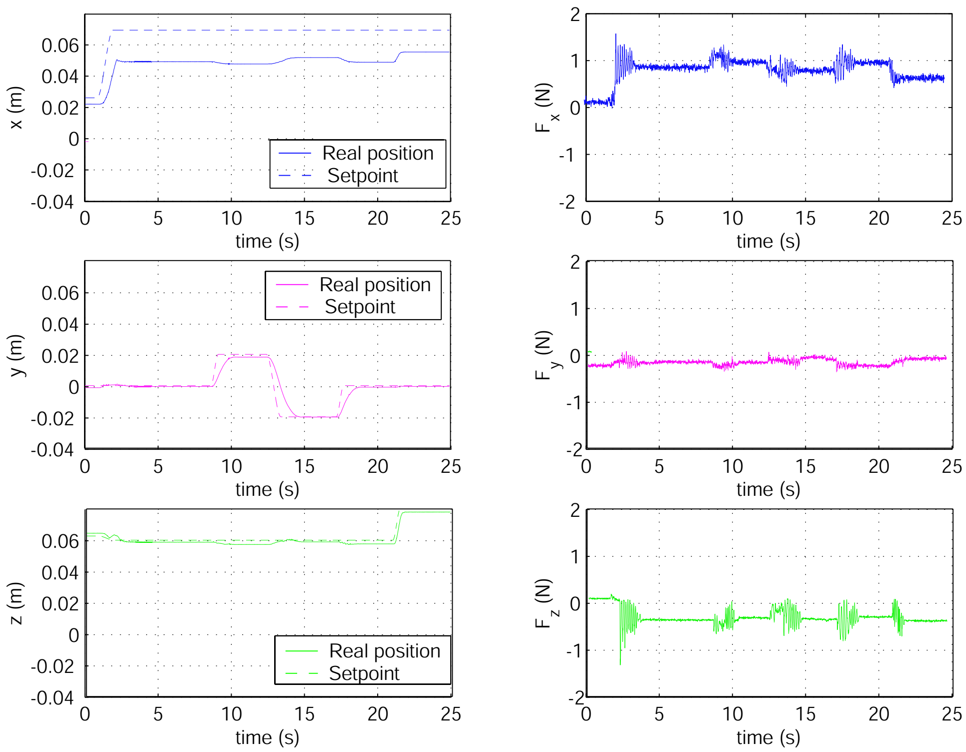

Figure 5.28: Interaction of the robotic finger (steered by an admittance controller) with an obstacle placed in $x_b = const$.

- friction and unmodeled dynamics of the finger;

- singularity conditions of the kinematic structure.

The result is a robotic system whose end-point has a smooth behavior decoupled in different directions of the workspace, and stable during the interaction with a wide class of objects.

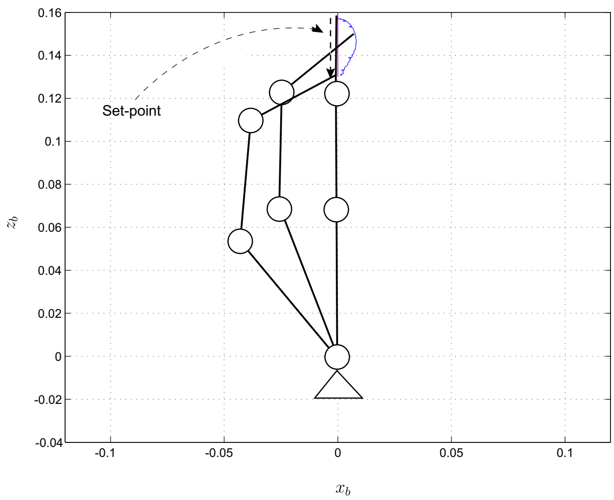

Figure 5.29: Tracking of a trajectory starting from a singularity condition with the complete admittance control.

Chapter 6

Towards a new kind of dexterous robotic hands

This Chapter describes the development, from the early idea to a working prototype, of a new kind of articulated robotic fingers, which is the basic element for a new hand for dexterous manipulation. This research summarizes in real terms the idea developed over this thesis and in this sense it is the right conclusion of the overall work; in particular it shows how, by means of a proper integration between the design of the physical structure (mechanical frame as well as sensory equipment) and the choice of the control strategies, it is possible to achieve a general simplification of robotic devices for dexterous manipulation.

6.1 Issues in robotic end-effectors design

As reported in Chapter 2, in the last two decades, a number of advanced robotic end-effectors has been developed in the laboratories of universities and institutions (e.g. [2, 3, 4, 5, 6, 7]). Main aim of these robotic devices is to reproduce the functional capabilities (and often the structure) of the human hand, and hence are usually named “hands”.
In the ‘80s, the seminal works of Salisbury and Jacobsen paved the way for dexterous robotic hands, that is hands able to deal with unknown objects, in a possibly unstructured environment. Afterwards several devices have been designed with the main purpose of achieving dexterity. These end-effectors are characterized by different mechanical structures, sensory equipments and control strategies, but all of them share a common drawback, that is the *complexity* of both the hardware and the software.
As a matter of fact dexterous manipulation requires a high number of controlled degrees of freedom and consequently a large number of actuators, which must be hosted in an extremely small space (if a self-contained device is aimed). Salisbury [89] showed that a minimum of 9 dofs are necessary to perform manipulation tasks, under the hypothesis of hard contact model,

but if soft contacts are considered this number grows.
At the same time, in order to achieve dexterity, an adequate sensing apparatus, including ,besides the standard position sensors, other sensors able to detect forces/torques exchanged during the interaction with the environment, is necessary (see Sec. 2.3). If the richness of force and tactile information greatly contributes to the overall dexterity of a hand (as well demonstrated by the human beings), on the other side it requires a noticeable growth of complexity.
Therefore, a structure, with the typical dimensions of a human hand, must host actuators, mechanical transmissions, sensors and electronics. In order to cope with this very limiting constraint, a natural solution is to jointly design the hand and the arm (examples of this approach are the Robonaut hand [5], the UB-Hand II [2]), reproducing in some way the human model. As a matter of fact, in an *integrated system* (hand + arm) the constitutive components can be distributed in the whole structure. In particular, the choice of integrating the hand and the arm with simultaneous design allows the placement of actuators (which, because of the available technology, are usually very bulky) in the forearm. But an obvious drawbacks arises from this choice, that is the impossibility of separating the hand from the arm.
Conversely, some hands have been designed independently on the carrying robot manipulator (examples of this approach are the DLR Hands [3, 4], the Barret Hand [35],...), and because all the components must be placed in their structure, the size of such modular hands is larger with respect to the human hand, the grasping forces are often weaker and the overall design seems complex and not enough reliable.
Often the hand design is neither *integrated* nor *modular*, but the actuation system is simple located remotely, in a separated structure. These devices are usually laboratory tests, developed to show the effectiveness of a particular kinematic structure and of a certain sensory equipment but without the precise target to produce a "usable" robot hand. The same impression comes out from the fact that in these projects, reliability and costs are factors often underestimated if not at all neglected. Conversely, if we consider commercial hands, like the Barret hand, this issues are prevalent, at the expense of a lower functional effectiveness.

6.2 An integrated approach to the development of a new robotic hand

If dexterous hands are too complex, and conversely commercial hands have low functional capabilities, is it possible to find a trade-off between these opposite trends? If so, how can this trade-off be found? In the following, a possible answer to these basic questions is given.
In the design of a new robotic finger(/hand), problems like:

- complexity,
- reliability,
- costs,

have been faced since the beginning, together with functional specifications, adopting a mechatronic approach. That may sound obvious: as a matter of fact, all the examples of robotic hands reported in Chapter 2 show a deep integration between mechanic and electronic parts.

Nevertheless, according the definition of mechatronics given by IRDAC (Industrial Research and Development Advisory Committee) of the European Union [90] it is evident that often robotic hand design and development are not strictly mechatronic. As a matter of fact, this definition states that:

> *The term mechatronics refers to a synergistic combination of precision engineering, electronic control and system thinking in the design of products and manufacturing process. It is an interdisciplinary subject that both draws on the constituent disciplines and includes subjects not normally associated with one of the above.*

Conversely, in robotic hand design, the third element commonly recognized in a mechatronic design, that is information technology and control theory [90, 91], is often added in a second stage, after the design of the hardware (see Fig. 6.1.a). In this way, the control algorithms must be compliant to a specific structure, and cope with the drawbacks that such a structure may present. This approach adds complexity to complexity (as a matter of fact control strategies must already manage a large number of actuators and an equally large number of sensors in order to get the desired capabilities). In particular, side effects of the mechanical design need sometimes heavy compensations. For instance, friction phenomena or backlashes in the motion chain require the adoption of additional sensors (e.g. joint position sensors or torque/force sensors) as well as suitable (and not always completely effective) control strategies. An example of this design approach, actually widespread in the dexterous manipulation field, is reported in Chapter 5: an impedance controller, able to steer the fingers of the DLR Hand II during manipulation tasks, has been constructed on the basis of the structure and the features of the hand itself; obviously the final control scheme is quite complex (as shown in Fig. 5.26), despite the controller itself is an attempt to simplify the system.

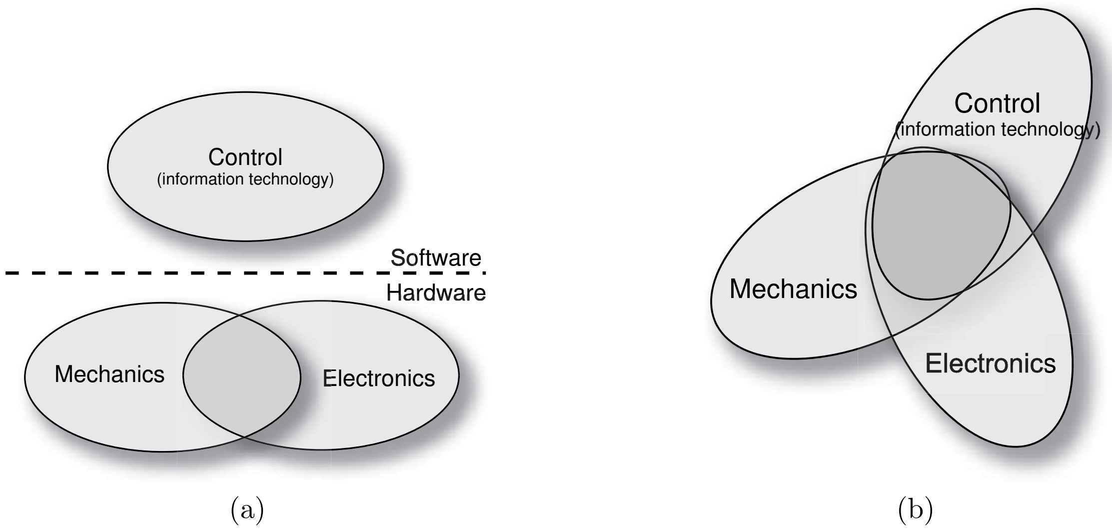

Figure 6.1: Traditional approach to robotic hand design (a) and fully mechatronic design approach (b).

In order to reduce the overall complexity of an articulated robotic hand preserving its dexterity, in this research activity, a traditional mechatronic approach has been assumed, and, besides the mechanics and the electronics, also control issues have been taken into account from the beginning. In this way it has been possible to exploit the positive features of each component, and to optimally balance each part.
Since, as stated in the definition of mechatronics this approach is strongly interdisciplinary and requires the interaction of researchers belonging to different areas, the development of this new robotic hand is done jointly with the colleagues of the mechanical department (DIEM) and in particular with the research group of Professor Vassura. The contribution given by this thesis concerns:

- the choice of a suitable sensory equipment;
- the development of the most adequate control strategies.

However, it is worth to highlight the strong integration with the mechanical design.

6.3 A "nontraditional" robotic finger design

The starting point of this research activity has been considerations about the appropriateness of the traditional mechanical solutions applied to dexterous robotic hands. Despite several hands have been successfully developed according these criteria, they show (as stated in Sec. 6.1) heavy limitations in terms of high complexity and cost, low reliability ... Mechanical structures inspired to biological models (in particular to the obvious model given by the human hand) may enhance the success of the overall design, concerning in particular its simplicity. Therefore, it has been defined a new finger structure based on the so called "compliant mechanisms", i.e. chains of rigid links connected through elastic hinges allowing relative motion between them. The interest towards compliant mechanisms and the investigation on their properties and design criteria have been rapidly growing in the last years, with significant applications in many fields, including MEMS (micro electro mechanical systems) and robotics [92], but application of compliant mechanism concepts to robotic end-effectors has been so far limited to small-scale manipulation grippers [93].
The new structure tries to reproduce the biological model, whose frame is obtained by separate bones connected by ligaments. In particular the endoskeletal concept, which is the base of the new design, can easily integrate distributed sensing capabilities as well as an external "skin" reproducing the tissues of the human hand. As a matter of fact, it has been shown that the presence of an external soft layer can greatly improve the manipulation capabilities of robotic fingers [45], in terms of stability of the interaction (because of dissipation introduced by the nonlinear visco-elastic behavior of the compliant layer) and of the grasp (due to the conformability to the object), and also enhances the reliability of the underlying (mechanical and electronic) structure.
Moreover the whole articulated structure is particularly suitable to be realized by a single piece (e.g. a moulded plastic item) composed of rigid and elastic parts (hinges); this structure greatly simplifies manufacturing and assembly operations, reduces costs, improves reliability.
Several morphological solutions have been defined, according to a systematic design approach

[94], [95], and different designs have been implemented and experimentally evaluated.
At present, only three parallel joints have been implemented: the adduction-abduction joint is not present. The proximal and the medial joints are independently actuated, while the distal joint is coupled to the movement of the medial joint. Joint actuation is provided by remote motors, and transmission is obtained with guided flexures, that can be directly integrated with the finger structure in PTFE, as well as obtained in different material, e.g. delrin (a plastic material often employed to construct deformable objects and devices) or high-strength steel.
In Fig. 6.2 the first implemented prototype is reported; in this case, both the finger structure and the tendons are obtained from the same piece of PTFE.

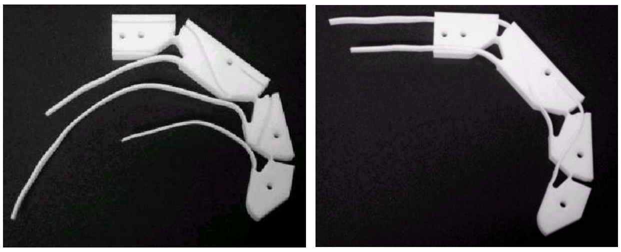

Figure 6.2: First prototype of the finger.

6.4 Interactions between mechanics, electronics and control

The optimization process of the mechanical structure, and in particular of the hinges, make use of theoretical considerations and experimental tests [94, 95]. But, as stated in Sec. 6.2 and shown in Fig. 6.3 this is only a part of the overall project. Side by side with the mechanical implementation of the basic idea, the study of a suitable sensing apparatus and adequate control strategies has been proceeding. Obviously, this research activity takes into account the main features of the proposed mechanical design, as well as the specifications tied to the desired target, that is a robotic hand able to interact with environment and perform *dexterous* manipulation. Conversely, the achieved results, in the both fields of electronics and control, have strong effects on the mechanical structure, which, because of its simple manufacture process (see Fig. 6.2), is intrinsically suitable for rapid prototyping and can be easily and rapidly modified.
In the following, the steps, which have leaded to the current state of this research activities are reported in the chronological order to give a precise idea of the development process and of the strong integration between the different parts (mechanics, electronics, control).

6.5 The early experimental tests

In order to validate the mechanical design of the finger and infer useful observations about its properties, a number of experimental tests have been performed on the different components of the finger, namely:

- skeletal frame;

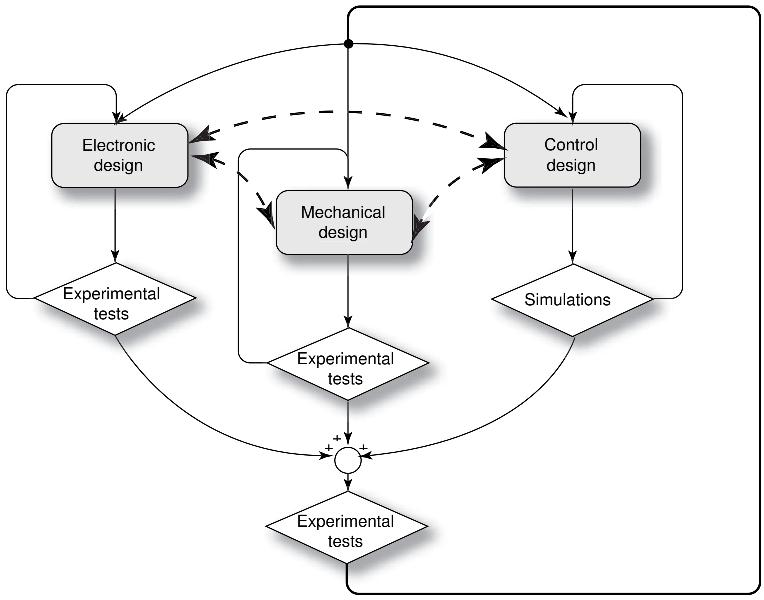

Figure 6.3: Approach followed in the development of the new robotic hand.

- soft material for the finger pads;

6.5.1 The skeletal frame

The prototype used for the tests on the mechanical frame is shown in Fig. 6.2, while its structure is reported in Fig. 6.4. In this case, to actuate the two degrees of freedom of the finger (the last two joints are coupled), only two flexure are used, and therefore they must work both under tension and under compression load.

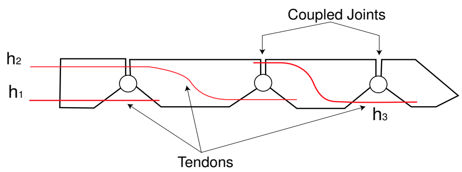

Figure 6.4: Possible structural scheme of the endoskeleton.

The way the two flexures act during the free motion depends on the kinematic design and on the structural design of hinges, the stiffness of which must be overcome by flexures. By adopting a relaxed configuration of the finger frame with angles of 45^o between each pair of links (like in the prototype under evaluation), it is necessary to apply compression loads only when the finger is opening, while only tension loads occur during closure and, most important, when a contact on the internal surfaces (normally used for grasping and manipulation) happens.
In order to impose controlled linear displacements on flexures, the setup shown in Fig. 6.5.a has been built. It is composed by two brushless motors and two ball screws which transform the

rotative motion into a linear one.

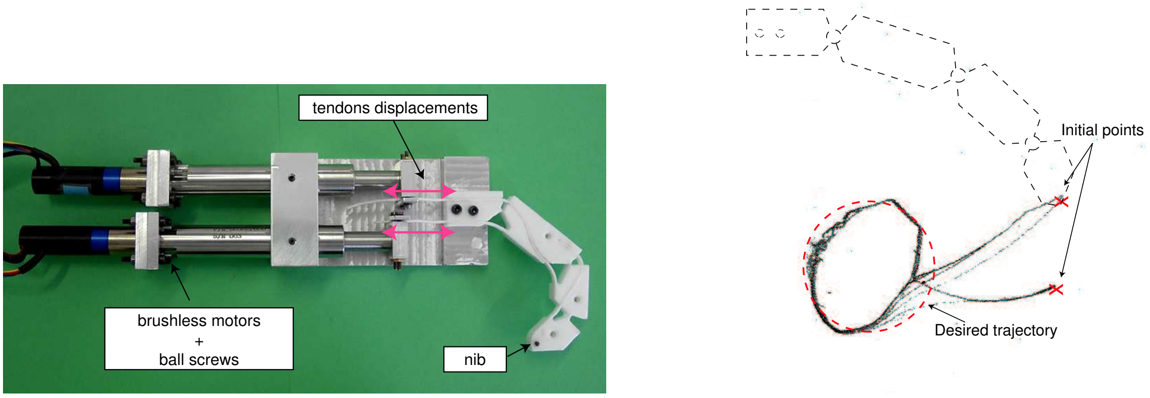

(a) (b)

Figure 6.5: Experimental setup for the endoskeleton (a) and trace of the desired motion (b).

Through a nib placed on the fingertip, the trajectory in the workspace can be recorded. In this way it is possible to verify the kinematic properties of the finger, comparing the desired trajectory with the real one.
In fact, due to their peculiar structure, the hinges do not generate exactly rotative motions, and in some conditions (e.g. when compression load occurs) the flexures may be not completely stretched out, being subject to undesired deformations (e.g. bending) and other non-idealities. Anyhow, in order to plan desired motions, the following theoretical kinematic relation between tendons displacement (h_i) and joint variables (θ_i) has been adopted (in addition to the "traditional" kinematic relation for a 3-dof planar manipulator with revolute joints):

$$h_i = d_i \; \theta_i \; \frac{\sin(\frac{\theta_{i0}-\theta_i}{2})}{\sin(\frac{\theta_i}{2})}$$

being θ_{i0} the joint angle corresponding to the initial configuration, d_i a mechanical parameter shown in Fig. 6.6. This equation is computed under the hypothesis of ideal revolute pairs (see Fig. 6.6) and does not take into account nonlinear effects, as shown in Fig. 6.5.b where a repetitive circular motion of the fingertip is reported. The same trajectory has been repeated several times, with different initial positions: although the tracking errors are not negligible, it is worth to notice that the behavior of the finger is perfectly repetitive.

The main cause of error has been recognized in the flexures, which in some case must work under compression loads; when this occurs they are subject to bending and are not able to drive the finger as planned. For example by means of only two flexures it is impossible to completely extend the finger skeleton. Moreover, the flexures show a strong elastic behavior: in Fig. 6.7 the elongation of a tendon due to the applied force is reported. This test has been performed by pulling the tendon (which is fixed at the other end) with a known force, and measuring the achieved displacement. The total length of the tendon is about 160mm and the overall stiffness $k = 1.5Nmm^{-1}$;

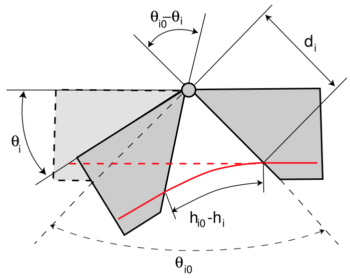

Figure 6.6: Ideal model of the hinges.

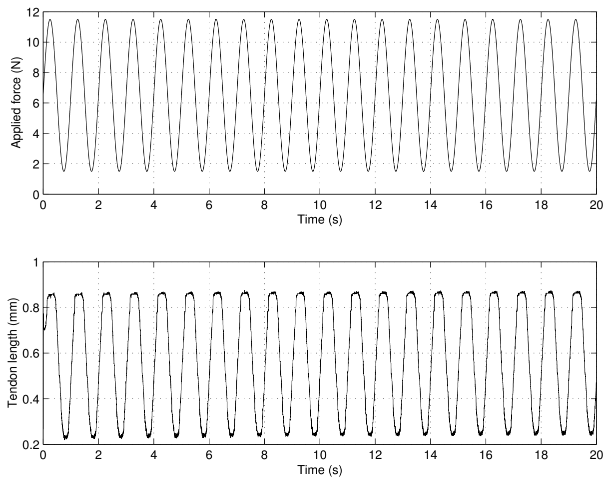

Figure 6.7: Tendon elongation due to the applied forces.

6.5.2 The soft material for the finger pads

Currently, the finger frame is tested without any soft layer, but tests tending to choose (and characterize) the material for the external compliant shell have been also performed.
In particular a suitable material has been identified in Technogel®, a polyurethane gel, which shows a softness quite close to the human skin, a nonlinear viscoelastic behavior (with a related dissipation that can contribute to stabilize of the grasp) and other promising features (for a complete analysis see [96]); among the different tests performed, the more significant is depicted in Fig. 6.8.b, where the dynamic responses of the Technogel® (obtained by means of the experimental setup shown in Fig. 6.8.a) to compressive loads and the following shape recovery are reported (6 mm is the thickness of the specimen at rest).
It is evident the non-linear behavior of the material, and it is also worth to notice that the recovery time is perfectly compatible with our application (the gel is able to go back up to the 80% of the rest thickness in less than one second).

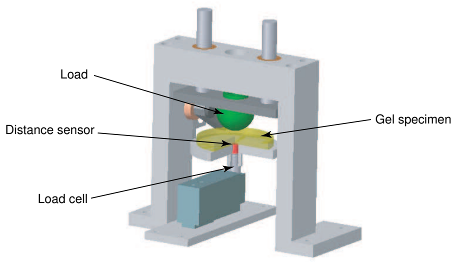

(a)

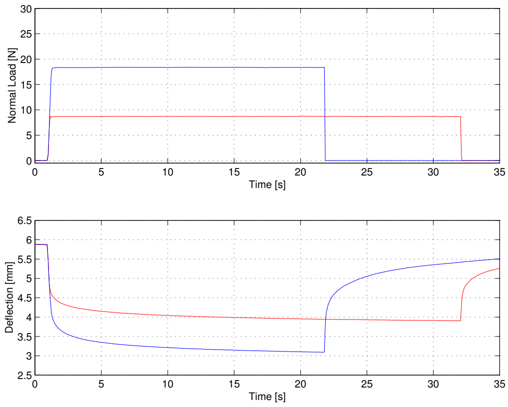

(b)

Figure 6.8: Experimental setup for the polyurethane gel (a) and response of Technogel® to a compressive loads and shape recovery (b).

6.6 Control strategy and actuation modalities

As stated in Sec. 6.2, this project is an attempt to improve the integration of the structure and control design. The target is not only the optimization of some parameters of the mechanical structure according the features of the adopted control strategies and *vice-versa*, but also to determine the most suitable mechanical solutions in order to carry out a given control (which is in turn inspired by the structure of the finger frame) [91].

In fact, a number of theoretical works have faced the problem of dexterous manipulation and control of robots interacting with the environment [97, 84, 98], but the results they show, although interesting, remain often unapplied (or with applications limited to simple test setups purposely developed, e.g. 1-dof manipulators), because of the gap between the assumed hypothesis and the real conditions. The target is to reduce this difference.

In Ch. 5 *impedance control* has been recognized as the most suitable strategy to perform robotic manipulation, when an interaction with an unstructured environment occurs. In particular, among the possible approaches for the implementation of such a controller, one seems well fitting with this application, that is impedance controller based on the passivity concept. This approach, deeply described in Sec. 5.5, consists in coupling the robotic finger with a target impedance

$$\mathbf{F}_z = \mathbf{K}(x_z - x_0) + \mathbf{B}(\dot{x}_z) \tag{6.1}$$

which leads to the control

$$\tau_{act} = -\mathbf{J}^T(\theta)\ \mathbf{K}\ (\mathbf{L}(\theta) - x_0) - \mathbf{J}^T(\theta)\ \mathbf{B}\ \mathbf{J}^{-1}(\theta)\dot{\theta} \tag{6.2}$$

where $\mathbf{K}$, $\mathbf{B}$ are the stiffness and the damping of the impedance regulator, $\mathbf{J}(\theta)$, $\mathbf{L}(\theta)$ are the Jacobian and the forward kinematics of the robotic finger (described by joint variables θ).

As shown in 5.5 by means of the Hamiltonian formalism, the controller (6.2) has very robust properties of stabilities during the interaction with the environment. Furthermore, it is robust towards two classes of crucial nonidealities and side-effects which characterize the mechanical structure of the robotic finger, namely:

a) *large errors in finger kinematic equations*, due to tendons bending and elongation;

b) *unmodeled interface dynamics* between the finger and the environment (e.g. soft pads); as a matter of fact the soft layer, that will cover the endoskeletal structure, can, as stated in Sec. 6.3, aid the stability of the system if a proper control (e.g. a passive controller) is adopted; conversely, because of their nonlinear behavior [84], the pads can compromise the stability.

If an error affects the kinematic model of the finger, and hence the (wrong) position of the fingertip in the work-space is computed as

$$x' = \mathbf{L}'(\theta)$$

the Hamiltonian of the controller becomes

$$\mathbf{H}'_Z(q) = \mathbf{H}_Z(\mathbf{L}'(\theta) - x_0) \tag{6.3}$$

The total energy of the system (finger structure and control) is, according to (5.21) where interactions with the external environment are neglected,

$$\mathbf{H}'_C(p, q) = \mathbf{H}_F(p, q) + \mathbf{H}'_Z(p, q) \tag{6.4}$$

The temporal derivative of (6.4) is

$$\frac{d\mathbf{H}'_C}{dt} = -\dot{\theta}^T \tau_{fric} - \dot{x}'^T \mathbf{B} \dot{x}' \tag{6.5}$$

where $\dot{x}'$ is the velocity corresponding to the wrong kinematics

$$\dot{x}' = \mathbf{J}'(\theta)\dot{\theta}$$

Equation (6.5) is equivalent to (5.25), with $\mathbf{F}_{ext} = 0$, therefore the same conditions for the stability hold. And the same happens if an interaction with the external environment is considered. Therefore, despite the large errors in the kinematic model which characterize the finger structure (as shown by the first experimental tests), the finger, steered by a simple impedance, will be stable if an interaction with an object, stable in isolation, happens.

Concerning the effects of the soft layer, which will cover the finger endoskeleton, the stability of the whole system (controller, finger, soft interface, environment) can be proved by means of simple energetic considerations. If the interface dynamics are stable in isolation, the environment is stable in isolation, and the manipulator (with the impedance controller) is stable in isolation, then the total energy of the coupled system is the sum of the energies of the components and never increases. Therefore dynamic interaction between these three systems cannot cause

instability.
Considering a visco-elastic material, the soft interface can be described through

$$q_i = x - x_e$$

where x, x_e are the position coordinates of the fingertip and of the environment. Its dynamic behavior is

$$\mathbf{F}_i = \mathbf{K}_i(q_i) + \mathbf{B}_i(\dot{q}_i) \tag{6.6}$$

where $\mathbf{K}_i(q_i)$ and $\mathbf{B}_i(\dot{q}_i)$ (with $\dot{q}_i^T\mathbf{B}_i > 0$ for $\dot{q}_i \neq 0$) represent respectively the elastic and the damping terms. The corresponding Hamiltonian (potential function of the elastic part) is

$$\mathbf{H}_i(q_i) = \int \mathbf{K}_i(q_i)dq_i \tag{6.7}$$

which is assumed to be a positive-definite nondecreasing function of q_i.
The Hamiltonian $\mathbf{H}_T$ for the coupled system may be obtained by adding the individual Hamiltonians

$$\mathbf{H}_T(p_t, q_t) = \mathbf{H}_C(p, q) + \mathbf{H}_E(p_e, q_e) + \mathbf{H}_i(x - x_e) \tag{6.8}$$

Therefore, the rate of change of $\mathbf{H}_T$ is

$$\frac{d\mathbf{H}_T}{dt} = -\dot{q}_e^T\mathbf{D}_e + \dot{x}_e^T\mathbf{F}_e - \dot{\theta}^T\tau_{fric} - \dot{x}^T\mathbf{B}\dot{x} + \dot{x}^T\mathbf{F}_{ext} - \dot{q}_i^T\mathbf{B}_i + \dot{q}_i^T\mathbf{F}_i \tag{6.9}$$

Since the power generated by the coupling is zero

$$\mathbf{F}_e^T\dot{x}_e + \mathbf{F}_{ext}^T\dot{x} + \mathbf{F}_i^T\dot{q}_i = 0 \tag{6.10}$$

by substituting (6.10) in (6.9) the rate of change becomes

$$\frac{d\mathbf{H}_T}{dt} = -\dot{q}_e^T\mathbf{D}_e - \dot{\theta}^T\tau_{fric} - \dot{x}^T\mathbf{B}\dot{x} - \dot{q}_i^T\mathbf{B}_i \tag{6.11}$$

Thus the properties of the environment, the manipulator, the simple impedance[1], and the surface are sufficient that the Hamiltonian for the couple system

1. is locally positive-definite;

2. never increases.

The coupled system is therefore locally asymptotically stable.

[1]see Sec. 5.5.

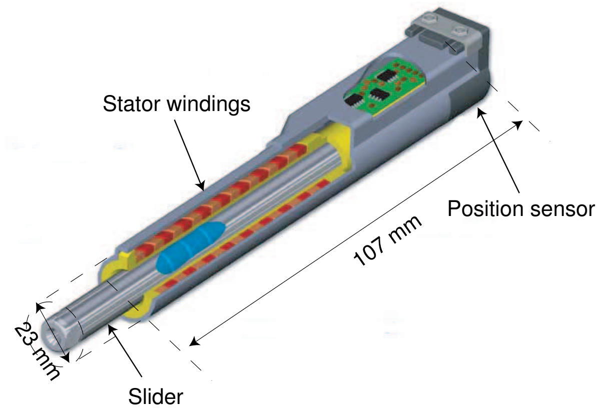

Figure 6.9: Sketch of the linear motor used to actuate the finger.

6.6.1 Choice of the actuation system

Besides its properties of stability, the passivity-based approach for the implementation of an impedance control provides further advantages. In particular, as clearly shown by eq. (6.2), the controller does not need any force feedback, and therefore, in a *minimal* approach, the use of force sensors, which are usually cause of high complexity and low reliability, can be avoided.
On the other hand, the implementation of such a controller requires two main conditions:

1. the back-drivability of the actuation chain;
2. the co-location of position sensors.

In particular its performances are strictly depending on the friction. For this reason, as shown in Ch. 5, this control strategies is often unapplicable in robotic hands. As a matter of fact the mechanisms that allow high reduction ratio (e.g. harmonic drive) and that are often necessary in order to provide sufficient forces by means of small (concerning sizes and therefore supplied forces/torques) actuators, likewise yield high friction levels [83].
From the last consideration, it follows the need of limiting the friction as much as possible, both in the kinematic chain and in the actuation system. As the transformation of a rotational motion into a linear one normally produces such effects and often requires complicated and/or not-back-drivable mechanical solutions, linear motors have been chosen for the actuation.
This kind of technology, not yet extensively adopted in robotics, allows a simple and direct connection with the flexures. In this way, it is possible to have back-drivable transmission chain and with limited frictions. Moreover, in the motors used for our application (produced by LinMot® [99]) the position sensor is integrated in the structure (thus the problem of sensor co-location is automatically solved), that is a simple tubular stator with a moveable slider, see Fig. 6.9. Despite the quite small dimensions, suitable for an integration into the forearm of a hand/arm system, the performances of these actuators are appropriate to actuate the fingers, as shown in Tab. 6.6.1. Since, in this approach, the motors are used as an ideal source of force, some experiments have been performed in order to test their capabilities (with the standard control boards which implement the basic current/force controller) to supply desired linear forces. For

Peak force	33 N
Continuous force	9 N
Max accel.	280 m/s^2
Max velocity	2.4 m/s
Position resolution	1 μm

Table 6.1: Main characteristics of the linear motors used for the finger actuation.

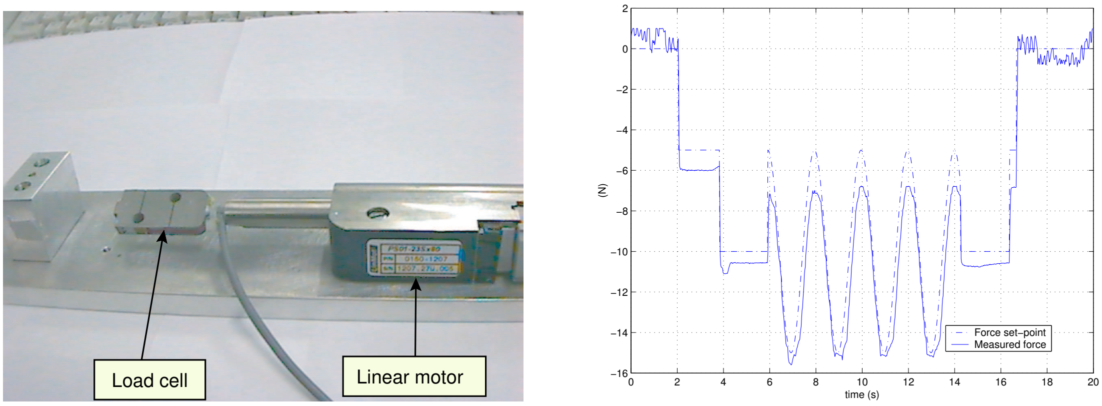

(a) (b)

Figure 6.10: Experimental setup used to test linear motors behavior (a) and applied forces (b).

this purpose, the simple setup of Fig. 6.10.a has been constructed: it allows to measure, by means of a (strain-gauges based) load cell directly installed on the motor slider, the forces that the motor is applying. Therefore, some force set-points have been provided to the motor control board, and the real force measured. The results are reported in Fig. 6.10.b, in the static case (application of a step set-point) as well as in dynamic conditions (sinusoidal set-point). In the worst case the difference, probably due to frictional phenomena, is about 20%. If better performances (in terms of precision of the applied forces) are required, the load cells can be used for control purposes, but this is not problematic because they can be easily integrated in the forearm and they are co-located [85] (that is directly installed on the actuators).

6.7 Implementation and experimental validation of the impedance control

In order to demonstrate its effectiveness, the control strategy (6.2) has been experimental implemented. As a matter of fact, the models used for simulations can not take into account all the dynamic effects that characterize the finger structure, the tendons, the actuators...
To this purpose, a new setup, reproducing the final working conditions of the finger in a complete robot hands, has been built. In Fig. 6.11, this setup is shown: three linear motors, equipped

with load cells installed on the slider, actuate the flexures/tendons, whose length is quite large to reproduce their routing in the final robotic hand. As a matter of fact, in order to include

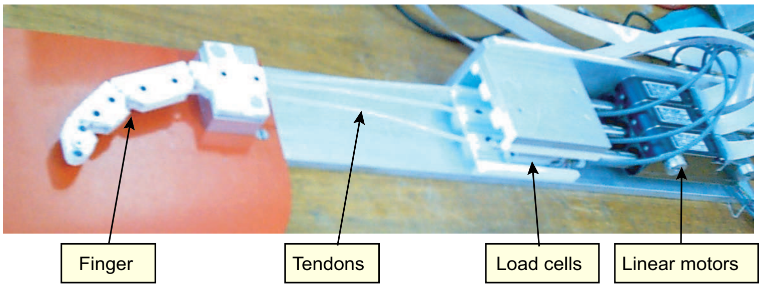

Figure 6.11: Experimental setup used to validate the control strategies.

all the components in a self-contained device, the integration between the hand and the arm is considered, and thus the motors will be located in the forearm, quite far from the actuated fingers.
Moreover, to overcome the problem of flexures bending (within the finger and along the path from actuators to the finger), a new one has been added to the structure. In this way they work all the time with tensile load, and also threadlike tendons can be used. This new finger prototype is shown in Fig. 6.12: the degrees of freedom are still two (the last two joints are coupled by means of h_4), but the shape of the hinges and the connection of the tendons (that in this case are separated from the endoskeleton) are quite different from the early prototype presented in Sec. 6.5.

In order to implement the control algorithm (6.2), it is necessary to map the required joint torques τ_{act} into the forces F_h which the linear motors can apply to the tendons. The steps necessary for the implementation of the overall controller are therefore:

1. Considering a planar robot (depicted in Fig. 6.12) with three standard revolute joints but two degrees of freedom (because of the mechanical coupling between the last two joints), from (6.2), it is possible to compute the torques τ_{act}, which must be provided to the joints.

2. From τ_{act}, according to the static relation between joint torques and tendon forces, the force set-points F_{act} for the linear motors can be computed. Note that it must be guaranteed that F_{acti} are all positive (the tendons must work under tension loads).

6.7.1 Kinematic model of the new prototype

In order to implement the impedance control, it is necessary to derive the relation between joint positions and tendon lengths (corresponding to the linear actuator positions) and between joint torques and tendon forces.
By considering the finger structure depicted in Fig. 6.12, the relation between joint angles θ_i

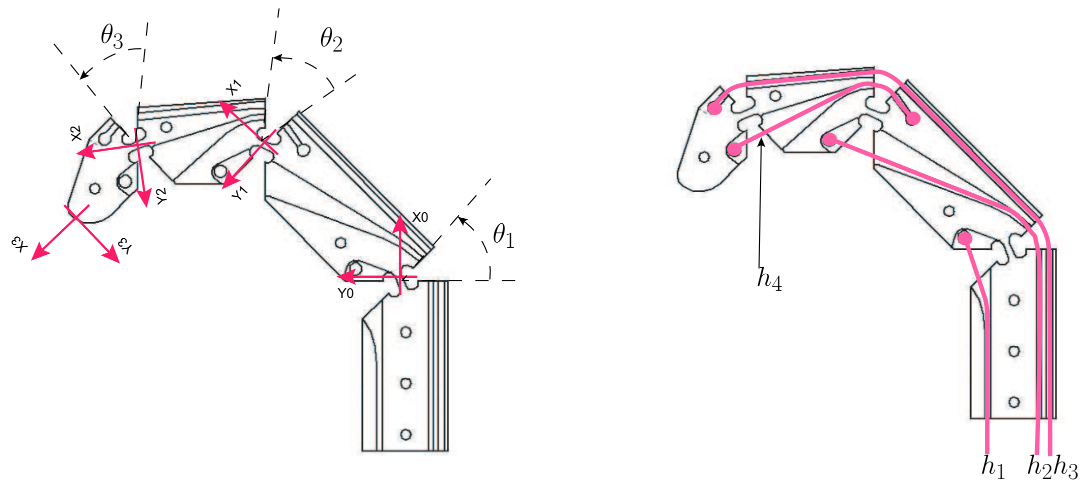

(a) (b)

Figure 6.12: Reference frames of the finger endoskeleton (a) and tendons configuration (b).

and tendon lengths h_i is

$$\begin{cases} h_1 = h_{10} - \sqrt{r_{11}^2 + d_{11}^2 - 2r_{11}d_{11}\cos(\theta_{10} - \theta_1)} \\ h_2 = h_{20} - \sqrt{r_{22}^2 + d_{22}^2 - 2r_{22}d_{22}\cos(\theta_{20} - \theta_2)} - r_{21}\theta_1 \\ h_3 = h_{30} - r_{31}\theta_1 - r_{32}\theta_2 - r_{32}\theta_2 \\ h_4 = h_{40} - \sqrt{r_{43}^2 + d_{43}^2 - 2r_{43}d_{43}\cos(\theta_{30} - \theta_3)} - r_{42}\theta_2 = const \end{cases} \tag{6.12}$$

where r_{ji}, d_{ji} and θ_{i0} are mechanical parameters reported in Fig. 6.13 (j refers to the considered tendon and i to the joint).

By differentiating (6.12) with respect to the time, it follows

$$\begin{cases} \dot{h}_1 = \frac{r_{11}d_{11}\sin(\theta_{10}-\theta_1)}{\sqrt{r_{11}^2+d_{11}^2-2r_{11}d_{11}\cos(\theta_{10}-\theta_1)}}\dot{\theta}_1 \\ \dot{h}_2 = \frac{r_{22}d_{22}\sin(\theta_{20}-\theta_2)}{\sqrt{r_{22}^2+d_{22}^2-2r_{22}d_{22}\cos(\theta_{20}-\theta_2)}}\dot{\theta}_2 - r_{21}\dot{\theta}_1 \\ \dot{h}_3 = -r_{31}\dot{\theta}_1 - r_{32}\dot{\theta}_2 - r_{32}\dot{\theta}_2 \\ \dot{h}_4 = \frac{r_{43}d_{43}\sin(\theta_{30}-\theta_3)}{\sqrt{r_{43}^2+d_{43}^2-2r_{43}d_{43}\cos(\theta_{30}-\theta_3)}}\dot{\theta}_3 - r_{42}\dot{\theta}_2 = 0 \end{cases} \tag{6.13}$$

From last equation of (6.13) it is possible to achieve the relation between $\dot{\theta}_3$ and $\dot{\theta}_2$, which are rigidly coupled, and finally obtain

$$\begin{pmatrix} \dot{h}_1 \\ \dot{h}_2 \\ \dot{h}_3 \end{pmatrix} = \mathbf{P}(\theta) \begin{pmatrix} \dot{\theta}_1 \\ \dot{\theta}_2 \end{pmatrix} \tag{6.14}$$

By classical duality argument between forces and velocities

$$\begin{pmatrix} \tau_{\theta 1} \\ \tau_{\theta 2} \end{pmatrix} = \mathbf{P}(\theta)^T \begin{pmatrix} F_{h1} \\ F_{h2} \\ F_{h3} \end{pmatrix} \tag{6.15}$$

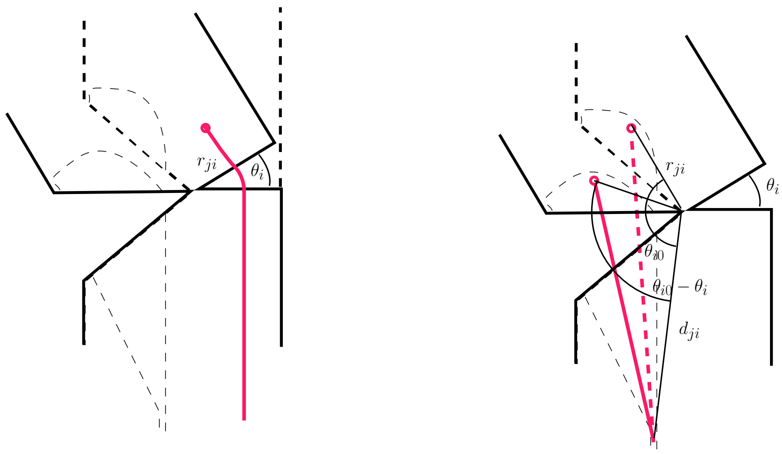

(a) (b)

Figure 6.13: Relation between angular displacements and tendon length.

where F_h are the tendon forces and

$$\tau_{\theta 2} = \tau_{\theta}{}'_2 + \tau_{\theta}{}'_3$$

is the overall contribution of the torques on the last two joints ($\tau_{\theta}{}'_2$ and $\tau_{\theta}{}'_3$).

6.7.2 Implementation of the controller

Given the desired torques

$$\tau_{act} = \begin{pmatrix} \tau_{act1} \\ \tau_{act2} \end{pmatrix}$$

provided by (6.2), where $\mathbf{J}^T(\theta)$ defines the relation

$$\begin{pmatrix} \tau_1 \\ \tau_2 \end{pmatrix} = \mathbf{J}_{2\times 2}(\theta)^T \begin{pmatrix} F_x \\ F_y \end{pmatrix} \tag{6.16}$$

in principle, the control scheme can be implemented by mapping τ_{act} into the linear forces F_{act}, which must be applied to the tendons

$$F_{act} = \mathbf{P}(\theta)^+ \tau_{act} + F_{actN}$$

where $\mathbf{P}(\theta)^+$ is the pseudo-inverse of $\mathbf{P}(\theta)^T$ and $F_{actN} \in ker(\mathbf{P}(\theta)^T)$ is an internal force which insures that all tendon tensions are positive. Obviously F_{actN} will be chosen as small as possible, so that the tendons remain taut but are not subject to excessive internal forces.

However, in this way, it is guaranteed that the actuated tendons are always pulled, while the state of the internal tendon h_4 (which must also work under tension load) is completely neglected.

Therefore, a different approach is preferable. By separately considering the equilibrium of the torques in each joint, the following relations hold:

$$\begin{cases} -r_{21}F_{h2} - r_{31}F_{h3} + f_1(\theta_1)F_{h1} = \tau_{\theta 1} \\ -r_{32}F_{h3} - r_{42}F_{h4} + f_2(\theta_2)F_{h2} = \tau_{\theta 2}' \\ -r_{33}F_{h3} + f_4(\theta_3)F_{h4} = \tau_{\theta 3}' \end{cases} \tag{6.17}$$

where

$$f_i(\theta_j) = \frac{r_{ij}d_{ij}\sin(\theta_{j0} - \theta_j)}{\sqrt{r_{ij}^2 + d_{ij}^2 - 2r_{ij}d_{ij}\cos(\theta_{j0} - \theta_j)}}$$

Therefore, given the desired torques

$$\tau_{act} = \begin{pmatrix} \tau_{act1} \\ \tau_{act2}' \\ \tau_{act3}' \end{pmatrix}$$

computed on the basis of (6.2), where $\mathbf{J}^T(\theta)$ defines, in this case, the relation

$$\begin{pmatrix} \tau_1 \\ \tau_2' \\ \tau_2' \end{pmatrix} = \mathbf{J}_{3\times 2}(\theta)^T \begin{pmatrix} F_x \\ F_y \end{pmatrix} \tag{6.18}$$

from the third equation of (6.17), which considers the equilibrium of the torques in the last joint, it is possible to choose F_{act3} which guarantees that $F_{h4} > 0$ (and in particular that $F_{h4} = \varepsilon$, with $\varepsilon = 1N$)

$$F_{act3} = \frac{f_4(\theta_3)\varepsilon + \tau_{act3}'}{r_{33}} \tag{6.19}$$

By substituting the value of F_{act3} (and F_{h4}) into

$$F_{act2} = \frac{r_{42}F_{h4} + r_{32}F_{act3} + \tau_{act2}}{f_2(\theta_2)} \tag{6.20}$$

the value of the force F_{act2} can be obtained, and finally, by substituting F_{act2} in

$$F_{act1} = \frac{r_{21}F_{act2} + r_{31}F_{act3} + \tau_{act1}}{f_1(\theta_1)} \tag{6.21}$$

F_{act1} can be computed.
At this point, it must be verified that

$$F_{act2} > 0$$

$$F_{act1} > 0$$

If these conditions are not satisfied the internal forces must be increased, by adding to F_{act} a vector $F_{actN} \in ker(\mathbf{P}(\theta)^T)$. In particular $ker(\mathbf{P}(\theta)^T)$ is a one-dimensional vector space, which can be represented by means of

$$F_{act}{}^* = \begin{pmatrix} F_{act1}^* \\ F_{act2}^* \\ 1 \end{pmatrix}$$

If F_{act1} or F_{act1} or both are less than zero the additive contribution is simply

$$\begin{pmatrix} F_{act1} \\ F_{act2} \\ F_{act3} \end{pmatrix}_N = m \; {F_{act}}^* \tag{6.22}$$

with

$$m = \left| \min \left\{ \frac{F_{act1}}{F_{act1}^*}, \frac{F_{act2}}{F_{act2}^*} \right\} \right|$$

An experimental result of the overall control algorithm, given by (6.2), (6.19), (6.20), (6.21) and (6.22) is shown in Fig. 6.14. In this case the finger is interacting with an object along the x direction, and by changing the position set-point it is possible to change the exerted forces. Note that, despite an obstacle is present, the finger position changes. This is due to the rotation of the fingertip that is not a point, as supposed, and to some couplings between task-space directions which have been not compensated. However the interaction is stable. In Fig. 6.15 the motor efforts needed to guarantee the task-space forces are reported. It is worth to notice that all the forces are obviously positive and that h_3 must provide very low (and quite constant) levels of force and hence can be substituted by a passive element (such as a spring).

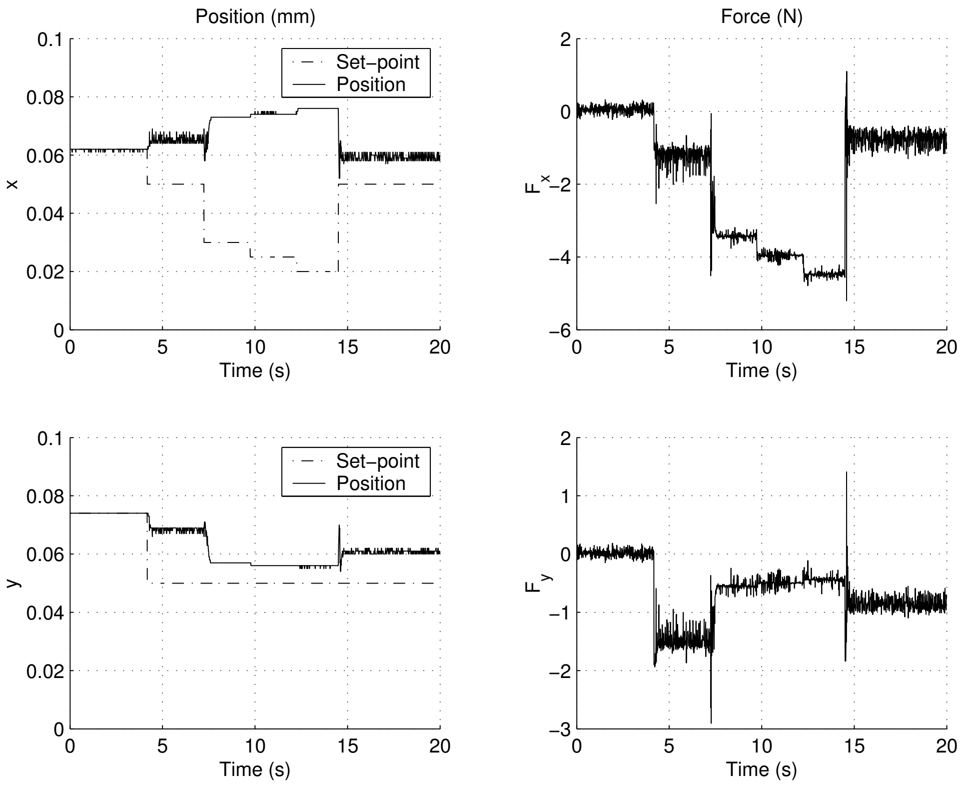

Figure 6.14: Physical interaction of the finger, steered by an impedance controller, with the environment.

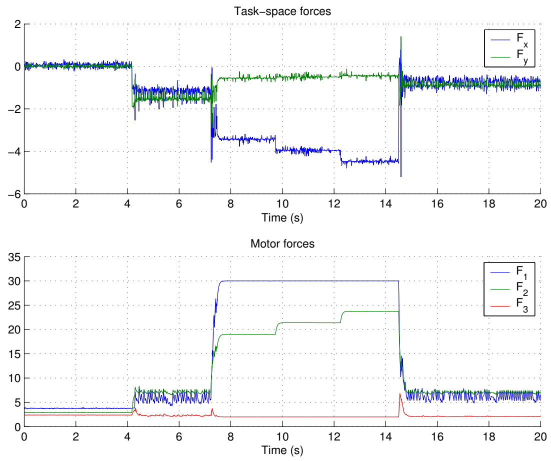

Figure 6.15: Mapping between work-space forces and motor efforts.

6.8 Design of the sensing apparatus

In the *minimal* approach, shown in Sec. 6.7, the finger, steered by the impedance controller, performs interaction tasks without any force information, but based only on motor position sensors. Nevertheless, in order to enhance the capability of the robotic end-effector the adoption of a suitable set of sensors (including position sensors on the joints and distributed tactile sensors, as shown in Fig. 6.16) seems necessary [100]. As a matter of fact, the estimation of the joint

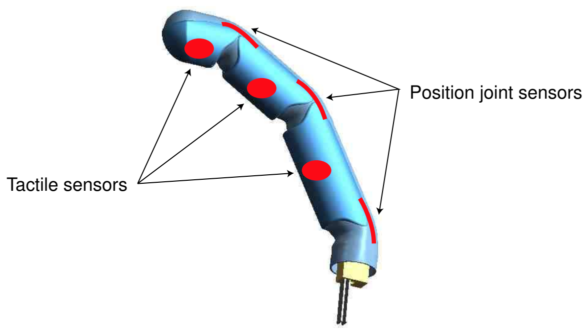

Figure 6.16: Sensory equipment of the finger.

angles from the tendon lengths, obtained by means of (6.12), leads to large errors (mainly due to tendon elongation). Moreover, to compensate for inevitable friction phenomena and allow fine manipulation tasks, which involve small forces, or to properly plan the manipulation operations force and tactile sensors must be used.

6.8.1 Position sensors

In order to know the relative positions between the links of the finger, a measure based only on tendon lengths is not sufficient. On the other hand, the peculiar structure of the joints (without a fixed rotation center) makes it difficult to find a suitable position sensor. In fact, the standard robotic technologies (e.g. potentiometers or hall-effect based sensors) require well defined paths.

A possible solution could be a special purpose sensor (see Fig. 6.17.a), directly built on the hinges of the endoskeleton. This solution is based on strain gauges, glued on the deformable structure. Nevertheless, in this manner only a partial compensation of kinematic errors is possible, such as those produced by tendons bending, but not of errors directly imputable to the hinges.

An alternative solution is based on flex-sensors, Fig. 6.17.b, usually used in data gloves to measure the bending of human fingers. These sensors are based on piezoresistive effect, and provide a variation of resistance proportional to the bending angle. In this case, the position information can compensate for all the kinematic errors, because the sensor is physically separated from the finger structure. A characterization of this sensor has been performed, by means of a mechanical setup, which mimics the structure of the finger joints, but in this case the center of rotation is fixed (see Fig. 6.18). It is therefore possible to compare the angular displacements, estimated by means of a potentiometer, with the measurements provided by the flex sensor, which has been arranged as reported in Fig. 6.18.b, with an end fixed to the structure and the other one free of sliding. The results, based on a number of measurements, are reported in Fig. 6.19. The Figure (a) shows the static relation existing between the angular displacement and the voltage output of the sensor: this relation is nonlinear but monotone, and hence can be easily inverted. In particular, it is enough the second-order polynomial

$$Y = -0.00089{\cdot}x^2 + 0.02{\cdot}x + 3.7 \tag{6.23}$$

to interpolate the points, with very small errors (0.02 rad).

The Figure (b) shows the dynamic behavior of the sensor: in particular the actual output that it provides, and the ideal output that it should provide (according the static characteristic) are compared, when the joint moves with a sinusoidal velocity. It is clear that, in this case, the behavior of the sensor is acceptable only for intermediate angular values, but probably this drawback is due to the mechanical arrangement, which should be redesigned. Further tests are needed, maybe directly integrating the sensor in the finger endoskeleton.

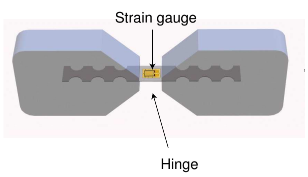

(a)

(b)

Figure 6.17: Joint position sensors: special purpose sensor (a), commercial flex sensor (b).

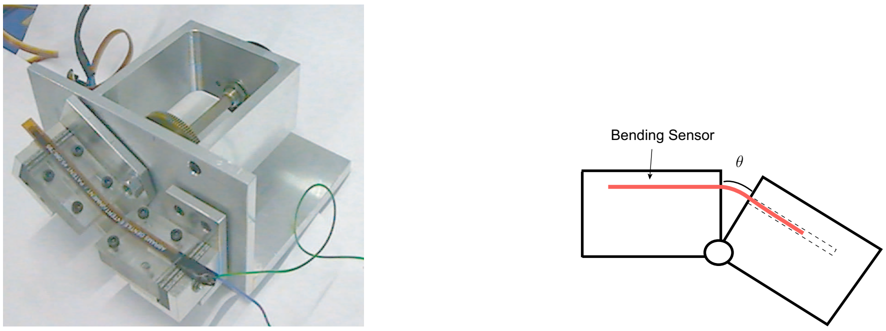

(a) (b)

Figure 6.18: Setup for the characterization of the bending sensor (a) and its functional scheme (b).

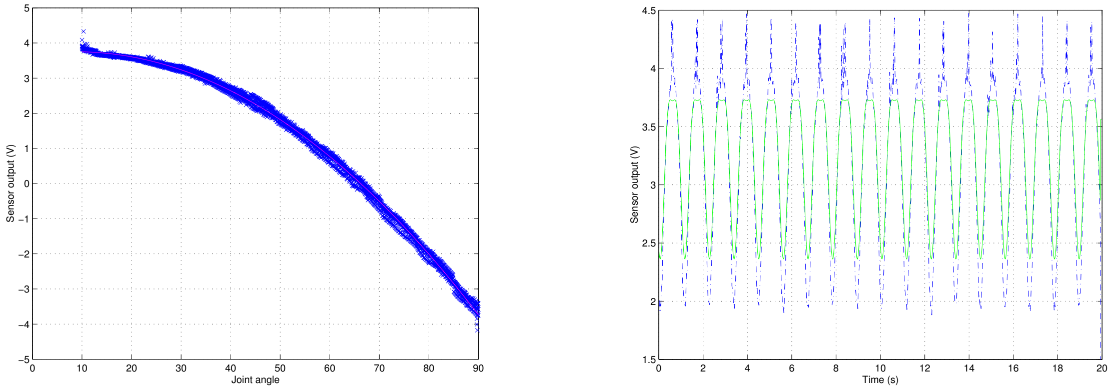

(a) (b)

Figure 6.19: Static characteristic (a) and dynamic behavior of the flex sensor (b).

An alternative solution which allows to keep the finger structure (and hence the overall end-effector) as simple as possible, is the use of a camera to estimate the finger configuration. This possibility, currently under evaluation, appears the most adequate for those tasks, which in any case need a visual feedback.

6.8.2 Force sensors

In order to exert very small forces on the environment, an implicit force control based on motor current(/force) control appears not to be an optimal solution. Additional force/tactile sensors seems necessary, also in the task planning phase, in order to have a sufficiently precise estimate of exchanged forces and to known the exact location of the contact points. Two are the possible solutions:

- tactile array sensors [100];

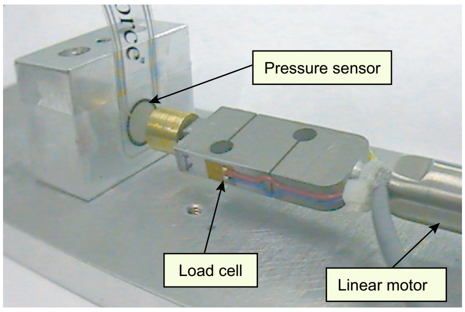

(a)

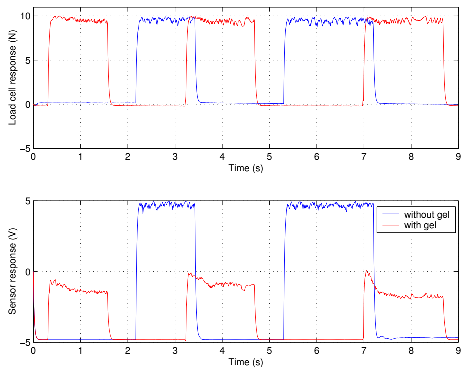

(b)

Figure 6.20: Setup for the characterization of the pressure sensor (a) and response of the pressure sensor to the application of a force of 10 N with and without soft cover(b).

- intrinsic tactile sensors [100].

The former set includes a number of different devices, able to detect the amplitude of the normal forces exerted on their surface (usually planar) and the contact shape. They can have different spatial resolutions and different sensitivities to the applied forces according to their degree of complexity. For the present application, inspired by criteria of simplicity and reliability, the use of a commercial single element pressure sensors has been investigated. In particular, the FlexiForce® manufactured by Tekscan [101], has been tested in order to verify the suitability of its integration in the finger design. Therefore, the focus has been the study of the interactions between the sensor and the other elements of the robotic finger, in particular the polyurethane gel for the pads. As the sensors must be placed under this soft cover, a setup to measure how the force is transmitted to the sensor through the gel has been designed (see Fig. 6.20.a). By means of this setup the response of the force sensor to a known force has been recorded, with and without a layer of gel.

As shown in Fig. 6.20.b, where the achieved results are reported, the presence of the gel layer (3 mm thick) reduces the sensitivity of the sensor, and above makes the dynamic of the sensor very slow. The reason of this behavior is due to the polyurethane gel which, after the initial application of the external force, changes its configuration, distributing the external pressure on the overall underlying surface (also outside the sensitive area of the sensor). This filtering effect of the Technogel® makes the use of this sensor for control purposes very difficult.
A solution which seems more suitable for the proposed finger are intrinsic tactile sensors, directly built on the finger frame. As a matter of fact this kind of sensor, able to detect the magnitude of the applied force/torque and the position of the contact centroid, provides a measure of the forces/torques resultant, and therefore it is insensitive to the above mentioned effects of gel; nevertheless a deeper analysis seems necessary, in order to test the interactions between the gel layer and an IT sensors.

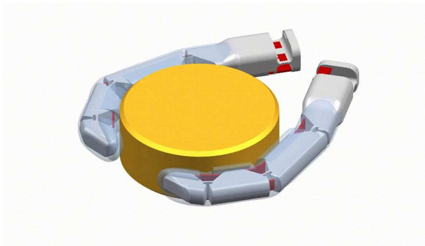

(a)

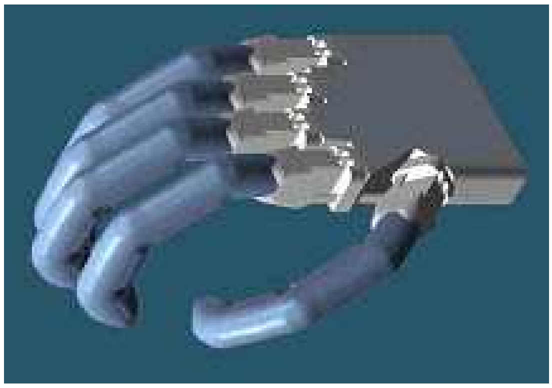

(b)

Figure 6.21: Conceptual scheme of a 2-jaw end-effector based on compliant mechanisms (a) and design of a robotic hand based on compliant mechanisms (UB-Hand III)(b).

6.9 Conclusion and future work

In this Chapter the design of a innovative robotic finger has been reported. The basic idea is the adoption of so the called "compliant mechanisms" in the field of robotic hands, which appears still too tied to traditional criteria of robot design. Because of the lack of suitable technological solutions (e.g. artificial muscles), these criteria lead to complex, costly and not enough reliable structures. Conversely, the proposed design shows attractive characteristics, such as a small size, which allows the adoption of a visco-elastic cover (similar to the human hands) and an easy integration with the sensory system, and above all a simplicity, also in the production process, that could lead to a wider diffusion of robot hands. On the other side, the first experimental activity has shown some drawbacks of the prototype, concerning in particular the difficulty of modelling the kinematics of the finger as well as its overall dynamic behavior (including elastic tendons, hinges and soft pads). Therefore, the control strategies and the sensory system have been designed in order to solve these specific problems in the more effective (and possibly simplest) way, influencing in turn the choice of particular mechanical solutions (e.g. the actuation system by means of linear motor).
The result is a simple, reliable and low-cost system. Moreover, thanks to its structure the finger is suitable for modular designs of robotic end-effectors. Therefore the target can an anthropomorphic robot hand with 4 upper fingers and an opposable thumb (whose sketch is depicted in Fig. 6.21.b), but also more simple structures, such as the articulated 2-jaws gripper shown in Fig. 6.21.a.

Bibliography

[1] A. Bicchi. Hands for dexterous manipulation and robust grasping: a difficult road toward simplicity. *IEEE Transactions on robotics and automation*, 16(6), 2000.

[2] C. Bonivento and C. Melchiorri. Towards dexterous manipulation with the u.b. hand ii. In *12th. IFAC World Congress*, Sydney, Australia, 1993.

[3] J.Butterfass, G.Hirzinger, S.Knoch, and H.Liu. Dlr's multisensory articulated part i: Hard- and software architecture. In *Proc. IEEE International Conference on Robotics and Automation, ICRA98*, 1999.

[4] J. Butterfass, M. Grebenstein, H. Liu, and G. Hirzinger. Dlr-hand ii: Next generation of a dextrous robot hand. In *Proc. IEEE International Conference on Robotics and Automation, ICRA01*, Seoul, Korea, 2001.

[5] R.O. Ambrose, H.Aldridge, R.S.Askew, R.R. Burridge, W.Bluethmann, M.Diftler, C.Lovchik, D.Magruder, and F.Rehnmark. Robonaut: Nasa's space humanoid. *IEEE Intelligent System*, 2000.

[6] S.C. Jacobsen et al. Design of the utah/mit dexterous hand. In *Proc. IEEE International Conference on Robotics and Automation, ICRA86*, 1986.

[7] G.A. Bekey, R. Tomovic, and I. Zeljkovic. Control architecture for the belgrade/usc hand. In T. Iberall S.T. Venkataraman, editor, *Dexterous Robot Hands*. Springer-Verlag, 1990.

[8] T. Iberall and C.L. MacKenzie. Opposition space and human prehension. In T. Iberall S.T. Venkataraman, editor, *Dexterous Robot Hands*. Springer-Verlag, 1990.

[9] R.L. Clatzky and S. Lederman. Intelligent exploration by the human hand. In T. Iberall S.T. Venkataraman, editor, *Dexterous Robot Hands*. Springer-Verlag, 1990.

[10] A. Bicchi, A. Marigo, and D. Pratichizzo. Dexterity through rolling: Manipulation of unknown objects. In *Proc. IEEE int. Conf. on Robotics and Automation, ICRA99*, 1999.

[11] A.M. Okamura and M.R. Cutkosky. Haptic exploration of fine surface features. In *Proc. IEEE int. Conf. on Robotics and Automation, ICRA99*, 1999.

[12] M. R. Cutkosky. On grasp choice, grasp models, and the design of hands for manufacturing tasks. *IEEE Transactions on robotics and automation*, 5(3), 1989.

[13] N.Fukaya, S. Toyama, T. Asfour, and R. Dillmann. Design of the tuat/karlsruhe humanoid hand. In *Proc. IEEE/RSJ Int.Conf.on Intelligent Robots and Systems, IROS'00*, 2000.

[14] A. Bicchi and R. Sorrentino. Dexterous manipulation through rolling. In *Proc. IEEE int. Conf. on Robotics and Automation, ICRA95*, 1995.

[15] W.T.Townsend. Mcb - industrial robot feature article- barrett hand grasper. *Industrial Robot: An International Journal*, 27(3), 2000.

[16] K.S. Salisbury and B.Roth. Kinematics and force analysis of articulated mechanical hands. *Journal of Mechanims, Transmissions and Actuation in Design*, 105, 1983.

[17] C.S. Lovchik and M.A. Diftler. The robonaut hand: a dexterous robot hand for space. In *Proc. IEEE International Conference on Robotics and Automation, ICRA99*, 1999.

[18] C.Melchiorri and G.Vassura. Mechanical and control features of the ub hand version ii. In *Proc. IEEE/RSJ Int.Conf.on Intelligent Robots and Systems, IROS'92*, 1992.

[19] C. Melchiorri and G. Vassura. Mechanical and control issues for integration of an arm-hand robotic system. In Raja Chatile and Gerd Hirzinger, editors, *Experimental Robotics II, the 2nd Int. Symposium.* Springer-Verlag, 1993.

[20] G. Hirzinger, B. Brunner, J. Dietrich, and J. Heindl. Sensor-based space robotics - rotex and its telerobotic features. *IEEE Transactions on robotics and automation*, 9(5), 1993.

[21] R.A. Grupen, T.C. Henderson, and I.D. McCammon. A survey of general-purpose manipulation. *Int.J.Robot.Res.*, 8(1), 1989.

[22] D.I. McCloskey. Kinesthetic sensibility. *Int.J.Robot.Res.*, 58(4), 1978.

[23] K.B. Shimoga. A survey of perceptual feedback issues in dexterous telemanipulation. i. finger force feedback. In *Virtual Reality Annual International Symposium*, Seattle, WA, USA, 1993.

[24] R.D. Howe and M.R. Cutkosky. Dynamic tactile sensing: perception of fine surface features with stress rate sensing. *IEEE Transactions on robotics and automation*, 9(2), 1993.

[25] L. Biagiotti, C. Melchiorri, and G. Vassura. Experimental activity on grasping objects in free-floating conditions. In *6th ESA Workshop on Adv.Space Techn. for Rob. and Aut.,ASTRA 2000*, ESTEC, Noordwijk, NL, 2000.

[26] J. Butterfass, G. Hirzinger, S. Knoch, and H. Liu. Dlr's multisensory articulated hand. i. hard- and software architecture. In *Proc. IEEE Int. Conf. Robotics and Automation, ICRA98*, 1998.

[27] H.R. Nicholls and M.H. Lee. A survey of robot tactile sensing technology. *Int. J. of Robotics Research*, 3(3), 1989.

[28] H.R. Nicholls and M.H. Lee. Tactile sensing for mechatronics - a state of the art survey. *Mechatronics*, 9, 1999.

[29] C. Melchiorri. Tactile sensing for robotic manipulation. In S. Nicosia, B. Siciliano, A. Bicchi, and P. Valigi (eds.), editors, *Ramsete: Articulated and mobile robots for services and Technology*, volume 270. Springer-Verlag, 2001.

[30] T. Okada. Computer control of multijointed finger system for precise object handling. In *International Trends in Manufacturing Technology - Robot Grippers*, 1986.

[31] T.A. Chase and R.C. Luo. A capacitive tri-axial tactile force sensor design. In *Proc. IEEE/ASME International Conference on Advanced Intelligent Mechatronics*, 1997.

[32] R.S. Fearing. Some experiments withtactile sensing during grasping. In *Proc. IEEE International Conference onRobotics and Automation, ICRA87*, 1987.

[33] I.D. McCammon and S.C. Jacobsen. Tactile sensing and control for the utah/mit hand. In T. Iberall S.T. Venkataraman, editor, *Dexterous Robot Hands*. Springer-Verlag, 1990.

[34] D. Johnston, P. Zhang, J.M. Hollerbach, and S.C. Jacobsen. A full tactile sensing suite for dextrous robot hands and use in contact force control. In *Proc. IEEE Int. Conf. Robotics and Automation, ICRA96*, Minneapolis, 1996.

[35] Barret hand webpage. `http://www.barretttechnology.com/robot/products/hand/handarfr.htm`.

[36] H. Liu, J. Butterfass, S. Knoch, P. Meusel, and G. Hirzinger. A new control strategy for dlr's multisensory articulated hand. *IEEE Control Systems Magazine*, 19(2), 1999.

[37] J.P. Gazeau, S. Zeghloul, M. Arsicualt, and J.P. Lallemand. The lms hand: force and position controls in the aim of fine manipulation of objects. In *Proc. IEEE International Conference on Robotics and Automation, ICRA01*, Seoul, Korea, 2001.

[38] A. Caffaz and G. Cannata. The design and development of the dist-hand dextrous gripper. In *Proc. IEEE int. Conf. on Robotics and Automation, ICRA98*, 1998.

[39] Dist hand webpage. `http://www.graal.dist.unige.it/research/activities/DISThand/DISThand`

[40] Robonaut webpage. `http://vesuvius.jsc.nasa.gov/er_er/html/robonaut/robonaut.html`.

[41] K. Lee and I. Shimoyama. A skeletal framework artificial hand actuated by pneumatic artificial muscles. In *Proc. IEEE International Conference on Robotics and Automation, ICRA99*, Detroit, Michigan, 1999.

[42] H. Kawasaki, H. Shimomura, and Y. Shimizu. Educational-industrial complex development of an anthropomorphic robot hand 'gifu hand'. *Advanced Robotics*, 15(3), 2001.

[43] H. Kawasaki, T. Komatsu, K. Uchiyama, and T. Kurimoto. Dexterous anthropomorphic robot hand with distributed tactile sensor: Gifu hand ii. In *Proc. IEEE SMC '99 Conference on Systems, Man, and Cybernetics*, 1999.

[44] Shadow hand webpage. `http://www.shadow.org.uk/`.

[45] K.B. Shimoga and A.A. Goldenberg. Soft materials for robotic fingers. In *Proc. IEEE International Conference on Robotics and Automation, ICRA92*, Nice, France, 1992.

[46] S. Schulz, C. Pylatiuk, and G. Bretthauer. A new ultralight anthropomorphic hand. In *Proc. IEEE International Conference on Robotics and Automation, ICRA01*, Seoul, Korea, 2001.

[47] F. Lotti and G. Vassura. A novel approach to mechanical design of articulated fingers for robotic hands. In *Proc. IEEE/RSJ Int.Conf.on Intelligent Robots and Systems, IROS'02*, Lausanne, Switzerland, 2002.

[48] Underactuated robotic hands webpage. `http://wwwrobot.gmc.ulaval.ca/recherche/theme04_a.html`.

[49] A. Bicchi and A. Marigo. Dexterous grippers: Putting nonholonomy to work for fine manipulation. *Int. Jour. of Robotics Research*, 21(5-6), May-June 2002.

[50] D.L. Brock. Enhancing the dexterity of a robot hand using controlled slip. In *Proc. IEEE int. Conf. on Robotics and Automation, ICRA88*, 1988.

[51] R.D. Howe and M.R. Cutkosky. Practical force-motion model for sliding manipulation. *Int.J.Robot.Res*, 8(6), 1996.

[52] S. Payandeh. Planning controlled slips in dexterous manipulation. In *Proc. IEEE int. Conf. on Robotics and Automation, ICRA97*, 1997.

[53] A. Bicchi and R. Sorrentino. Dexterous manipulation through rolling. In *Proc. IEEE int. Conf. on Robotics and Automation, ICRA95*, 1995.

[54] M. Moll and M.A. Erdmann. Dynamic shape reconstruction using tactile sensors. In *Proc. IEEE int. Conf. on Robotics and Automation, ICRA02*, 2002.

[55] P. Putz. Space robotics. In P. Ehrenfreund at al., editor, *Laboratory Astrophysics and Space Research*. Kluwer Academic Publishers, 1999.

[56] G. Hirzinger, B. Brunner, J. Dietrich, and J. Heindl. Sensor-based space robotics-rotex and its telerobotic features. *IEEE Transactions on robotics and automation*, 9(5), 1993.

[57] R. Mugnuolo, S. Di Pippo, P.G. Magnani, and E. Re. The spider manipulation system (sms): the italian approach to space automation. *Int. J. on Robotics and Autonomous System*, 23(1-2), 1998.

[58] C. Melchiorri, G. Vassura, G. Ferretti, C. Maffezzoni, G. Magnani, and P. Rocco. A three finger, three degree-of-freedom gripper for space robotic manipulation. In *Proc. 5th ESA Work. on Adv. Space Technol. for Rob. and Aut., ASTRA'98*, 1998.

[59] F. Fabbri. *Progetto, costruzione e sperimentazione di un organo di presa robotico finalizzato ad applicazioni spaziali*. Master thesis, University of Bologna, 1999.

[60] C. Melchiorri. Slip detection and control using tactile and force sensors. *IEEE Trans. on Mechatronics, special Issue on Advanced Sensors for Robotics*, 5(3), 2000.

[61] L. Biagiotti. *Pinza Robotica per Applicazioni Spaziali: Controllo e Verifiche sperimentali.* Master thesis, University of Bologna, 2001.

[62] J.K. Salisbury. Active stiffness control of a manipulator in cartesian coordinates. In *Proc. 19th IEEE Conference on Decision and Control*, 1980.

[63] Rtai webpage. `http://www.rtai.org/`.

[64] A. Macchelli and C. Melchiorri. Real-time control system for industrial robots and control applications based on real-time linux. In *Proc. 15th IFAC World Congress*, 2002.

[65] S. Hutchinson, G.D. Hager, and P.I. Corke. A tutorial on visual servo control. *IEEE Transactions on robotics and automation*, 12(5), 1996.

[66] B. Mishra and M. Teichmann. Three finger optimal plannar grasp. Technical report, New York University, 1995.

[67] J. Ponce and B. Faverjon. On computing three-finger force-closure grasps of polygonal objects. *IEEE Transactions on robotics and automation*, 11(6), 1995.

[68] D.J. Montana. The condition for contact grasp stability. In *Proc. IEEE Int. Conf. Robotics and Automation, ICRA91*, 1991.

[69] R. Carloni. *Manipolazione Robotica: Strategie di Presa Ottima di Oggetti Planari.* Master thesis, University of Bologna, 2002.

[70] E. Rimon and J. Burdick. Mobility of bodies in contact i: a new 2nd order mobility index for multiple-finger grasp. In *Proc. IEEE Int. Conf. Robotics and Automation, ICRA94*, 1994.

[71] E. Rimon and J. Burdick. Mobility of bodies in contact ii: How forces are generated by curvature effects. In *Proc. IEEE Int. Conf. Robotics and Automation, ICRA94*, 1994.

[72] D.M. Gorinevsky, A.M. Formalsky, and A. Yu. Schneider. *Force Control fo Robotic Systems.* CRC Press, 1997.

[73] Dlr miniaturized force/torque sensor webpage. `http://www.robotic.dlr.de/mechatronics/minift/`

[74] M. Gavesi, F. Palma, and B. Riccò. Novel low-cost mechanical stress sensor. *Alta Frequenza*, 12(4), 2000.

[75] W. E. Spear and M. Heintze. The effect of applied and internal strain on the electronics properties of amorphous silicon. *Philosophical Magazine B*, 54(5), 1986.

[76] M.Tanimoto, F. Arai, T. Fukuda, I. Takahashi, and M. Negoro. Force display method for intravascular neurosurgery. In *Proc. IEEE Int. Conf. on Systems, Man, and Cybernetics*, 1999.

[77] Dlr hand ii webpage. `http://www.robotic.dlr.de/mechatronics/hand/`.

[78] R.M. Murray, D.C. Deno, K.S.J. Pister, and S.S. Sastry. Control primitives for robot systems. *IEEE Transaction on Systems, Man, and Cybernetics*, 22(1), 1992.

[79] B. Siciliano and L. Villani. *Robot Force Control*. Kluwer Academic Publishers, 1999.

[80] N. Hogan. Impedance control: an approach to manipulation. part i-iii. *ASME Journal of Dynamic Systems, Measurement, and Control*, 107, 1985.

[81] H. Asada. *Studies on Prehension and Handling by Robot Hands with Elastic Fingers*. PhD thesis, Kyoto University, 1979.

[82] V. Nguyen. Constructing force-closure grasps. *Int. J. Robotics Research*, 3(7), 1988.

[83] T. Doersam and P. Duerrschmied. Compensation of friction in mechanical for a three fingered robot gripper. In *Proc. IEEE/RSJ Int.Conf.on Intelligent Robots and Systems, IROS'96*, 1996.

[84] N. Hogan. On the stability of manipulators performing contact tasks. *ASME Journal of Dynamic Systems, Measurement, and Control*, 4(6), 1988.

[85] S.D. Eppinger and W.P. Seering. Three dynamic problems in robot force control. *IEEE Transactions on Robotics and Automation*, 8(6), 1992.

[86] H. Liu and G. Hirzinger. Cartesian impedance control for the dlr hand. In *Proc. IEEE/RSJ Int.Conf.on Intelligent Robots and Systems, IROS'99*, 1999.

[87] A. Albu-Schaeffer and G. Hirzinger. Cartesian impedance control techniques for torque controlled light-weight robots. In *Proc. IEEE Int. Conf. Robotics and Automation, ICRA02*, 2002.

[88] L. Sciavicco and B. Siciliano. *Modelling and Control of Robot Manipulators - 2nd Edition*. Springer-Verlag, 2000.

[89] M.T. Mason and J.K. Salisbury. *Robot Hands and the Mechanics of Manipulation*. MIT Press, 1985.

[90] J. van Amerongen. The role of control in mechatronics. *Engineering Science and Education Journal*, 9(3), 2000.

[91] Q.Li, W.J. Zhang, and L. Chen. Design for control - a concurrent engineering approach fo mechatronic system design. *IEEE/ASME Trans. on Mechatronics*, 6(2), 2001.

[92] L.L. Howell. *Compliant mechanisms*. John Wiley & Sons, 2001.

[93] J. M. Goldfarb and N. Celanovic. A flexure-based gripper for small-scale manipulation. *Robotica*, 17, 1999.

[94] F. Lotti and G. Vassura. A novel approach to mechanical design of articulated fingers for robotic hands. In *Proc. IEEE/RSJ Int. Conf. on Intelligent Robots and Systems '02, IROS 02*, 2002.

[95] F. Lotti and G. Vassura. Sviluppo di soluzioni innovative per la struttura meccanica di dita articolate per mani robotiche. In *Associazione Italiana per l'Analisi delle Sollecitazioni (AIAS) XXXI Convegno Nazionale*, 2002. in italian.

[96] P. Tiezzi, F. Lotti, and G. Vassura. Polyurethane gel pulps for robotic fingers. In *International Conference on Advanced Robotics, ICAR03*, 2003.

[97] S. Stramigioli, C. Melchiorri, and S. Andreotti. A passivity-based control scheme for robotic grasping and manipulation. In *Proc. of the 38th IEEE Conference on Decision and Control*, 1999.

[98] A. Bicchi and V. Kumar. Robotic grasping and manipulation. In A. Bicchi, S. Nicosia, B. Siciliano, and P. Valigi, editors, *Articulated and Mobile Robotics for SErvices and TEchnologies (RAMSETE)*. Springer Verlag, 2001.

[99] Linmot webpage. `www.linmot.com`.

[100] C. Melchiorri. Tactile sensing for robotic manipulation. In A. Bicchi, S. Nicosia, B. Siciliano, and P. Valigi, editors, *Articulated and Mobile Robotics for SErvices and TEchnologies (RAMSETE)*. Springer Verlag, 2001.

[101] Tekscan webpage. `www.tekscan.com/flexiforce/flexiforce.html`.